

Metals and Ceramics Division

**Heavy Vehicle Propulsion Materials Program
Quarterly Progress Report for
April through June 2003**

**D. R. Johnson
Technical Project Manager**

**Prepared for
U.S. Department of Energy
Assistant Secretary for Energy Efficiency and Renewable Energy
Office of FreedomCAR and Vehicle Technologies Program
EE 07 01 00 0**

**Prepared by the
OAK RIDGE NATIONAL LABORATORY
Oak Ridge, Tennessee 37831-6066
Managed by
UT-Battelle, LLC
for the Department of Energy
Under contract DE-AC05-00OR22725**

CONTENTS

Materials for Fuel Systems

Smart Materials for Diesel Fuel Injector (Detroit Diesel Corporation)

Cost-Effective Smart Materials for Diesel Engine Applications (ORNL)

Low-Cost Manufacturing Processes for Ceramic and Cermet Diesel Engine Components (SIU-C)

Intermetallic-Bonded Cermets (ORNL)

Low Cost–High Toughness Ceramics (ORNL)

Materials for Exhaust Aftertreatment

Materials for Exhaust Aftertreatment (Caterpillar Inc.)

Development of NO_x Sensors for Heavy Vehicle Applications (ORNL and Ford Motor Company)

Ultra-High Resolution Electron Microscopy for Characterization of Catalyst Microstructures and De-activation Mechanisms (ORNL)

Microstructural Changes in NO_x Trap Materials under Lean and Rich Conditions at High Temperatures (ORNL and Ford Motor Company)

Aftertreatment Catalyst Materials Research (Cummins Inc.)

Materials for Air Handling, Hot Section, and Structural Components

Lightweight Valve Train Materials (Caterpillar Inc.)

Thick Thermal Barrier Coatings (TTBCs) for Low Emission, High Efficiency Diesel Engine Components (Caterpillar Inc.)

Processing and Characterization of Structural and Functional Materials for Heavy Vehicle Applications (North Carolina A&T State University)

NDE Development for Ceramic Valves for Diesel Engines (Argonne National Laboratory)

Durability of Diesel Engine Component Materials (ORNL)

Life Prediction of Diesel Engine Components (ORNL and Caterpillar)

Low-Cost Manufacturing of Precision Diesel Engine Components (ORNL)

Diesel Exhaust Filter Temperature Measurement and Cost-Effective Machining of Titanium Alloys (University of Michigan)

Advanced Cast Austenitic Stainless Steels for High-Temperature Components (ORNL and Caterpillar Inc.)

Microstructure and Creep Properties of Hot-Extruded TiAl/Ti₃Al In-Situ Composites (Lawrence Livermore National Laboratory)

Synthesis of Powders for Titanium Carbide/Nickel Aluminide Cermets (University of Colorado)

Laser Surface Texturing of Lubricated Ceramic Parts (ORNL)

High-Density Infrared Surface Treatment of Materials for Heavy-Duty Vehicles (ORNL)

Test and Materials Standards

Surface Modification of Engineering Materials for Heavy Vehicle Applications (NIST)

Implementing Agreement for a Programme of Research and Development on Advanced Materials for Transportation Applications (ORNL)

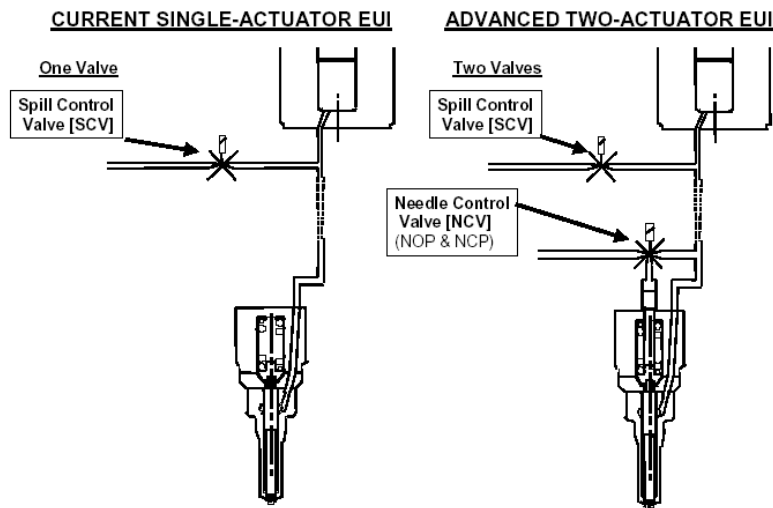
Mechanical Property Test Development (NIST)

Smart Materials for Diesel Fuel Injector

Urvish Joshi, Yury Kalish, and Craig Savonen – Detroit Diesel Corporation
Vijay Venugopal, Naeim Henein – Wayne State University

Objective/Scope

The objective of this project is to accelerate the pursuit of the application of emerging piezoelectric materials to the requirements of future diesel engine fuel injectors. Specific requirements of this material application and challenges of the operating environment are to be quantified. Whereas previous project effort included conceptual design and hydraulic analysis of a two-actuator fuel injector, the current work includes an experimental evaluation of the dual actuator fuel injector with contrast to single actuator systems. Performance and emission advantages of the dual actuation system are to be quantified relative to an advanced single actuation system. The incremental performance advantages of applying advanced material actuation to either the single actuator system or the dual actuator system will be evaluated by a combination of baseline experimental results, material characterization, and advanced electro-mechanical-hydraulic analysis.



A technical objective of this project is to substantiate a design/application strategy, through the use of computational and experimental methods, to maximize the advantage of piezoelectric materials, as compared to conventional solenoid materials, in a diesel fuel injector environment. The premise of the base piezoelectric material advantage is that it can provide:

- An order of magnitude reduced response time.
- Much higher force.
- More precise control of the start, rate-shape, and duration of the main injection event.
- More precise timing and delivery quantity of a multiple injection event.
- Less energy consumption.

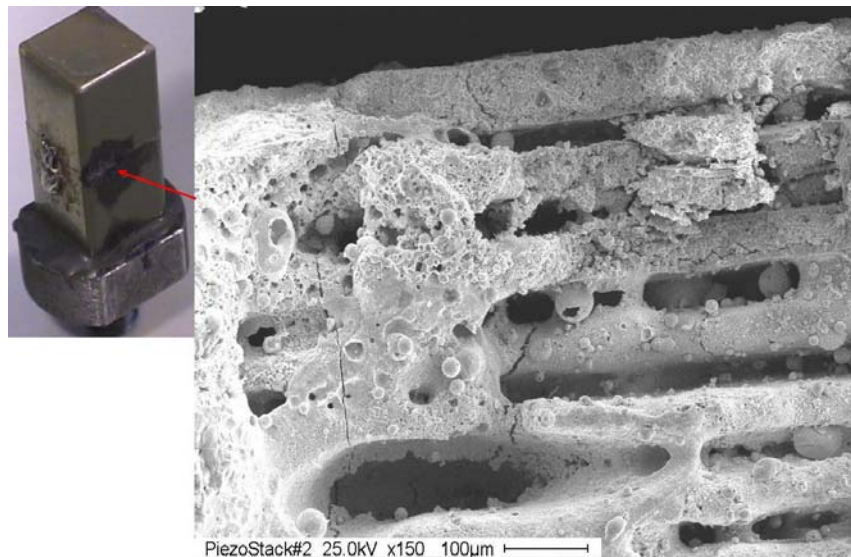
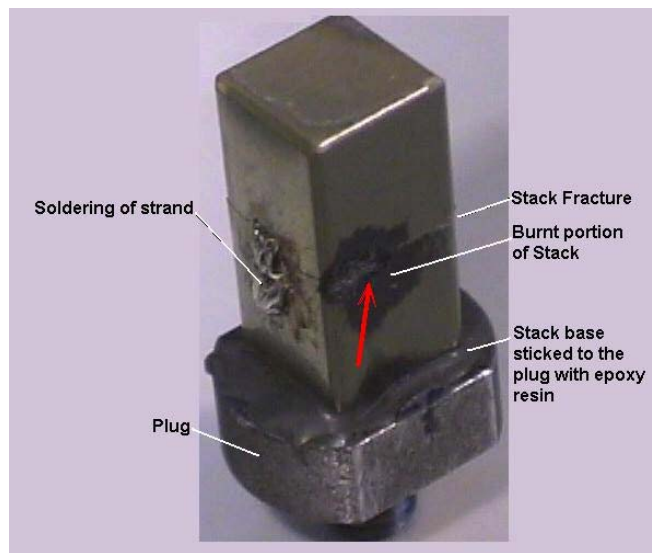
Recent Technical Highlights

Two failure modes on the bench test apparatus were clarified. Sensitivity of the piezoelectric stack to its operating environment were illustrated. Post-mortem analysis included SEM and

calculation of apparent dynamic forces during the event(s). Remedies were determined and adjustments to bench apparatus were made, while the implications of this experience are captured for future design reference.

When the actuator is driven at low (or no) preload, the negative acceleration, following a short pulse, induces tensile force. The tensile force is maximum at the center of the actuator. If it exceeds the tensile strength of the material, the actuator cracks in the center of the stack while the outer and intermediate elements move rapidly away from each other. At the shortest possible load time, the preload must compensate the acceleration force of the actuator.

The crack mostly causes an arc of the stored energy of the actuator. The electrodes get short-circuited resulting in sparks and heat that melts the bond and the insulation. This leads to the destruction and meltdown of the crack surfaces and the surrounding regions of the stack.



Similarly, the design of the marriage between the piezoelectric stack and its encapsulating structure must ensure that the loads subjected to the stack are substantially co-axial with the stack axis. Similarly, the mating surfaces between the stack and the encapsulating structure must be within a predetermined tolerance of parallelism, influenced by local perpendicularity and planarity.

Design and fabrication of a hydraulic amplification system was completed. Iterations on the design have led to considerable simplification, crucial to ultimately achieving a production feasible assembly. Upcoming bench testing of the actuation system aims to quantify performance status of the final design in this project. Measurements should include dynamic displacement, response, rise time, and delay time at different voltages, currents, frequencies, preloads, and number of pulses.

Cost-Effective Smart Materials for Diesel Engine Applications

J. O. Kiggans, Jr., F. C. Montgomery, B. M. Evans, and T. N. Tiegs
Oak Ridge National Laboratory

Objective / Scope

There are two objectives for this project. The first is to evaluate the cost-effectiveness and maturity of various “Smart Materials Technologies,” which are under consideration for diesel engine applications, such as fuel injection systems. The second is to develop “Smart Materials” to be incorporated into working actuators and sensors.

Task 1 - Multilayer Electroded Laminates

The purpose of this study is to find satisfactory methods for the preparation of PZT laminates with internal electrodes from tape cast materials. There is no new data on this task to include in the present report.

Task 2 – Compositional Alteration of PZT-4

A major task of this project is to develop cost-effective PZT compositions and processing methods that will give PZT powders that will sinter to high density at a temperature below 960°C. This goal is driven by the need to lower the cost of multilayer PZT actuators by reducing the cost of the interlayer electrodes. Commercial hard PZT powders require sintering at temperatures exceeding 1200°C and, thus, multilayer devices must use costly Pd/Ag electrodes. There is no new data on this task to include in the present report.

Task 3 – Fabrication and initial testing of a PZT actuator fatigue test system

The objective of this task is to fabricate a reliability testing system for PZT actuators. This system is designed to cycle a multiple layer piezoelectric actuator and measure the electrical and mechanical properties of the stack during testing. A fixture is used in conjunction with a computer-based data acquisition system that controls testing of the piezoelectric ceramic materials and records conditions during the test. This setup will provide for continuous cycling of PZT actuators and measure changes in piezoelectric parameters during cycling to determine the effects of fatigue on the electric and mechanical properties of the piezoelectric stacks.

A test fixture has been developed which will hold the PZT stack and apply a known preload to that stack. The preload is applied with a heavy-duty spring and is adjustable from 0 to greater than 100 lb with a threaded collar. The amount of preload is measured with a load cell. The load cell can also be used to determine the force during cyclic testing. A known field is applied to the PZT stack with a Trek 609E-6 amplifier. The amount of displacement is measured with a Capacitech Model 4100 capacitance probe.

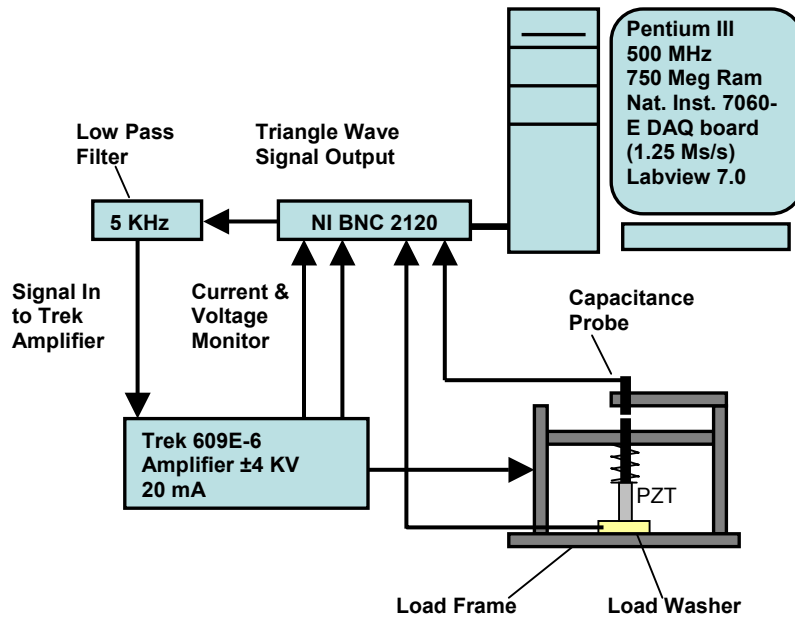


Figure 1: Schematic of the ORNL multilayer PZT actuator testing fixture and data acquisition system.

A National Instruments 7060-E multifunction data acquisition board is used to control cycling of the stack by providing the output signal for the amplifier and to record the data from the experiment. In tests performed to date, a 100 Hz or lower frequency signal has been used to drive the piezo stack. A 5 kHz low pass filter is used between the analog output of the data acquisition board and the amplifier to remove the “steps” from the digital to analog conversion, smooth the signal, and reduce noise. The voltage and current output are recorded from the Trek amplifier.

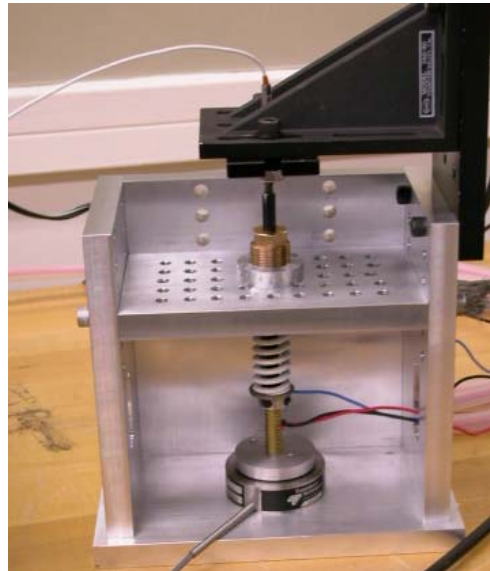


Figure 2: Load Frame with load washer and EDO PZT.

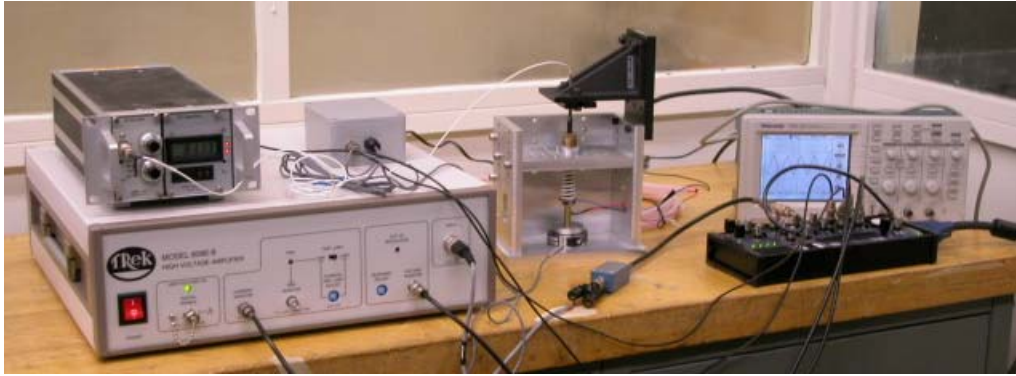


Figure 3: Experimental setup with Trek amplifier, Capacitech 4100 displacement gage, Load frame, load washer, power supply BNC 2120, and oscilloscope to monitor output from DAQ card.

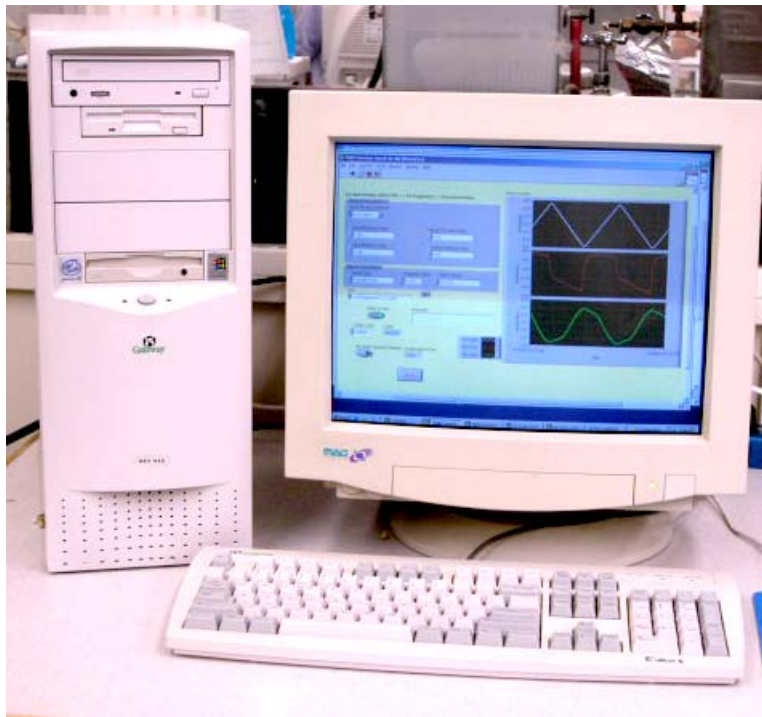


Figure 4: Computer data acquisition system. Shown on screen are voltage, current, and displacement signal monitors.

Several initial experiments have been performed with this setup. An EDO model E100-P4 actuator was cycled over 7 million times during the setup of this system. Some of the history of this actuator is unknown and it is possible that the actuator was overloaded at times during the setup. Its behavior was somewhat unpredictable at the end of 7 million cycles. A second EDO model E100-P4 is currently undergoing fatigue testing with this system and has survived over 40 million cycles.

The EDO E100-P4 actuators are 26 mm in length and 8.25 mm in diameter. They consist of 44 layers that are approximately 0.5 mm thick. The frequency range of these actuators is DC to 1000 Hz. The voltage range is 0-800 Volts. The recommended preload range is 10-200 lb. The

current actuator is being cycled with a triangle wave that ranges from 0 to 600 Volts at 50 Hz. Two full cycles of voltage, current, and displacement data are stored every 25,000 cycles for the first 15 million cycles, then every 100,000 cycles until failure. 2,000 points for each parameter are stored. A 25-lb preload is applied to the stack during cycling. Load data can be stored as well, but is not currently being stored to decrease the data I/O requirements.

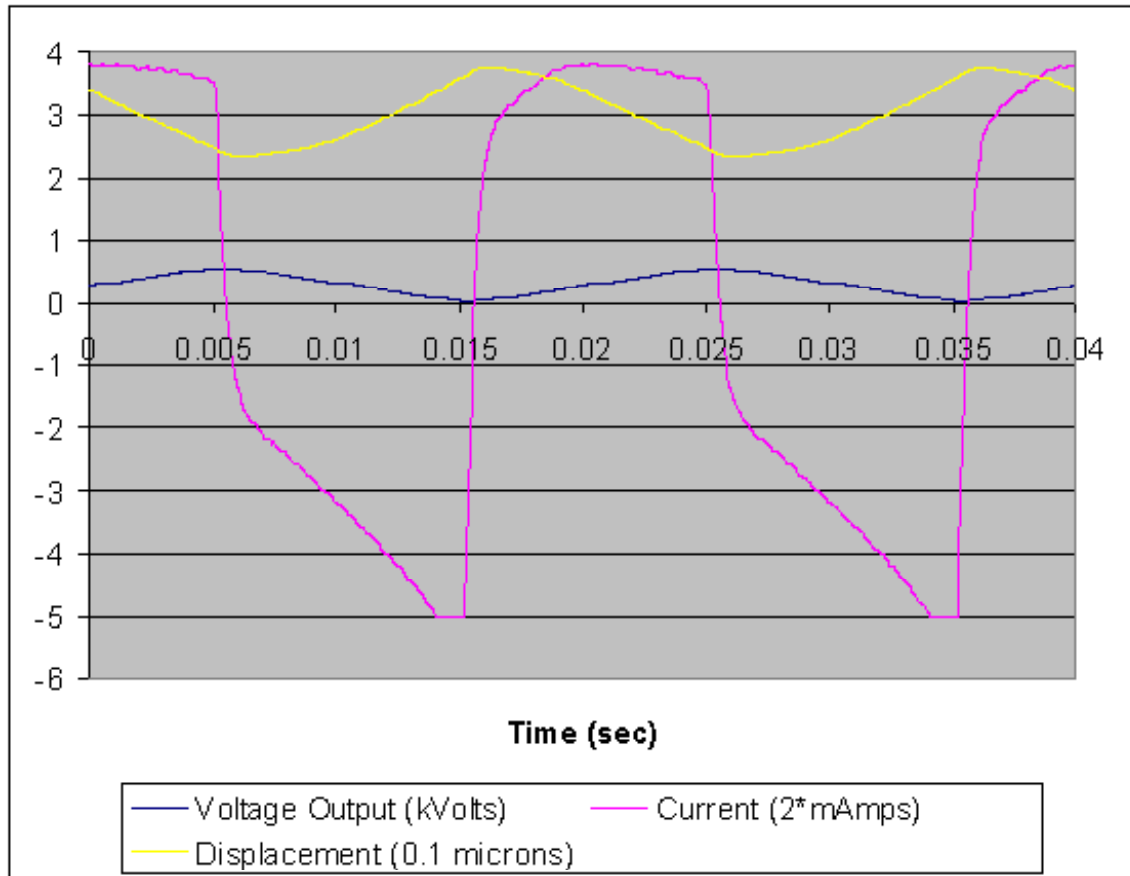


Figure 5: Data output for two cycles of PZT excitation.

Results and Discussion

Figure 5 shows the raw output from the data acquisition board during fatigue cycling of the PZT actuator. The triangle excitation is shown with the 180 degree offset current signal and the displacement signal. The capacitance gage gap signal is representative of the displacement motion of the actuator. As the actuator expands, the gap in the capacitance gage decreases. The smaller gap corresponds to a larger displacement. The current output is a voltage proportional to the current and is slightly clipped due to the ± 5 V gain setting on the board. This setting was used because the other signals are smaller than the current signal and allows a better overall resolution. The clipping of the current signal was not apparent on the Labview front-panel display, but was present in the raw data. The front-panel display was used to optimize the settings, before the experiment was started.

The voltage output is a feedback signal proportional to the actual voltage applied by the amplifier. The input signal is slightly attenuated by the 5 kHz low pass filter. The voltage signal

is used to determine the field applied to the capacitor in the hysteresis and displacement loops. The current signal is numerically integrated to determine the charge on the PZT device.

The gain setting used results in a 2.5-mV resolution with the 12-bit A-D conversion. The excitation voltage and frequency were chosen in order for the current to get as close to -5 V as possible without going above or below ± 5 V. This limitation occurs because the current system is not using true simultaneous multichannel data acquisition card. The individual points of data are taken sequentially and are offset by 1 microsecond. A new data acquisition system under development will utilize a true multi-channel data acquisition board such that the gains can be set for the channels individually. This system will allow the maximum data resolution per channel.

A similar error can occur with the analog output signal out as well, because the data acquisition board outputs a series of “steps” representing the triangle wave. The low pass filter corrects for this at the frequency and voltage used presently, however at slower frequencies and lower voltages this becomes a problem. The analog output of our board is 12 V. A 10-Hz, 100 mA triangle wave has 20 vertical steps that are 2.4 milliseconds (410 Hz) in duration. This signal was unusable by the current test system. We are investigating methods for removing this error by recalibrating the output voltage of the card. Another method would be to use an arbitrary waveform generation card or an external programmable waveform generator.

Figure 6 shows the polarization curves and displacement curves for the EDO actuator for the first 40 million cycles. The most notable characteristic of these curves is the decrease in stroke with increasing cycles. This appears to be due a loss in the poling of the sample with cycling, even though no negative voltage is used in this experiment. There is a significant drop in the maximum displacement over the first 100,000 cycles, and then a steady decline in the maximum displacement with each subsequent 5 million cycles. Some drop in the maximum charge is noted with continued cycling, as well. This appears to be as much a shift in the polarization curves, however. The displacement data has been normalized such that the minimum displacement is always zero microns, and appears reversed because it corresponds to the size of the gap in the capacitance gage. No normalization has been performed on the polarization data. Note that two full cycles were plotted in each of these curves. Testing of this device is ongoing. We will be investigating the causes of the changes in poling and shifts in polarization curves in the next quarter. The next generation testing system will have increased stroking speeds and more capability for adjusting data for off-sets.

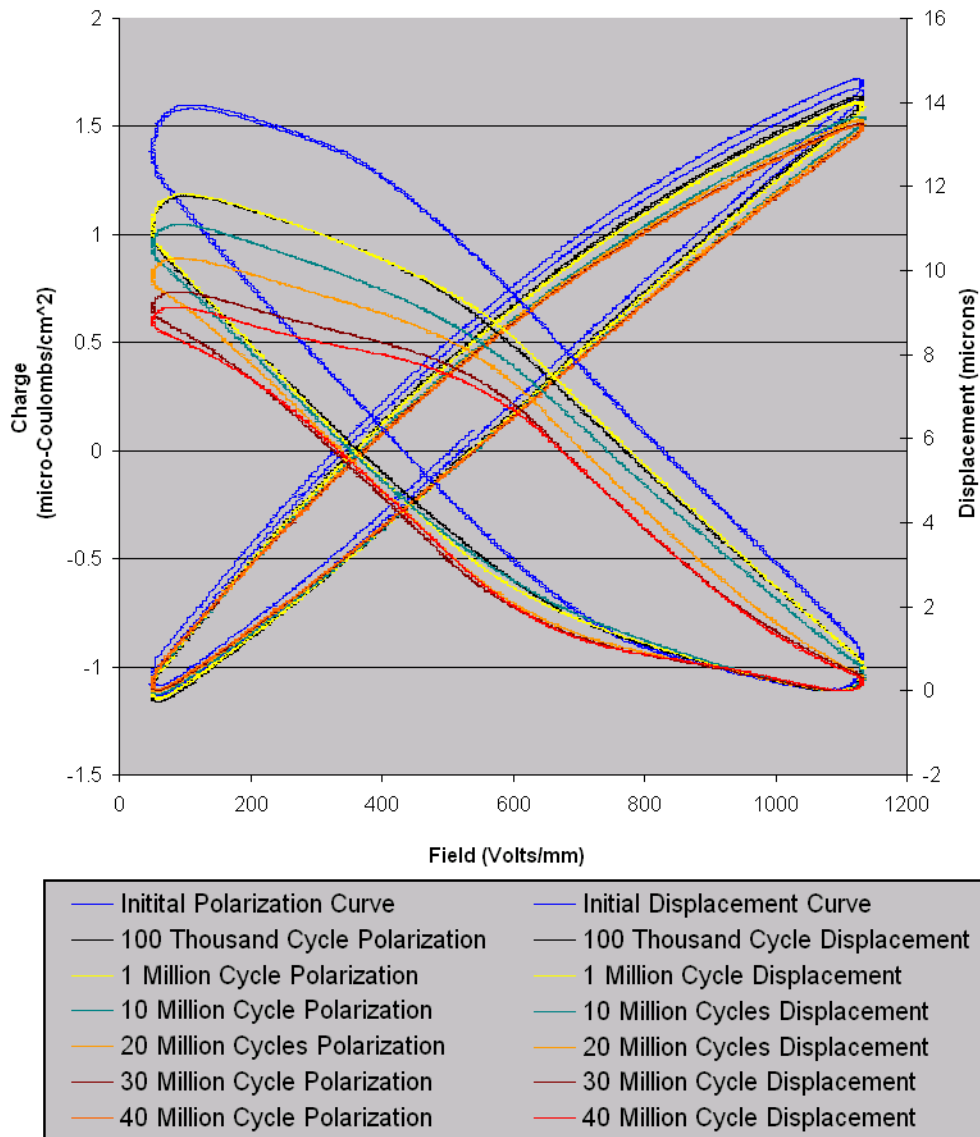


Figure 6: Polarization and displacement curves for the first 40 million cycles of the EDO PZT actuator.

Status of Milestones

1). Fabricate and characterize several multilayer PZT stacks using low temperature sintered PZT materials.

Status: This task has been started. Results will be presented in the next quarterly report

2). Fabricate a test fixture for stroking the multilayer PZT parts.

Status: This task is complete. Testing is now underway with the test system.

3). Make PZT powders with a nano-additive and characterize sintered discs for electromechanical and strength measurements.

Status: This milestone is complete; however additional data is being compiled. Additional PZT materials with nano-alumina addition have been prepared. Discs will be pressed, sintered, and tested during the next reporting period.

Low-Cost Manufacturing Processes for Ceramic and Cermet Diesel Engine Components

D. E. Wittmer
Southern Illinois University

Objective/Scope

The purpose of this work is to investigate the potential of low-cost manufacturing processes for ceramic and cermet diesel engine components. The primary task is to develop cost effective processing, forming and sintering methodologies for cermet and ceramic formulations, used by industrial diesel engine manufacturers.

Technical Highlights

Task 1. Collaboration with industrial partner(s).

This task involves the collaboration with industrial partners to assist them in processing and sintering of their diesel engine components. Our goal is to provide assistance in processing and sintering which may result in a reduction in surface reactions and part warping. Moreover, this may also provide an alternative sintering process that will allow improved throughput efficiency and manufacturing economy. Due to the proprietary nature of this task, any research data generated from this task is normally controlled by the terms of each specific confidentiality agreement. The reporting of this data and any results are the responsibility of the industrial partner(s).

During this reporting period a die was designed in order for us to produce a near-net shape injector plunger. Our goal is to prove to potential industrial partners that we have the capability of producing a prototype plunger of complex geometry by low-pressure injection molding. The die is currently being machined and is expected to be ready for injection trials during the next reporting period.

Task 2. Cost Effective Processing and Sintering

This task was completed and reported in previous quarterly report.

Task 3. Economic Comparison of Materials and Processing of Cermets for Use as Diesel Engine Components

This task involves the development of an economic model for comparing both materials and processing methods for cermets targeted for use as diesel engine components. The cermet is a combination of an intermetallic and TiC where the intermetallic can be nickel aluminide, chrome aluminide, nickel chromium. Modification of these intermetallics may be necessary to obtain the properties desired.

This task was completed during this reporting period. It is believed that with higher sintering rates, cermets can be manufactured to be competitive or lower cost than ceramics for these applications. The advantages of the cermets over the ceramics are:

- Lower sintering temperature
- Potentially faster sintering cycle
- Can be machined by EDM

The intermetallic phase of the cermet is available as an alloy or as independent metals or metallic compounds that can be reaction sintered to form similar alloys. The advantage of the reaction sintering is a reduced cost of the raw materials and the ability to produce finer grain structure in the finished cermet. Currently the powders used for reaction sintering are comparable with high-purity ceramics.

Task 4. Effect of High Heating Rates on Sintering of Cermets

This is a new task that was initiated during this reporting period. The goal is to evaluate the use of very high heating rates on the densification of selected intermetallic bonded-TiC cermets. During this reporting period reaction sintered 50% Ni₃Al-50% TiC was injection molded into test rods for the sintering trials. During the next reporting period, sintering rates of up to 750°C/min will be investigated. If extremely high heating rates can be used to sinter these cermets, it offers the opportunity to even further reduce the manufacturing cost.

Status of Milestones

Collaboration with Industrial Partners	On Schedule
Cost Effective Processing and Sintering of Diesel Engine Components	Completed
Economic Comparison	Completed
Effect of high heating rates	On Schedule

Communications/Visits/Travel

D. E. Wittmer met with Terry Tiegs for discussions on technical progress.

Problems Encountered

None

Publications and Presentations

“Low Pressure Injection Molding of Intermetallic-TiC Cermets,” Jeffrey Hazelwood, Dale E. Wittmer, and Joshua Steffen, SIUC, and Terry N. Tiegs, ORNL, poster presentation at PM2TEC 2003, Las Vegas, NV, June 8-12, 2003, received Poster of Merit Award.

Intermetallic-Bonded Cermets

P. F. Becher and S. B. Waters
Oak Ridge National Laboratory

Objective/Scope

The goal of this task is to develop materials for diesel engine applications, specifically for fuel delivery systems and wear components (e.g., valve seats and turbocharger components). This will require materials that have a minimum hardness of 11 GPa and a thermal expansion coefficient of between 10 to 15 x 10⁻⁶/°C. The material should also have excellent corrosion resistance in a diesel engine environment, flexure strength in excess of 700 MPa, and fracture toughness greater than 10 MPa√m to ensure long-term reliability. The material should also be compatible with steels and not cause excessive wear of the steel counter face. The upper temperature limit for fuel delivery systems applications is 200°C, and for the other wear applications, the limit is 815°C. Finally, the total material processing costs for these advanced materials should be competitive with competing technologies such as TiN or other ceramic coatings on high-speed tool steels.

Technical Highlights

A number of metering plungers of TiC-50 vol. % Ni₃Al were machined to specifications for insertion into a high pressure (> 315 MPa) fuel injection test. During preparation, the starting rods are machined to profile, a steel end cap is added by press fitting, and, finally, the end cap is machined to specifications. Four of these plungers were received for failure analysis and are shown in Figure 1: C10-3 & C10-7 (both failed during machining of press fit steel end cap), C10 (failed in 20-h overpressure test), C8-5 successfully completed the 20-h overpressure test.

Plungers C10-7 failed during the machining of steel end cap in the upper section near the steel end cap, Figure 2. The fracture origin was traced back to surface or near surface; however, a large chip was missing from this area making it impossible to identify a specific origin of failure. Plunger C10-3 also failed during machining of steel end cap in the upper section near end cap, Figure 3. It had been suggested that the laser scribing of the identifying numbers might have been the source of larger defects that caused failure. However, it appears that failure originated from the surface of the plunger nearly 180 degrees around the circumference from the scribed numbers, Figure 3. The fracture markings were traced to the region at or just below the machined surface, but no unusual defects or features could be identified. On the other hand two areas along the fracture surface-machined surface edge were noted, Figure 4, which might be thought to be the origins of fracture. However, the appearance of these two depressions in the edge suggest they might be the result of impacts, which could have occurred when the plungers failed during the grinding operation. These areas exhibit features similar to those associated the plastic deformation induced by indentation. Impact type damage was also indicated on C10-7 in the region of the large chip-out at the failure origin. Multiple cracks were observed on the machined surface and the fracture surface adjacent to the chip-out, Figure 5.

Finally, several pores (some with diameters ≥ 50 microns) and a large “linear” defect were observed on the fracture surfaces, Figures 3 and 5. Such defects would not be desirable for achieving the high strengths typically obtained with these cermets.

Plunger C10: Failed in the overpressure test. Observations reveal that failure first occurred in the upper section near the end cap, Figure 6. The overpressure test obviously continued as the cermet faces at this fracture made repeated contact causing considerable debris. In addition, the steel end cap bears evidence of considerable damage to its surfaces. The second fracture must have occurred at the very end of the test as these fracture faces show no evidence of damage. This fracture originated from the machined surface region, but no obvious defects were found. One might suspect that the stress configuration was fairly complex due to misalignment of the plunger by the action of the broken upper section.

Status of Milestones

On Schedule

Communication/Visits/Travel

None

Publications

E. Rocha-Rangel, P. F. Becher and E. Lara-Curzio, "Influence of Carbon on the Interfacial Contact Angle Between Alumina and Liquid Aluminum," *Surface and Interface Analysis*, 35: 151-155, (2003). .

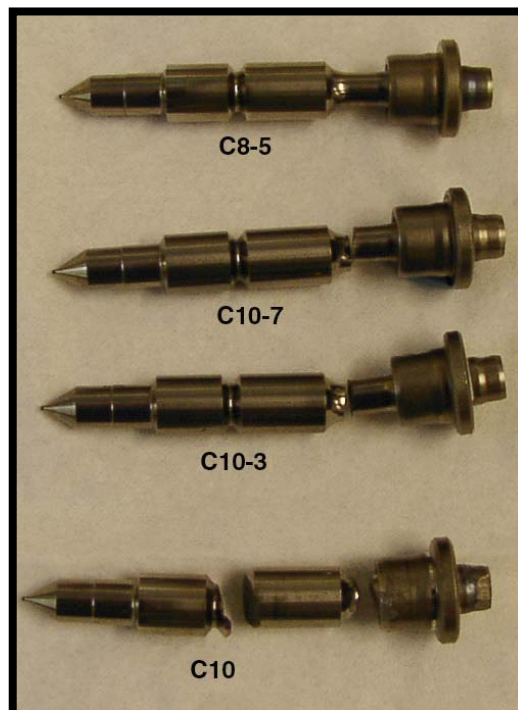


Figure 1. TiC-Ni₃Al cermet plungers.

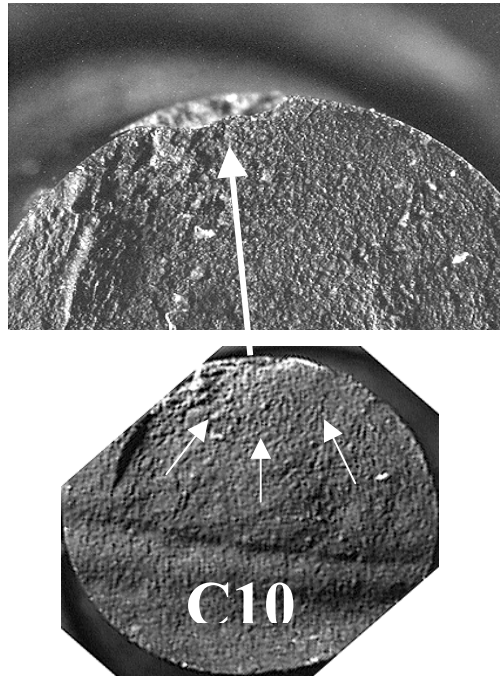


Figure 2. C10-7 fractured during machining of steel cap appear to originate in the cermet surface region, however, fracture origin is obscured by large missing chip.

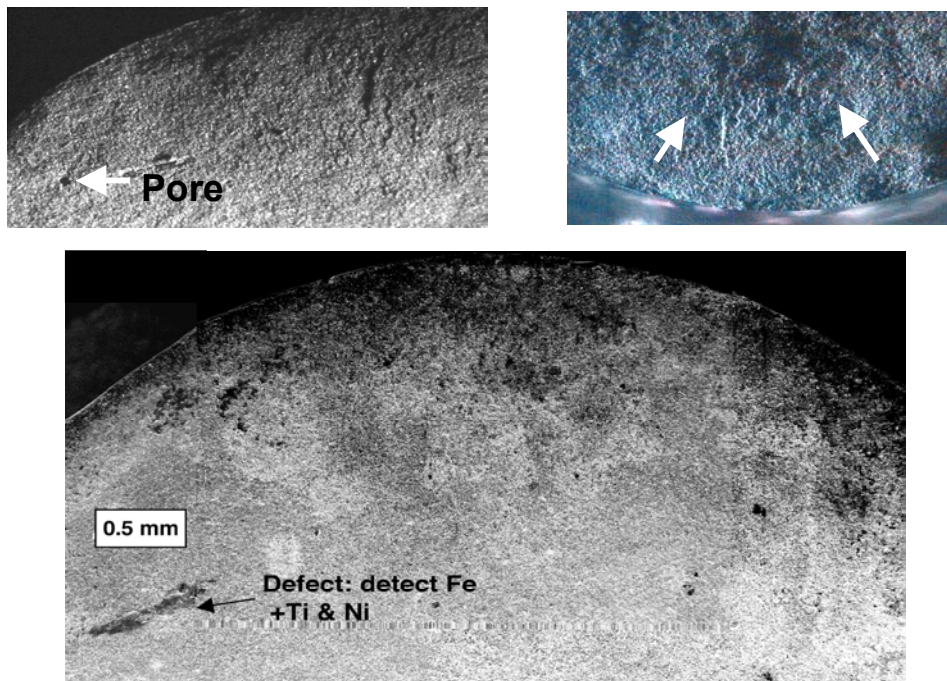


Figure 3. C10-3: Pores and defects found on fracture surface but not at surface fracture origin. Sample appears to have been damaged when failed during machining of end cap (I.e., scars on fracture surface and evidence of impacts at edge of fracture surface). Not clear if ones in fracture origin region occurred before or after fracture. Failure origin is not located near laser scribed numbers.

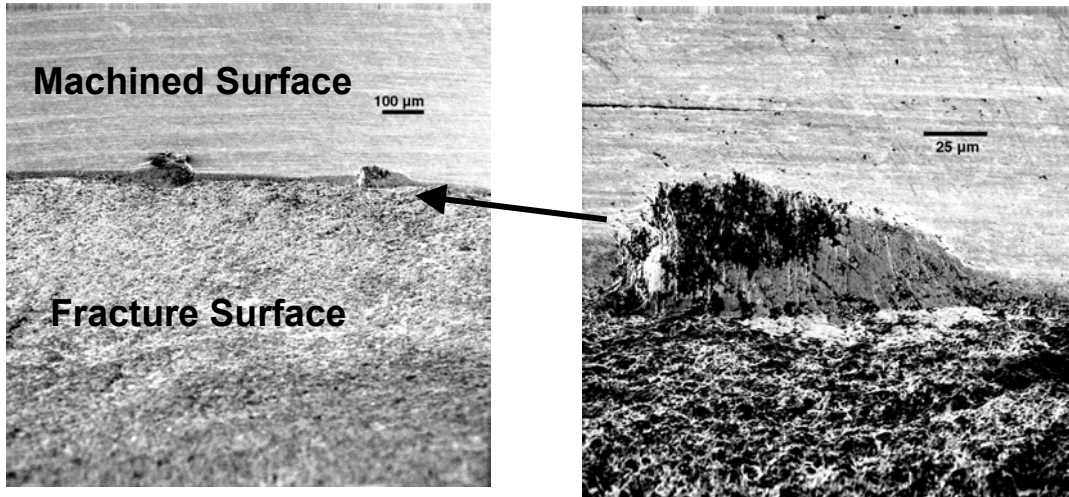
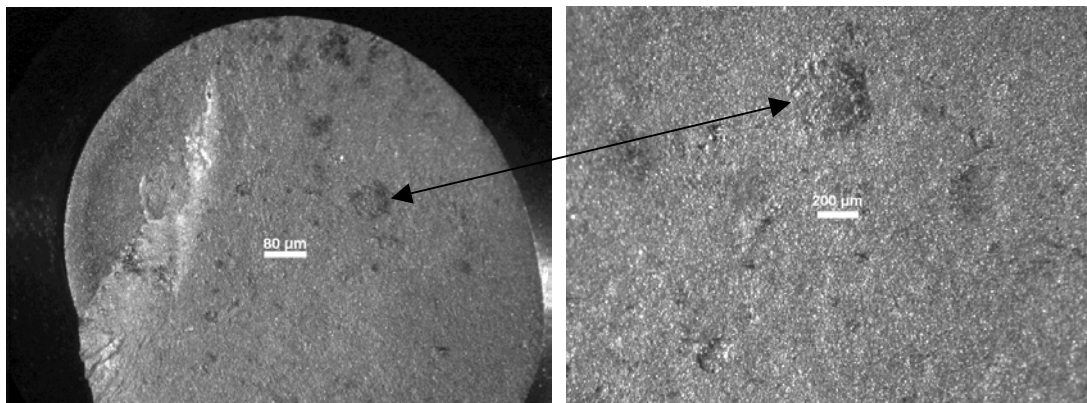
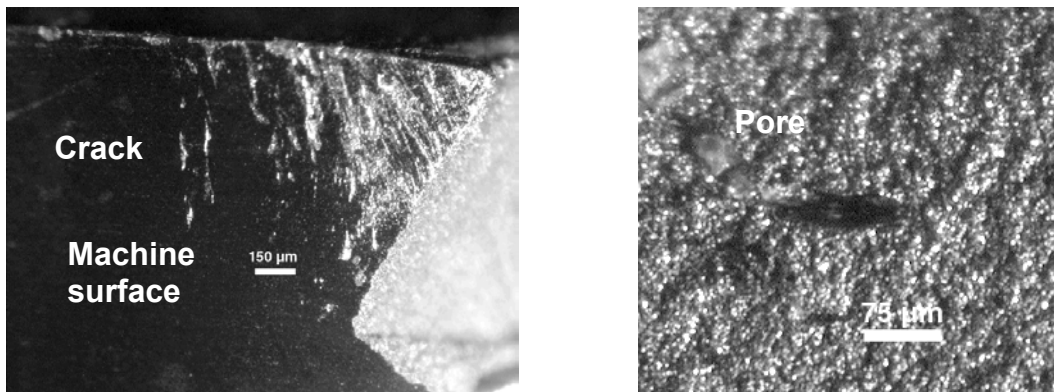


Figure 4. Fracture-machined surface edge in fracture origin region of C10-3. Appearance of depressions along edge suggest possible impact events as smooth areas reminiscent of indent impression are combined with fractured regions.



C-10 fracture surface in lower section



C10-7

Figure 5. Defects and damage observed in C-10 (failed in overpressure test) and C10-7 (failed during machining of steel end cap). As with C10-3, large defects were observed on fracture surfaces in the form of defects resembling flattened and lenticular pores.

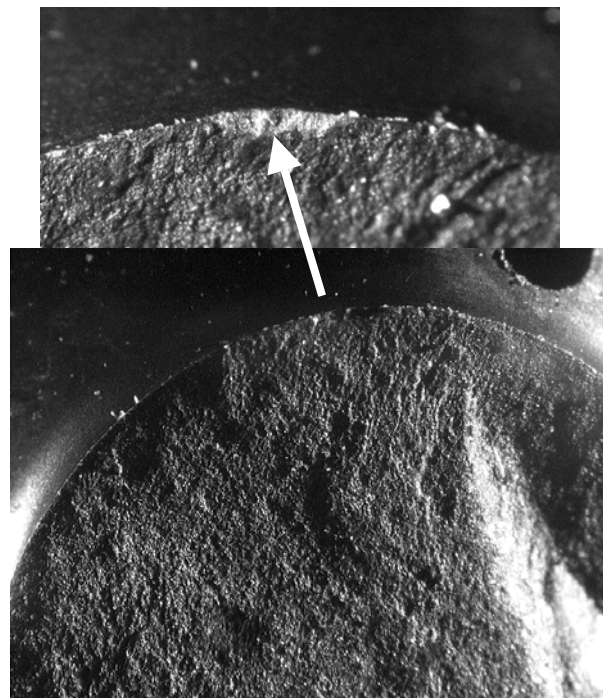
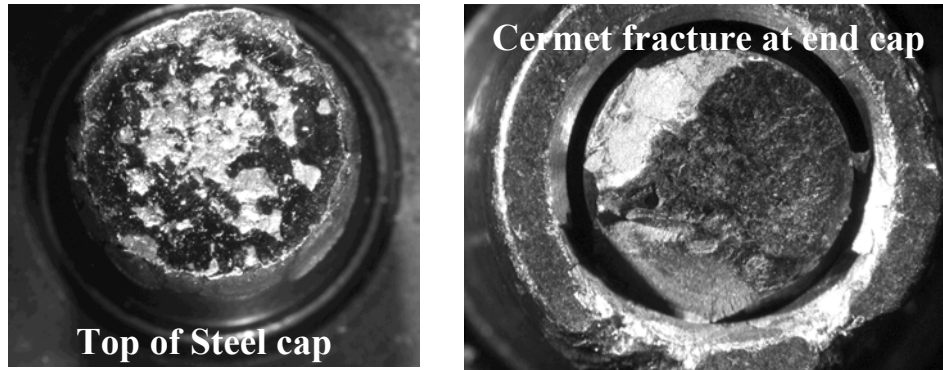


Figure 6. Plunger C10 failed during overpressure injector test. Observations indicate that the plunger first failed in the region near the steel end cap. This is concluded as both the steel cap and the cermet fracture surface suffered repeated impacts after fracture and extensive damage, upper images. As a result, the source/cause of failure cannot be determined. The fracture in the lower section of the plunger originated at the surface (lower images). This failure appears to have occurred at or extremely close to the point the test shut down, as there is no obvious damage to lower fracture surfaces indicating it was not subjected to cycling after fracture.

Low Cost-High Toughness Ceramics

T. N. Tiegs, F. C. Montgomery, and P. A. Menchhofer
Oak Ridge National Laboratory

Objective/Scope

Significant improvement in the reliability of structural ceramics for advanced diesel engine applications could be attained if the critical fracture toughness (K_{Ic}) were increased without strength degradation. Currently, the project is examining toughening of ceramics by incorporation of ductile intermetallic phases.

Technical Highlights

Previous studies have shown that the properties of the aluminide-bonded ceramics are attractive for diesel engine applications and consequently, development of these materials was started. At the present time, TiC-based composites with 40-60 vol % Ni_3Al are being developed because they have expansion characteristics very close to those for steel. Previously, the general property envelope has been studied and the compositions refined. Further processing studies are needed to examine lot-to-lot variation using statistically designed experiments, determine compaction behavior, assess dimensional control during sintering, identify suitable binders which will not add carbon ash during sintering, and develop a viable and cost-effective source of NiAl powder. The development effort is being done in collaboration with CoorsTek, Inc.

Alternate Precursors for Ni_3Al Formation - All previous work used a combination of Ni and NiAl for an in-situ reaction to form the Ni_3Al . Because the costs of the starting raw materials can be a significant fraction of the total cost of a component, alternative materials for fabricating the cermet are of interest. Ni and Al powders are produced in sufficient quantities to be relatively cost-effective and so tests were done to maximize their usage in the composites. Several different metal powder combinations were examined including: NiAl+Ni; Al-30 Ni+ Ni; NiAl+Ni+Al; and Ni+Al. Sintering behavior was acceptable for compositions utilizing Ni-Al precursors. When elemental Al was used the samples exhibited macroscopic cracking due to differential heating and shrinkage resulting from the exothermic reaction between the Ni and Al.

The two compositions that did not crack (i.e., the NiAl+Ni and the Al-30 Ni+ Ni) were examined in greater detail for mechanical properties and microstructures. The results on the fracture strength, toughness and hardness are summarized in Figs. 1, 2, and 3, respectively. As shown, the strength measurements for the sample made by the reaction of Al-30 Ni (catalyst precursor) and Ni were very poor strength in comparison to the other composite. Examination of the microstructures revealed no unusual features than normally observed in these types of composites (Figs. 4 and 5). While the TiC grains were larger for the sample made by the reaction of Al-30 Ni (catalyst precursor) and Ni, the sizes of the grains in the sample were not sufficiently large to be the main factor for the low observed strength. The fracture toughnesses were excellent for both of the composite compositions made with either NiAl or Al-30 Ni precursors. The main toughening mechanism in these composites is plastic deformation by the Ni_3Al binder phase and evidently it is effective for both composites. The hardness for the Al-30

Ni composite was lower than for the composite with NiAl. This is most likely due to the larger grain sizes and presence of a second phase in those materials.

Further examination of the samples at lower magnification revealed a significant amount of a second phase within the composite made with the Al-30 Ni (catalyst precursor) as shown in Figs 6 and 7. X-ray diffraction could not identify any other phases besides the TiC and Ni₃Al typically observed in these materials (Figs. 8 and 9).

Status of Milestones

On schedule.

Communications/Visits/Travel

Travel by T. N. Tiegs to Las Vegas, NV June 9-12, 2003 to present paper on ‘Effect of Ni-Al Precursor Type on Sintering and Properties of TiC-Ni₃Al Composites.’

Problems Encountered

None.

Publications

T. N. Tiegs, F. C. Montgomery, and P. A. Menchhofer, “Effect of Ni-Al Precursor Type on Sintering and Properties of TiC-Ni₃Al Composites,” to be published in Proceedings of International Conference on Powder Metallurgy and Particulate Materials, Las Vegas, NV, June 2003.

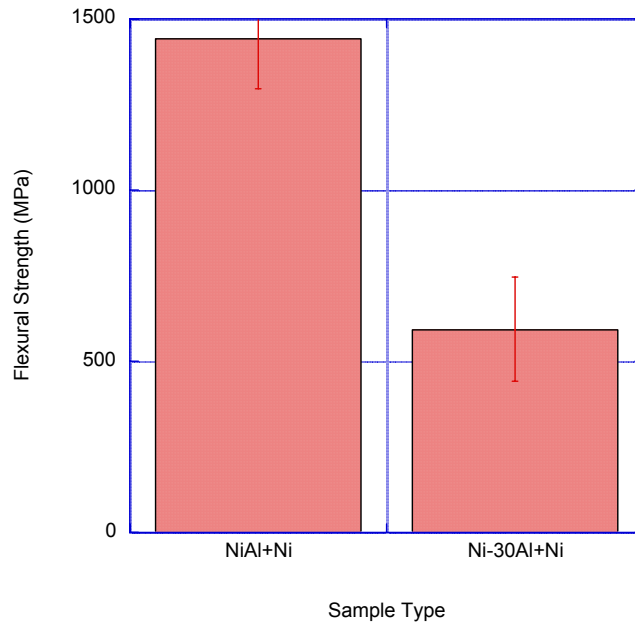


Fig. 1. Results on fracture strength of composites made with either NiAl+Ni or Al-30 Ni+Ni.

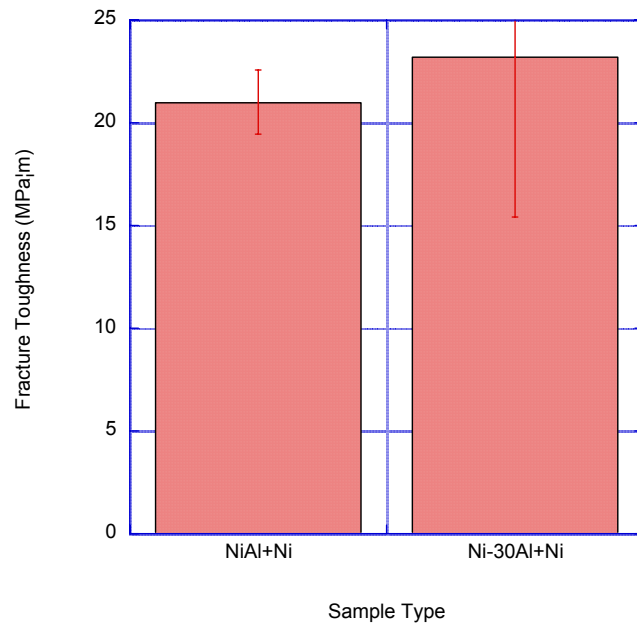


Fig. 2. Results on fracture toughness of composites made with either NiAl+Ni or Al-30 Ni+Ni.

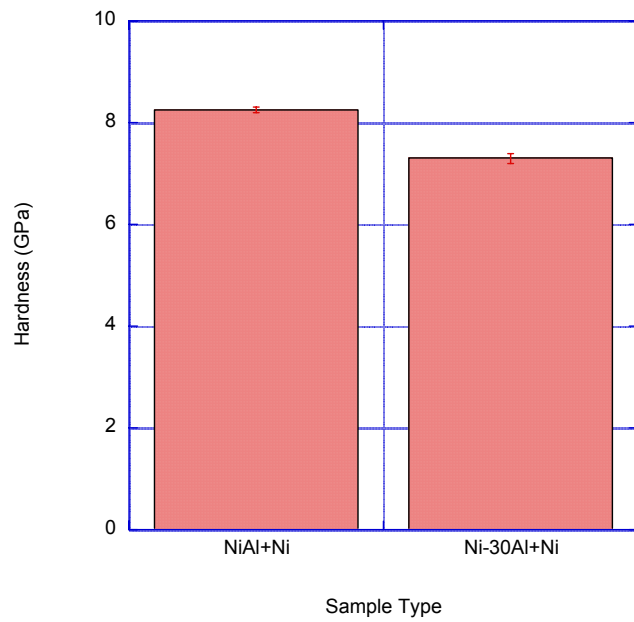


Fig. 3. Results on hardness of composites made with either NiAl+Ni or Al-30 Ni+Ni.

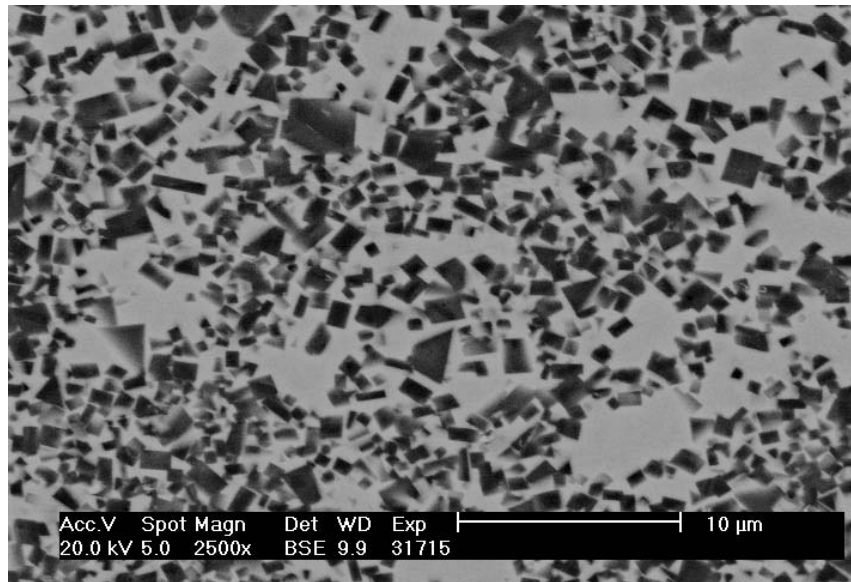


Fig. 4. Microstructure of sample made with NiAl+Ni showing fine TiC grains in Ni₃Al matrix.

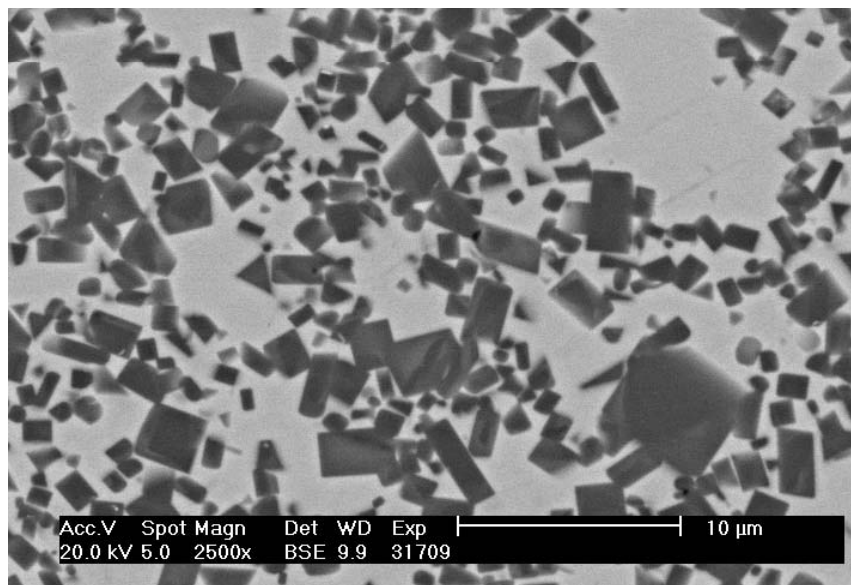


Fig. 5. Microstructure of sample made with Al-30 Ni+Ni showing large TiC grains in Ni₃Al matrix.

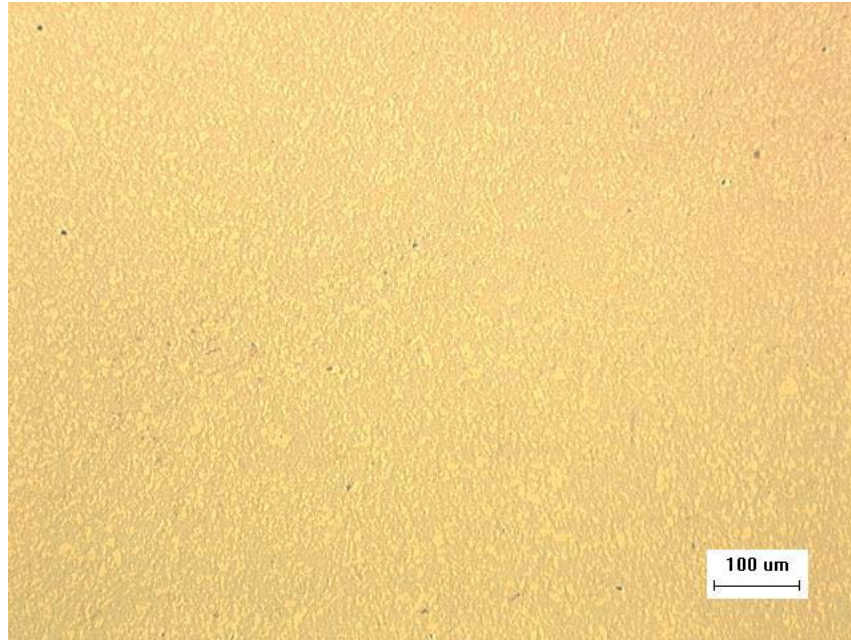


Fig.6. Microstructure of sample made with NiAl+Ni showing uniform distribution of TiC grains in Ni₃Al matrix and no secondary phases.

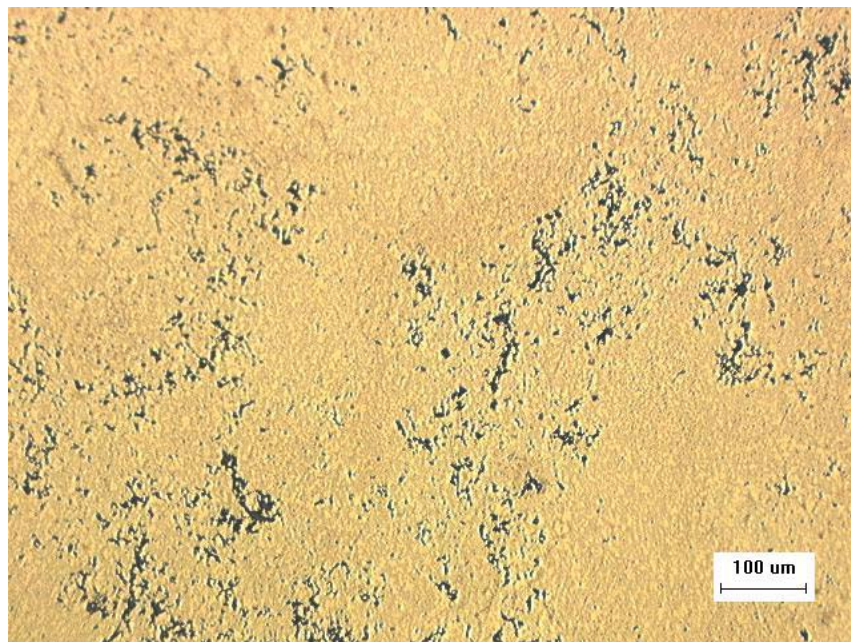


Fig.7. Microstructure of sample made with Al-30 Ni+Ni showing a second phase (black spots) distributed within the TiC and Ni₃Al.

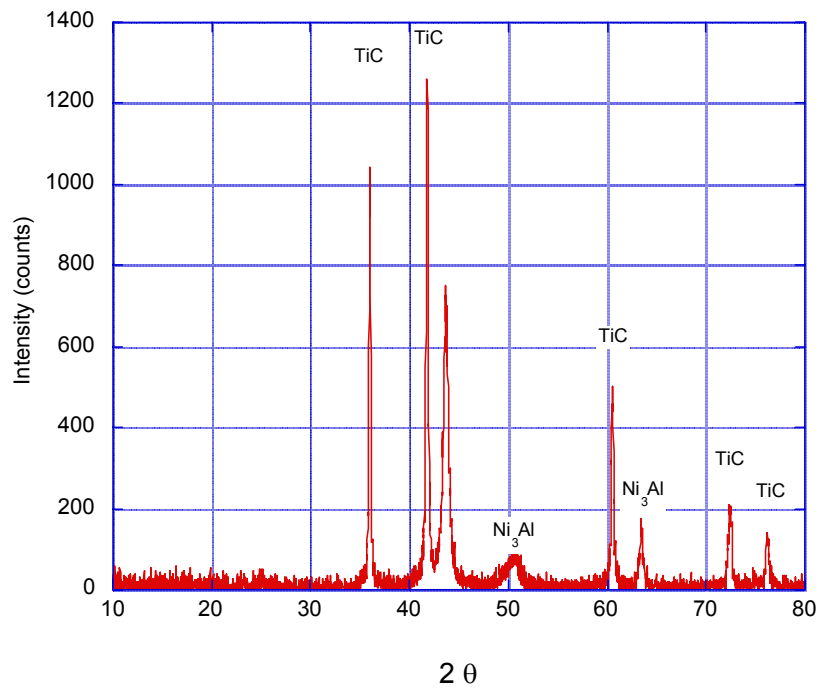


Fig. 8. X-ray diffraction scan of the composite made with NiAl+Ni.

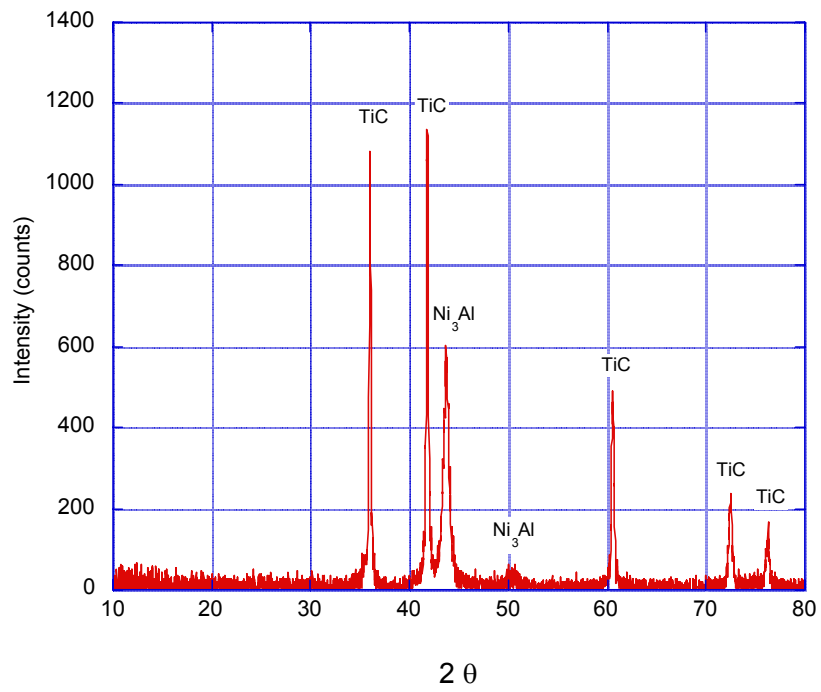


Fig. 9. X-ray diffraction scan of the composite made with Al-30 Ni+Ni .

Materials for Exhaust Aftertreatment

Paul W. Park, Alexander G. Panov, and Craig F. Habeger
Caterpillar Inc.

Objective/Scope

The objective of this effort is to develop and evaluate materials that will be utilized in aftertreatment systems for diesel engines. These materials include catalysts for NO_x abatement, filtration media for particulate abatement, and materials to improve NO_x sensing capabilities in the exhaust system. This project is part of a Caterpillar strategy to meet EPA requirements for regulated emissions in 2007 and beyond. This year's focus is on the durability of NO_x catalysts developed for lean burn applications in the presence of sulfur, evaluation of filtration properties of sintered metal media for application in diesel particulate filters (DPF), and evaluation of current NO_x sensor technologies while developing materials to improve sensing capabilities.

Technical Highlights

Lean-NO_x. The effect of various alcohols (ethanol, propanol, butanol, hexanol, octanol) on the performance of lean-NO_x catalysts (Ag/Al₂O₃, Cu- and Fe-ZSM5) has been examined using a powder bench system. The results showed that ethanol had the highest NO_x reduction among the tested alcohols (90% NO_x conversion, 350-400°C, 30,000h⁻¹). The high hydrocarbon chain alcohols, which may be more feasible for real applications than ethanol, also showed promising NO_x conversion (60-70%) at low temperatures (300-375°C). The relationship between catalyst formulation and reductant species will be investigated to achieve higher NO_x conversion.

The installation of the Xytel multi-reactor catalyst test bench system has been completed. This multi-reactor system will allow high throughput screening of catalyst materials in both powder and washcoated-core samples for various catalyst aftertreatment technologies including oxidation, ammonia-SCR, Lean-NO_x and NO_x-trap.

PM Trap. The goal for this quarter was to select the materials for a catalyzed deep-bed particulate filter and begin the development of the test protocols for evaluation of the catalyzed DPFs. The filtration properties of the sintered powder metal filters were evaluated with a diesel fuel burner. A set of samples prepared by tape casting and three samples from outside suppliers were evaluated. The deep bed and surface filtration efficiency of sintered powder metal and SiC filtration media (obtained from suppliers) will be evaluated. Development of the test protocol for evaluation of catalyzed DPFs has started. A diesel burner is used for deposition of soot on the catalyzed filter samples and the rate of soot oxidation is later tested with a flow catalytic reaction system.

NO_x Sensor. This past quarter, the test bench was debugged. The software appears to be functioning properly as well as the remainder of the controls. We have three sensors from outside parties to evaluate. The first sensor, based on the mixed potential measurement technique, had a major leak through the electrical connections and made evaluation difficult to perform. This sensor will be evaluated further after sealing the electrical connections. The second sensor, based on potentiometric measurement using a sodium ion conductor, was much easier to evaluate. However the sensor had poor measurement capabilities at 150°C that

degraded as the temperature was taken to 300°C. Initial evaluation was performed using NO or NO₂ in He to determine if the sensor would detect NO_x in a simple gas mixture. The simple gas mixture also reduces the complication of measuring other gas species due to cross sensitivity of the electrodes. This sensor will be evaluated further to determine the minimum amount of O₂ that is required for the electrode reaction to proceed and therefore detect the gas species. However a finite concentration of O₂ in the exhaust mixture may be a problem when trying to measure NO_x absorber performance, particularly during regeneration. The third sensor is expected to be evaluated during the next quarter.

Future Plans

- (1) Continue to characterize silver catalysts.
- (2) Improve catalyst durability.
- (3) Prepare catalyzed filters based on SiC and Sintered Powder Metal filtration media.
- (4) Complete modification of burner bench to accommodate catalyzed DPF testing.
- (5) Evaluate NO_x sensors.
- (6) Continue the interaction with sensor developers to meet heavy-duty diesel needs.

Travel

None.

Status of FY 2003 Milestones

- 1) *Catalyst Durability*: Improve catalyst durability for sulfur poisoning (in progress)
- 2) *Washcoat Technology*: Develop a controlled catalyst coating technique in order to fully demonstrate selected catalyst chemistries on a full size honeycomb monolith (in progress)

Publications

None

Development of NO_x Sensors for Heavy Vehicle Applications

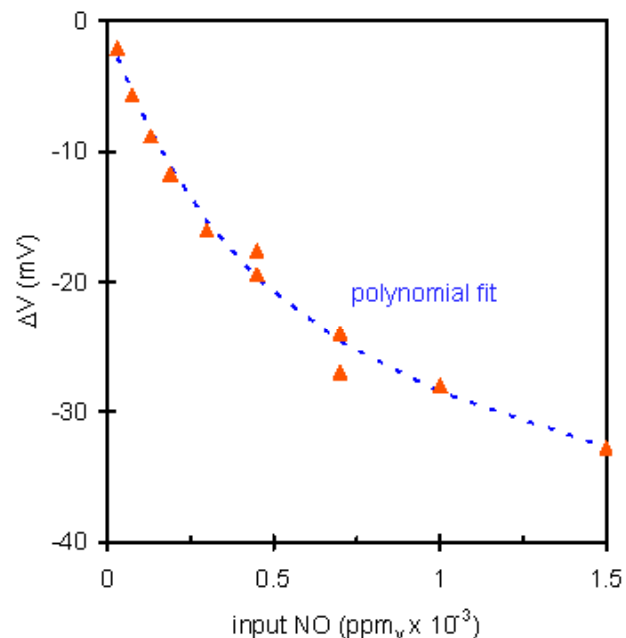
Timothy R. Armstrong, David L. West, Fred C. Montgomery
Oak Ridge National Laboratory
(CRADA No. ORNL 01-0627
with Ford Motor Company)

Objective

The proposed project seeks to develop technologies and materials that will facilitate the development of NO_x and ammonia sensors. The development of low-cost, simple NO_x will facilitate the development of ultra-low NO_x emission engines, directly supporting the OHVT goals.

Technical Highlights

1. During this quarter ORNL demonstrated that a larger sensor output signal could be achieved by replacing the Pt electrodes with an electrically conducting oxide such as lanthanum chromite. In some cases an improvement in the output signal of 50% was achieved.
2. The goal of this reporting period was to flush out the effects of an applied bias on sensor performance, determine the effects of current and voltage biases, bias strength, and electrode design for biasing.
3. The results of tests to determine whether the sensor should be current or voltage biased clearly indicate that optimal signal outputs for both NO and NO₂ were achieved with a current bias greater than 100 mA.
4. A variety of sensor designs for biasing were evaluated. In the end the optimal results were achieved when the bias current was applied between the sensing and working electrode.
5. A sensor operating with an applied current bias as developed at ORNL is a "Total NO_x Sensor" and will accurately measure the total NO_x (NO and NO₂) concentration in a gas stream. The dependence of the ORNL sensor on the NO_x concentration has been measured from 1 to 1500 ppm and found to have a logarithmic dependence on NO_x concentration (see Figure).
6. The data presented in the figure is the first ever reporting of an operational total NO_x sensor build around a mixed potential design.
7. During this quarter ORNL also was developed a super mixed potential sensor in which the working electrode and reference electrode are oppositely biased. It is currently under construction but anticipated to give larger more reliable outputs than previously observed.



Status of Milestones

Although this project had a late kick-off, we are ahead of schedule of most of the milestones:

1. Modify current sensor test stand for operation at 800°C (delayed at request of Ford)
2. Test NGK sensor in modified test stand (delayed at request of Ford)
3. Deliver NO_x catalyst assessment and program plan to Ford (completed 6/2002)
4. Construct NO_x electrode test stand. (Completed 12/2003)
5. Deliver report on initial test results (Completed 2/2003)
6. Design and procure screens for simplified NO_x sensor design. (Completed 12/2003)
7. Produce first simplified NO_x sensors for testing (delayed until December 2003).

Communications/Visits/Travel

1. A quarterly report will be delivered to Ford in July 2003.

Problems Encountered

None to date.

Publications

1. Electronically Conducting Oxides as Replacements for Noble Metals in Mixed-potential, Electro-ceramic Gas Sensors, submitted J. of Gas Sensors.

Intellectual Property Filed

1. Use of Electronically Conductive Oxides as Replacements for Noble Metals in High-Temperature Gas Sensors.
2. NO_x sensor with oppositely biased electrodes for enhanced signal output.

Ultra-High Resolution Electron Microscopy for Characterization of Catalyst Microstructures and De-activation Mechanisms

L. F. Allard, D. A. Blom, C.K. Narula and T. A. Nolan
Oak Ridge National Laboratory

Objective/Scope

The objective of the research is to develop and utilize new capabilities and techniques for ultra-high resolution transmission electron microscopy (UHR-TEM) to characterize the microstructures of catalytic materials of interest for reduction of NO_x emissions in diesel and automotive exhaust systems. The research is focused on understanding the effects of reaction conditions on the changes in morphology of heavy metal species on “real” catalyst support materials (typically oxides). These changes are being studied utilizing samples treated in both static bench reactors and a special ex-situ catalyst reactor system especially constructed to allow appropriate control of the reaction.

Technical Progress

We report here on the current status of the new EERE-funded Aberration-Corrected Electron Microscope (ACEM) project, and the Advanced Materials Characterization Laboratory being constructed adjacent to the HTML to provide the special quiet environment required for proper operation of the instrument.

The primary research thrust of the ACEM is to provide the capability for sub-angstrom (-Å) imaging to permit characterization of the structure of atomically dispersed heavy metals and metal clusters on catalyst supports. The ACEM is a combination transmission electron microscope (TEM) with scanning transmission (STEM) capabilities. The basic instrument, designated the 2200FS-AC, is being manufactured by JEOL Ltd., of Akishima, Japan. The sub-Å imaging will be realized primarily through the technique of “high-angle annular dark-field imaging,” which is provided by the STEM imaging capability of the instrument. The aberration corrector, a device which is being constructed by the CEOS Co. (Corrected Electron Optical Systems) of Heidelberg, Germany, is being placed in the illuminating system of the ACEM, to allow an improvement of the diameter of the focused probe from an uncorrected 0.14 nm down to a corrected 0.07 nm. Halving the probe diameter (at the same incident beam intensity) actually has the effect of improving the signal-to-noise (or contrast) by a factor of nearly 10 times. This is the biggest advantage of the inclusion of an aberration corrector in the new generation of electron microscopes, since it allows the formation of images with much shorter scan times (say 4s), or images with much higher resolution in standard scan times (say 40s). Figure 1 is a rendering of the expected appearance of the new ACEM, showing the position of the aberration corrector, and also an “in-column” energy filter that will allow the identification of chemical species and chemical bonding at the level of single atomic columns in a crystal structure. Figure 2 shows calculated probe profiles for 0.14 nm and 0.07 nm resolutions, illustrating the improvement in contrast expected for the aberration-corrected instrument. Early results on Pt/Al₂O₃ catalysts studied using a dedicated STEM instrument retrofitted with an

aberration corrector (the Vacuum Generators HB603U instrument in ORNL's Condensed Matter Sciences Division, Dr. Stephen Pennycook's group) have shown clearly the presence of Pt "trimers," or single atoms in triangular arrays distributed over the alumina surface, that are suspected to be the primary sites for reactions to occur. The ability to characterize catalyst structures "as-prepared" that have atomic dispersions will be a major jump in capability provided by the ACEM, since no instrument in an EERE laboratory in the country can make such images today.

As part of the ACEM project, JEOL has placed another 200 kV field emission electron microscope on consignment to the HTML: the 2010F TEM-STEM. With an ultra-high resolution objective lens pole piece, this instrument provides us with annular DF imaging at the 0.14 nm level (to make images roughly equivalent to Fig 2(a), and conventional bright-field TEM imaging of 0.19 nm. This instrument is being used to give the HTML staff experience in operation of a TEM-STEM so that our learning curve when the ACEM arrives will be much steeper. A special benefit will be to let us learn how best to operate between conventional TEM imaging and STEM imaging, since there are expected to be alignment issues between the two operating modes that will require a certain degree of operator skill, along with computer control capabilities that we hope to develop.

The ACEM will only be able to achieve its specified resolution if it is not degraded by the local environment. Such scanning instruments are influenced by environmental effects such as magnetic fields, air flow, temperature fluctuations, air pressure changes, microphonics and floor vibrations. For example, magnetic fields must be below 0.05 mG at 60 hz, temperature must be constant at better than 0.2°C/h, floor vibrations lower than 3 nm peak-to-peak in any direction, and air flow less than 5 cm/sec in a horizontal plane. All of these conditions are expected to be met by the design features of the AMCL (Figs. 3 and 4). This new lab features a "house-in-house" construction philosophy, where the instruments are housed within rooms with concrete masonry walls and concrete panel ceilings, that are in turn totally enclosed by the external shell of the building that also has concrete masonry walls and roof panels. Since the building shell is air conditioned, the instrument room temperatures, once equilibrated, will have little external influence, and so should be relatively easy to maintain at a constant level. A second major feature of the AMCL is the concept of a "control room" for each instrument. Since the new ACEM will be totally computer controlled (in fact, it does not have the standard fluorescent screen and binocular arrangement of standard TEMs), the operator(s) will sit in an adjacent room to operate the instrument, eliminating the influence of the operator on the instrument environment. This will also permit the instrument to be operated essentially from anywhere in the world just as easily as it can from the AMCL control room, and thus will be a major benefit to our national user program.

Finally, the schedule for both completion of the AMCL and delivery of the ACEM have been coordinated, so that the building will be ready when the instrument is delivered. Construction is expected to be complete to allow beneficial occupation of the lab by March 15, 2004. A 1-2 month period of commissioning is expected to suffice to "shake down" any problems in the

building, with the instrument delivery now planned for May 1, 2004. The basic ACEM without corrector will be tested by HTML staff at the factory in mid-January, and final tests of the corrected instrument are expected to be conducted by HTML staff in mid-March. Results of these tests will be reported in subsequent quarterlies.

Status of Milestones

The ex-situ catalyst reactor gas delivery system has undergone a complete re-design, to allow more functional control of simulated diesel and automotive exhaust compositions for TEM studies of a variety of catalytic materials. Also, Dr. Narula's new catalyst preparation laboratory is under development, to provide the capability for preparation of new experimental catalysts for NO_x traps and NO_x reduction catalyst development. First production and characterization of ceria-zirconia-lanthana mixtures on BaO-Al₂O₃ supports for trapping applications, with Ford Research Laboratory, will be reported in the next quarterly.

Communications/Visits/Travel

1. JEOL USA, Peabody, MA: Discussions of status of the ACEM project and installation issues for the 2010F TEM-STEM consignment instrument.

Publications

None this period.

References



Fig. 1. Artist's rendering of the JEOL 2200FS-AC "ACEM," showing location of aberration corrector

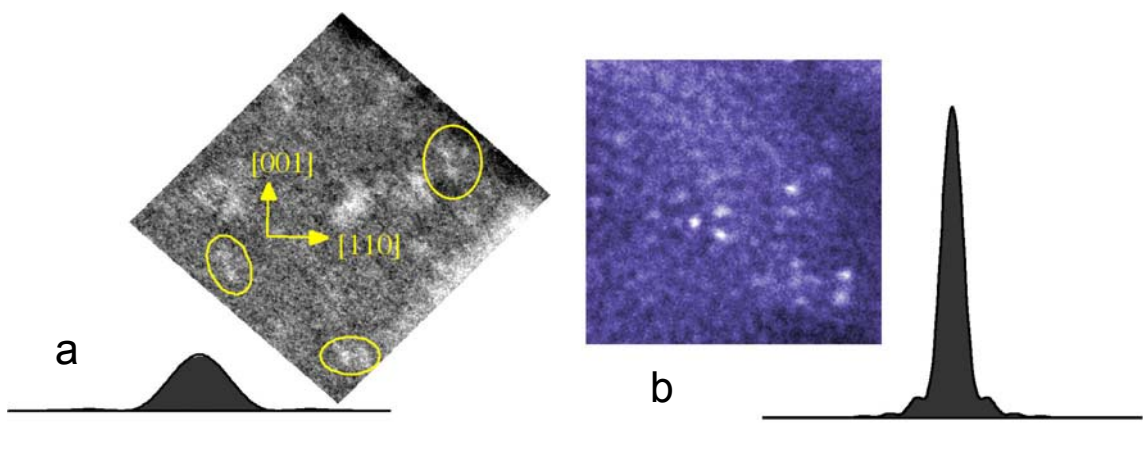


Fig. 2(a). Profile of 1.4 Å probe, with image of Pt atoms on alumina support.
(b) Profile of 0.7 Å probe, with image of similar Pt atoms on alumina, taken at about 0.8 Å resolution. Improvement in image resolution and contrast is clearly seen; with 0.7 Å resolution, the ACEM should make images slightly better than 2b. Images from the VG HB603U dedicated STEM instrument in Dr. Stephen Pennycook's laboratory in ORNL's Condensed Matter Sciences Division.



Fig. 3. Artist's rendering of Advanced Materials Characterization Laboratory. High bay section house laboratories for 4 ultra-sensitive electron beam instruments, including ACEM. View direction indicated below.

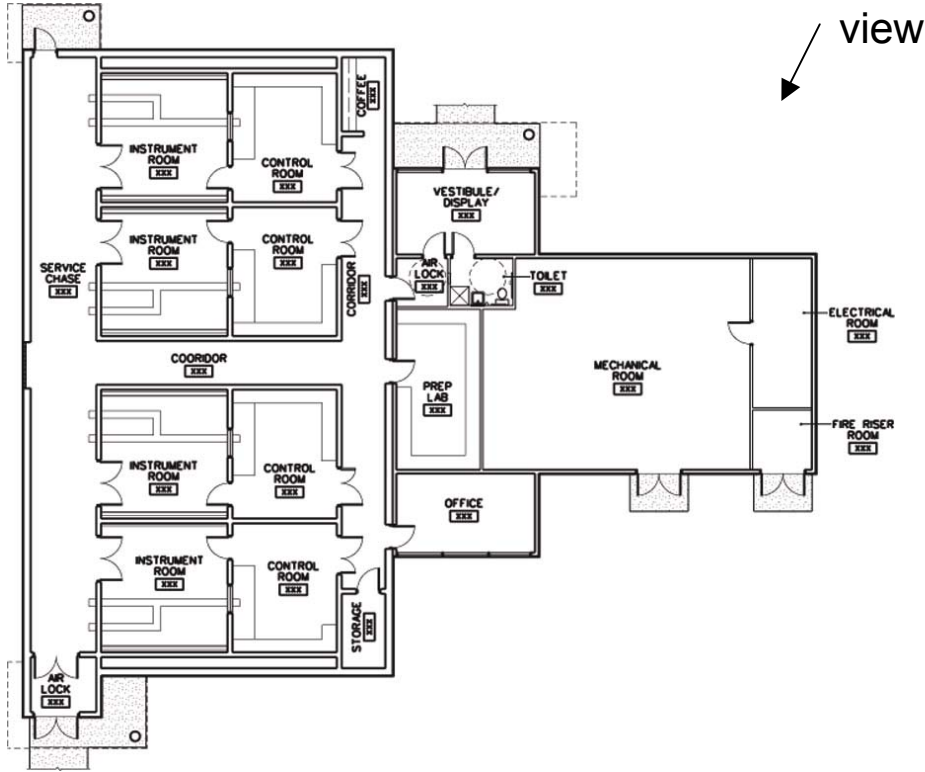


Fig. 4. Floor plan of AMCL, showing instrument and control room configuration in high-bay section, and separate mechanical section housing HVAC equipment and related services.

Microstructural Changes in NO_x Trap Materials under Lean and Rich Conditions at High Temperatures

C.K. Narula and L.F. Allard
Oak Ridge National Laboratory
and
C. Goralski and J. Li
Ford Motor Co.

Objective/Scope

NO_x traps are at the forefront of various strategies under investigation to treat NO_x from Diesel or Lean-gasoline engines [1]. NO_x traps collect engine out NO_x during lean operation and treat it during short rich operation cycles [2]. Fresh NO_x traps work very well but cannot sustain their high efficiency over the lifetime of vehicles. This is believed to be caused by aging due to high-temperature operation and sulfation-desulfation cycles necessitated by the sulfur oxides in the emissions from the oxidation of sulfur in fuel. In order to design a thermally durable NO_x trap, there is need to understand the changes in the microstructure of materials that occur during various modes of operation (lean, rich, and lean-rich cycles). This information can form the basis for selection and design of new NO_x trap materials that can resist the deterioration under normal operation.

The NO_x traps are derived from commercial three-way catalysts installed to treat emissions from engines operating at stoichiometric air-fuel ratios. As such, the basic components of NO_x traps are identical to three-way catalysts. The advance version of three-way catalyst is a two-layer system on a honeycomb substrate with the inner layer based on platinum-alumina and the outer layer on rhodium-ceria-zirconia. The NO_x traps derived from advanced three-way catalysts are identical to it with the exception of high baria content (the upper limit being close to 20%) in alumina layer. Thus, the aging can lead to intermixing of layers, crystallization of baria containing phases that are not good NO_x absorbers, and the sintering of precious metals. The first goal of the project is to determine if one or all of the microstructural changes take place and if these changes occur during lean, rich, or lean-rich cycles.

The tasks to achieve this goal are as follows:

- Complete microstructural characterization of fresh and thermally aged NO_x trap materials to determine the species formed as a result of aging.
- Complete microstructural characterization of fresh NO_x trap materials after exposure to lean conditions to determine the species formed during lean cycles.
- Complete microstructural characterization of fresh NO_x trap materials after exposure to lean conditions to determine the species formed during lean cycles.

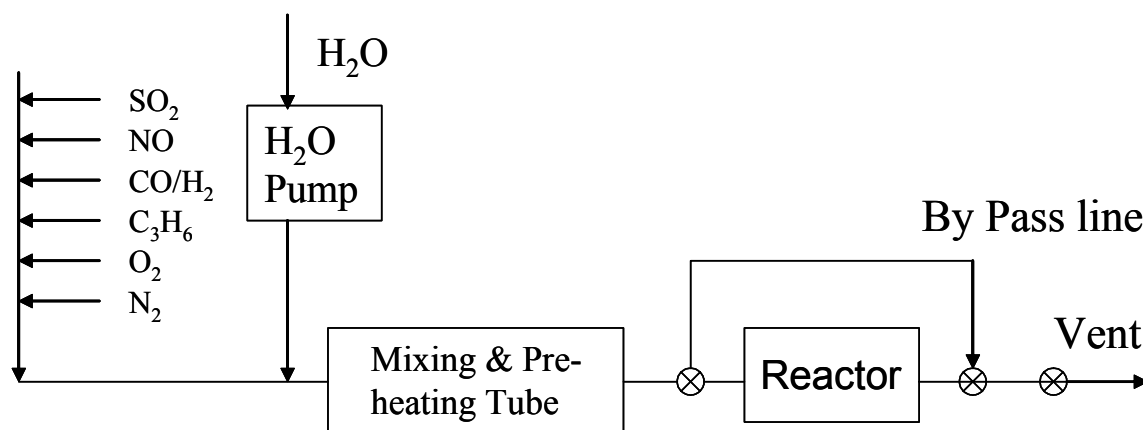
The second goal of the project is to investigate and design new materials that can withstand NO_x trap operating conditions without undergoing detrimental structural changes. The results from first goal will provide insights into changes that occur in NO_x trap materials at microstructural level upon extended exposure to NO_x trap operating conditions enabling selection and design of materials for the second goal.

Technical Highlights

We initiated the work by characterizing the microstructures of samples prepared by two methods. In the first method, a sample of Pt-alumina was impregnated with a barium compound and carefully pyrolyzed. In the second method, a sample of Pt-alumina was ball milled with a barium compound and then pyrolyzed. The samples have 2 wt % Pt and 18 wt % barium. The X-ray powder diffraction patterns of the samples show sharp peaks due to barium carbonate, suggesting that barium oxide component has reacted with atmospheric CO₂. The broad diffraction peaks due to microcrystalline γ -alumina can also be seen.

The TEM of the samples essentially confirmed the BaCO₃ crystallites in the samples. In the impregnated samples, the crystallites are needle shaped while the ball-milled samples show broken needles. These samples have been evaluated at a bench flow reactor at Ford for their NO_x trapping efficiency and thermal durability. The samples, aged on the flow reactor, are being sent back to us to microstructural characterization.

The next step for this research requires utilization of ex-situ reactor. The existing ex-situ reactor needed a complete redesign for this project. The new design of ex-situ reactor is as follows:



The gas controller system has been installed and calibrated for a total gas flow of 100 cc/min. The fabrication of gas lines is in progress. The water pump is on order.

Other activities

The synthesis laboratory is being equipped to enable preparation of NO_x trap materials. Several items are on order. A graduate student, Kelvin Lester, (Prof. A. Datye's group at University of New Mexico) has been identified to support this project. The process for his recruitment is in progress.

Communications/Visitors/Travel

The paperwork for a CRADA with Ford, jointly with NTRC, on “Measurement and Characterization of Lean NO_x Adsorber Regeneration and Durability for Diesel and Lean-burn Engines” is in process. The funding for model catalyst portion has also been received.

Problems Encountered

Ex-situ reactor required total redesign.

Publications

None

References

1. Miyoshi, N.; Matsumoto, S.; Katoh, K.; Tanaka, T.; Harada, J.; Takahashi, N.; Yokota, K.; Sigiura M., and Kasahra, K.; “Development of New Concept Three-Way Catalyst for Automotive Lean-Burn Engines”, SAE paper 95-0809.
2. Takahashi, N.; Shinjoh, H.; Iijima, T.; Suzuki, T.; Yamazaki, K.; Yokota, K.; Suzuki, H.; Miyoshi, N.; Matsumoto, S.; Tanizawa, T.; Tateishi, S.; and Kasahara, K.; “The New Concept 3-Way Catalyst for Automotive Lean-Burn Engine: NO_x Storage and Reduction Catalyst”, Catalysis Today, 1996, 27, 63-69.

Aftertreatment Catalyst Materials Research

**Randy Stafford, Matthew Henrichsen, and Thomas Yonushonis
Cummins Inc.**

Objective/Scope

The objective of this program is to explore (1) novel catalytic materials for more efficient oxidation of soot; (2) effects of non-conventional heating on the efficiency of soot regeneration; (3) advanced techniques for probing degradation of soot filters; and (4) sulfation/desulfation mechanisms for NO_x adsorbers.

Technical Highlights

The work completed in the reported period was conducted at Notre Dame with oversight and guidance by Matthew Henrichsen. Combinatorial chemistry techniques were used to synthesize CuFe₂O₄ and Cu_{1-x}Co_xFe₂O₄ powders. These powders were then tested for catalytic activity using thermalgravimetric analysis (TGA). In addition the crystal structure of the powders was examined using X-ray diffraction.

All sample powders showed catalytic activity; however, there was little differentiation in activity between the samples. All compositions showed essentially the same level of activity and similar behavior of decreasing activity with increasing reaction (sample preparation) temperature.

Future Plans

- (1) Continue combinatorial synthesis and testing with LiFe₅O₈ and substituted LiFe₅O₈ powders.
- (2) Conduct sulfation/desulfation work.

Travel

Trip to University of Notre Dame by Randy Stafford and Matthew Henrichsen to review combinatorial development with Prof. Paul McGinn.

FY 2003 Milestones

Complete studies on the effects of LST on the frictional behavior and microstructural changes produced on ceramic bearing surfaces. Submit final report. **(09/03)**

Publications

None this period.

Lightweight Valve Train Materials

**Mark J. Andrews
Caterpillar Inc.**

Introduction

Valve train components in heavy-duty engines operate under high stresses and temperatures, and in severe corrosive environments. In contrast, the valve train components in the light-duty engine market requires cost-effective reliable materials that are wear resistant and lightweight in order to achieve high power density. For both engine classes, better valve train materials need to be identified to meet market demand for high reliability and improved performance while providing the consumer lower operating costs.

Advanced ceramics and emerging intermetallic materials are highly corrosion and oxidation resistant, and possess high strength and hardness at elevated temperatures. These properties are expected to allow higher engine operating temperatures, lower wear, and enhanced reliability. In addition, the lighter weight of these materials (about 1/3 of production alloys) will lead to lower reciprocating valve train mass that could improve fuel efficiency. This research and development program is an in-depth investigation of the potential for use of these materials in heavy-duty engine environments.

The overall valve train effort will provide the materials, design, manufacturing, and economic information necessary to bring these new materials and technologies to commercial realization. With this information, component designs will be optimized using computer-based lifetime prediction models, and validated in rig bench tests and short-and long-term engine tests.

Program Overview

Information presented in this report is based on previous proprietary research conducted under Cooperative Agreement DE-FC05-97OR22579.

Ceramic Materials

Silicon nitride materials have been targeted for valve train materials in automotive and diesel industries since early 1980's. Some silicon nitride material grades have reached a mature level of materials processing, capable of implementing into production. Commercial realizations have been reported in both automotive and diesel valve trains, with large-scale production underway. The silicon nitride valve train components in production are used in high rolling contact stress applications and have exhibited superior wear resistance, and longevity.

Intermetallic Materials

Titanium aluminide based intermetallics retain their strength to elevated temperature and are highly corrosion-resistant. They are lightweight, and possess high fracture toughness. These alloys are actively being investigated for several aerospace and automotive applications.

Summary

Valve Test Rig

An investigation was initiated to examine the high contact stresses that occur when the valve having a terminal velocity of 200 mm/s makes contact with the seat insert. Evidence of silicon nitride particles from the valve was observed embedded in the seat insert after completing a 100-hour bench test. The focus of the investigation is to better understand reasons for the silicon nitride valves by observing the stress fields. Caterpillar software that was developed in-house is coupled with a finite element model for making the analysis.

The investigation used a modified surface mapping technique to estimate the contact stresses. The surface contact regions of the valve and seat insert can be seen as the surface of two annular rings from two cones. The analysis results suggest that the silicon nitride valve experiences compressive stresses as high as 10 GPa at the surface and just underneath the contact area. The analysis also indicated that the stress estimates were extremely sensitive to the contact regions. The silicon nitride with the 30° contact angle has significantly higher stresses than the silicon nitride valve with the 45° contact angle. This is due in part since the contact region of the corresponding seat insert; the 30° seat insert angle has a much smaller contact region than the 45° seat insert angle. Since there is some question regarding the use of the modified surface mapping techniques, the results of the analysis are considered inconclusive at this time.

To better understand variances in the surface mapping methodology, a standard series of ball-on-flat tests were conducted using the NT551 silicon nitride as the flat material. The surface mapping techniques for this geometry used are well established and accurate contact stresses can be estimated. The flat was subject to an increasing set of constant loads for 10^6 cycles in order to determine the load range when significant damage is observed. For future analyses, the SN235P silicon nitride was subjected to the same ball-on-flat cyclic tests. Figure 1 shows the results from the cyclic indentation tests for each material. Notice that the NT551 is less resistant to contact fatigue since more damage is observed with this material. These results will be analyzed in the next reporting period and compared to the previously made valve contact stress estimates.

The valve bench rig is adding an additional 400 hours of rig time to NT551 silicon nitride valves that have already accumulated 100 hours of test time. These valves will be examined using optical and NDE techniques after completing 500 hours. Table I shows the test parameters for the 500-hour test time. Note that an additional test parameter has been added to the study: the use of an out-of-alignment valve guide. This additional parameter has been added to represent an extreme out of tolerance condition between the valve and seat insert. The silicon nitride valve having the 30° contact angle has completed the 400 hours of rig tests making contact with a 30° seat insert, while the silicon nitride valve with the 45° contact angle and corresponding 45° seat insert is still on the test rig.

Machining Study

The cylindrical specimen geometry having a nominal diameter of 8 mm and a length of 75 mm has been chosen for the Alliance for Innovative Manufacturing (AIM) machining study. The Advanced Machine Research group at Caterpillar has devised this study in support of this program. The purpose of the study is to examine different finishing processes on silicon nitride

materials in order to reduce machining induced failures, the most common mode of failure found for ceramics.

A purchase of 400 test specimens made from SN235P has been received from Kyocera Industrial Ceramics. One of three different surface finishing techniques will be applied to the test specimens. A User Proposal was submitted and accepted at the High Temperature Materials Laboratory located within the Oak Ridge National Laboratory (ORNL) complex. This proposal will allow Caterpillar to conduct strength tests and analyze the test specimens using the lab's facilities and resourceful expert staff personnel. A machining vendor has been chosen to rough grind the test specimens as well as provide a set of specimens with explicit surface finish specifications.

Silicon Nitride Valve Blanks

Two of the 50 silicon nitride valve blanks fabricated by Kyocera were delivered to ORNL as a part of a machine grinding study to be conducted by Mr. Sam McSpadden. The ORNL will use a plunge grinding machine to fabricate the valve blanks to finish specifications. These valves will then be compared to the other 48 finish machined valves that will be machined using a different process.

Caterpillar has completed the oil ash environmental exposure test for 30 SN235P flexure test specimens. These specimens were coated with an ash generated from engine oil and then placed in the furnace for 1000 hours at 850°C. Flexure test specimens are also being exposed to simulated diesel exhaust gas mixture for 1000 hours at 850°C and the completion of this test will be in July. These specimens will be strength tested at ORNL under the direction of Dr. H. T. Lin to determine if the environmental exposures have any influence on strength.

Life Prediction of Ceramic Engine Valves

Efforts are underway to upgrade a life prediction code to accept newer versions of ANSYS finite element software. The output stress file from the finite element software has changed format and extracting the data from the binary files cannot be achieved without upgrading the software. Additional enhancements are being considered for the life prediction software such as offering a "boot strapping" technique to estimate confidence bounds for the data and introducing a damage accumulation fatigue model.

Intermetallic Materials Research

It is difficult to consistently cast long and slender sections of γ -TiAl, such as a valve stem, with appropriate dimensional control and without defects; therefore, it is desirable to use the high temperature capable γ -TiAl only in the valve head region while maintaining a lower cost material in the stem region, where temperature and stresses are significantly lower, as illustrated in Figure 2. This requires that a reliable stem-to-head joining technique be developed for these advanced materials.

Preliminary testing presented in earlier reports explored brazing and friction welding of γ -TiAl to various stem materials. From these joining techniques friction welding is more attractive for producing engine components since it is a more cost effective process. Also, friction welding is

currently used for producing engine valves, which would facilitate scaling up to industrial production.

The control parameters for the friction welding process that were explored include: rotational speed, friction load, and forging force. Different combinations of these parameters were used for joining round bars of γ -TiAl to Ti-6Al-4V and the quality of the joint was evaluated in terms of the ultimate tensile strength (UTS) of the friction-welded specimens.

Joint strengths in excess of the base intermetallic material were obtained. One of the specimens that failed away from the interface (Figure 3) was cut in half, and the transverse section was examined with scanning electron microscopy (SEM) using back-scatter electron detection for contrast enhancement. The mosaic of 4 images at 150X presented in Figure 4 shows the weld line.

ANL

Dr. J. G. Sun from Argonne National Laboratory visited Caterpillar in the current reporting period to discuss the current NDE capabilities that have been used on the NT551 silicon nitride valves. The AIM machining study will include a NDE assessment from ANL after finish machining the specimens and again after testing. Using this approach, the ANL NDE techniques will be assessed for the ability to identify and predict the strength-limiting flaws on the test specimens before strength testing.

Presentations

None

Future Work

Analysis of the ball-on-flat tests cyclic indentation tests will be completed and compared to the valve and seat insert contact stress analysis. Final print specifications for machining the Si_3N_4 valves will be completed and sent out to machining vendors for obtaining quotations. NT551 valves will continue to be tested on the bench test to 500 hours and then sent to ANL for NDE. Prototype γ -TiAl to Ti-6Al-4V valves will be produced using the parameters that result in the strongest welds for rig and engine testing.

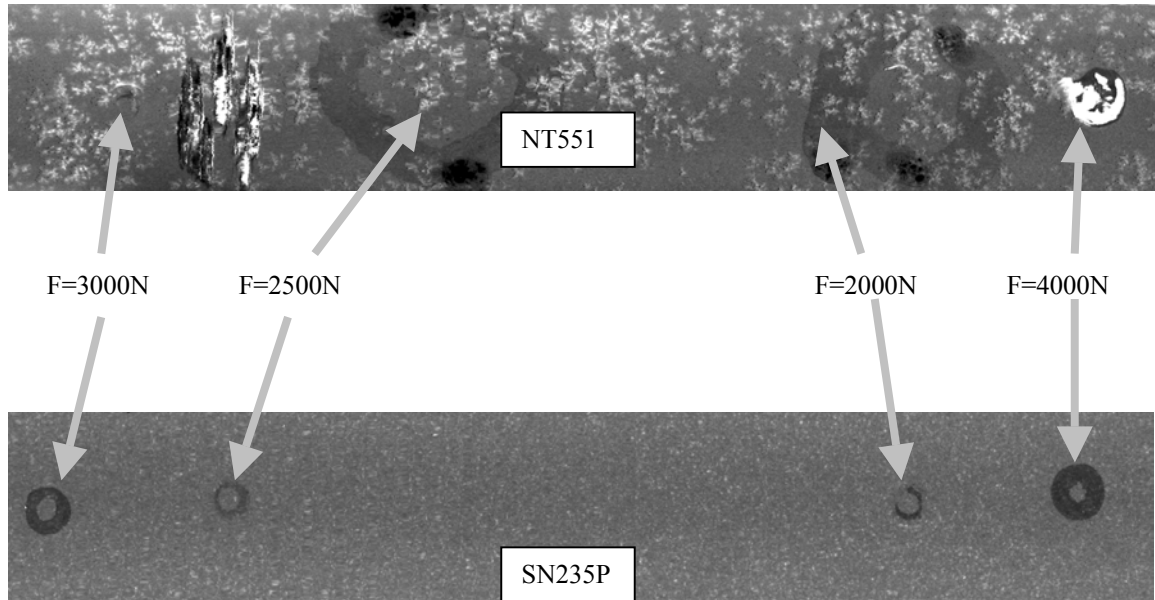


Figure 1. Results from 106 cyclic indentations for NT551 and SN235P silicon nitride. The NT551 shows a lower tolerance to cyclic contact loading than the SN235P. Note the “snowflake” imagery in the NT551 material (images by JG SUN, ANL).

Table I. Bench test matrix for completing 500 hours on valve rig.

Test Configuration	Valve contact angle (deg)	Seat insert contact angle (deg)	Valve guide
A	30	30	standard
B	45	45	standard
C	45	30	standard
D	30	30 – eccentric machined	standard
E	30	30	nonstandard
F	45	45	nonstandard
G	45	30	nonstandard
H	45	30 – eccentric machined	nonstandard

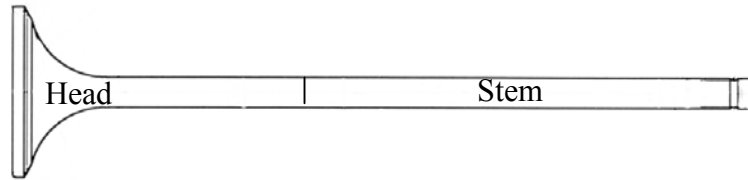


Figure 2 Sketch of a two-piece diesel engine valve indicating possible configuration. The valve head would be TiAl while the stem would be Ti-6V-4Al.

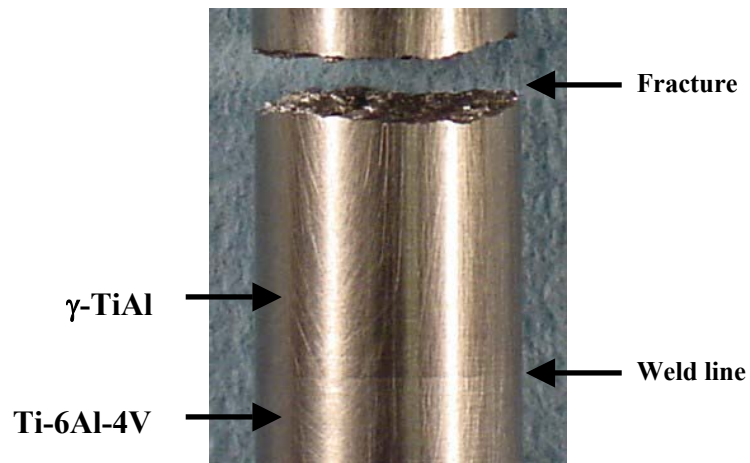


Figure 3 Specimen that failed in tension on the γ -TiAl, away from the interface or weld line.

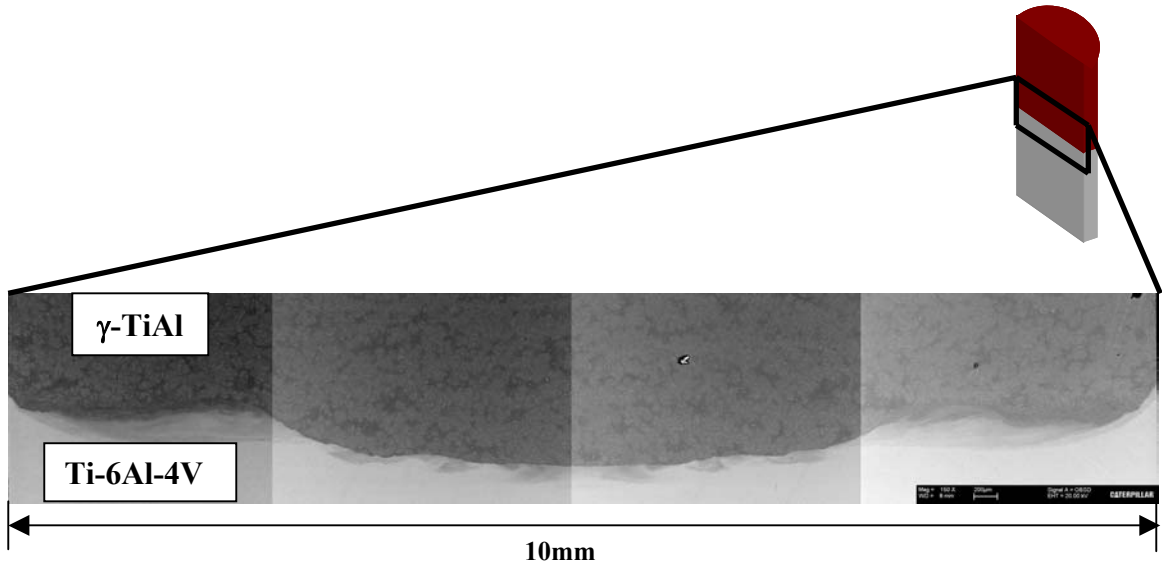


Figure 4. Back-scatter electron SEM image showing transversal section of the weld.

Thick Thermal Barrier Coatings (TTBCs) for Low Emission, High Efficiency Diesel Engine Components

**M. Brad Beardsley and Jesus G. Chapa-Cabrera
Caterpillar Inc.**

Objective/Scope

Engine testing of thermal sprayed coatings has demonstrated their use as thermal barriers and wear coatings can reduce fuel consumption, reduce wear and reduce component temperatures. The durability of thermal sprayed coatings, particularly thermal barrier coatings, remains as the major technical challenge to their implementation in new engine designs. New approaches to coating design and fabrication will be developed to aid in overcoming this technical hurdle. New laser technology of surface dimpling, cleaning and laser assisted spraying will be applied to enhance adherence and increase coating strength. Refinements of current seal coating technologies will be developed to further enhance the durability of the coating structure. New quasicrystalline materials will be evaluated as thermal barrier coatings as well as wear coatings for ring and liner applications and as low friction coatings for camshafts and crankshafts. Plasma spraying, D-Gun and HVOF processing will be used to develop these new coatings.

Technical Highlights

Laser Assisted Thermal Spraying – No effect was detected in the microstructure of the sprayed and laser treated samples. The laser beam was introduced both at the leading and trailing edge of the spray footprint without any detectable change in the coating microstructure. This may be due to either the high federates used (3 to 6 lb/h) or to the high melting point of the NiCrAlY bond coating sprayed. A consulting agreement with Fraunhofer USA is being negotiated in order to have discussions relating to this patented process with them.

Quasicrystals – Diffusion of the aluminum in the quasicrystal structure has been determined to be the critical factor in being able to use these new materials for TBC applications. Diffusion couple experiments are planned and will be run at the Materials Processing Center of the Ames Laboratory at Iowa State University. Samples will be sprayed with both the BT1 quasicrystal and bond coatings to determine what type of diffusion will occur within the TBC system.

Future Plans

Quasicrystal diffusion couple samples will be sprayed and the diffusion experiments begun.

Travel

None this quarter, no trips are planned for next quarter.

Status of FY 2003 Milestones

321. Determine the effect on TTBC bond strength due to laser micro-dimpling of the substrate surface prior to coating. (July 31, 2003)

No progress to report.

322. Determine the effect on TTBC coating strength and permeability due to laser shock peening after coating application. (July 31, 2003)

No progress to report.

323. Determine the effect on the hardness and microstructure of the TTBC due to laser assisted plasma deposition. (July 1, 2003)

Fraunhofer, USA, will be consultant as to the poor results of initial trials at Caterpillar of this technology.

324. Incorporate torsional fatigue testing results into life models. (Completed May 29, 2002)

325. Develop FEA models to aid in the design of life prediction tools for the TTBC system. (December 1, 2003)

No progress to report.

325. Evaluate the microstructure of the ceramic TTBC material using varying laser power.

The poor response of the metallic bond coating to the laser treatment to date makes processing of the ceramic of the TBC to be unsuccessful.

Publications

None this period.

Processing and Characterization of Structural and Functional Materials for Heavy Vehicle Applications

J. Sankar, Z. Xu, and S. Yarmolenko
North Carolina A & T State University

Objective/Scope

Continue to investigate the combustion chemical vapor deposition technique of fully stabilized zirconia (YSZ) thin films for solid oxide fuel cells.

Task

Investigate the techniques to enhance YSZ thin film deposition rate in Liquid fuel combustion chemical vapor deposition CCVD.

Technical Highlights

YSZ is an oxygen ion conductive material and has been conventionally used as an electrolyte in solid oxide fuel cell (SOFC) and oxygen sensors for pollution and safety monitoring, control and automation of industrial processes and energy conservation. Because of the relatively low electrical conductivity of the YSZ material (about $0.1 \text{ S}\cdot\text{cm}^{-1}$ at 1000°C), most of the ohmic loss is due to the resistance of the electrolyte. To reduce the ohmic loss and increase the power generating efficiency of the fuel cell, it is desirable to use thin film electrolyte. On the other hand, temperature as high as 1000°C is usually employed in order to obtain reasonable ion conductivity for YSZ material. This high temperature places a great difficulty on material selection and increases the product cost greatly. Reducing the thickness of the electrolyte will increase the conductivity at lower temperatures.

YSZ thin films were usually synthesized by chemical vapor deposition technique or electrochemical vapor deposition technique. The vacuum systems used by these techniques place limitations on the sizes of the parts and high costs of the products. Liquid fuel combustion chemical vapor deposition (CCVD) is a promising technique to produce YSZ thin films for industrial applications. Metal-organic reagents were dissolved in organic solvent (toluene). The solution was atomized into small sized aerosols with a nebulizer when it was mixed with oxygen, and then was ignited by a pilot flame. The CCVD works in open atmosphere. There is potential to have conformal deposition of films on non-flat surface. Moreover, because there is no any vacuum chamber needed for the process, there will be no size limitation of the part on which the film is deposited. Because of the relatively high precursor concentration in liquid fuel to that usually used for low-pressure CVD processes, CCVD is expected to have higher deposition rate. Therefore, CCVD will be a promise technique to produce YSZ thin films for industrial SOFC applications with lower cost than any other CVD/EVD techniques.

The reduce the cost of fuel cell manufacturing that using thin film technology, high growth rate of the films is of great interest. Upon finishing the fundamental researches of thin film depositions using CCVD in Center for Advanced Materials and Smart Structures (CAMSS), methods to enhance the growth rate of YSZ had been further studied. In this report, effects of thermophoresis, total-metal-concentration on the film growth rates will be discussed.

Results and Discussion

Thermophoresis is a thermal gradient directed flow of material from high temperature regions to low temperature regions. Thermophoresis had been found to be a strong factor in some CVD environments [3]. A temperature gradient across a diffusion boundary layer causes a thermophoresis effect. In our case, if the flame were hotter than the substrate, on average, the gas molecules from the substrate would have a smaller velocity than the gas molecules traveling toward the substrate. This creates a driving force for YSZ clusters formed in the direction toward the substrate. Stable gas species would not stick to the substrate, but any species that might be capable of sticking to the substrate would have a net flux to the substrate. A larger temperature gradient adjacent to the substrate increases the thermophoresis effect. The study of the effect of thermophoresis was carried out by film depositions at different substrate-to-nozzle distances from 51 mm (far into the flame) to 83mm (out of the visible end of the flame). The film thickness measured in Scanning Electron Microscopy (SEM) images is plotted versus the substrate-to-nozzle distance in Fig. 1 in solid line. The data can be fit by an exponential equation. With the increase of the substrate-to-nozzle distance, precursor concentration in the flame will be attenuated because of the expansion of the flame. Normalization was made in order to eliminate the effect of concentration dilution on the film growth rate. The normalized thickness data were again plotted in the same graph of the originally measured data, as is shown in Fig. 1 by the curve 2 in dashed line. It is apparently noticeable that after normalization, the growth rate of the film still follows the exponentially decaying mode with the substrate-to-nozzle distance. In other words, the parameter substrate-to-nozzle distance does play a role in film growth.

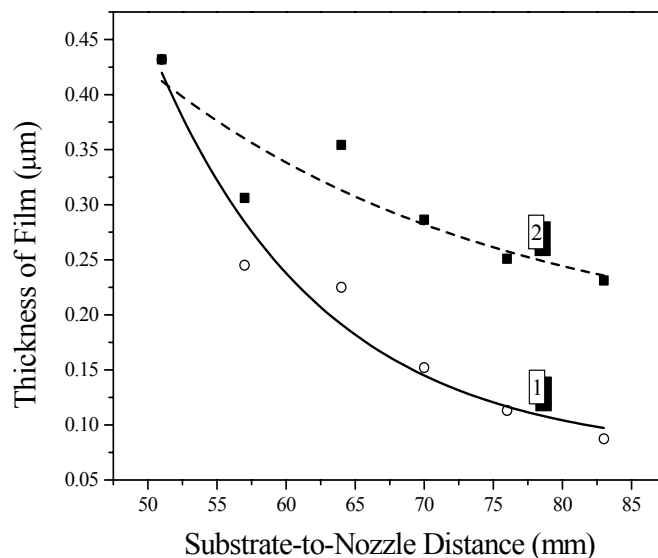


Figure 1. Film thickness as a function of the substrate-to-nozzle distance, line (1) for the original measured data, line (2) for the normalized data

Effect of the total-metal-concentration on the film growth rate is shown in Fig. 2. Within the range of the concentration employed in our experiments, a linear relationship was obtained between the film growth rate and the concentration. By observing the morphologies of the

samples (as shown in Fig. 3), the films had well crystallized and faceted particles as long as the total-metal-concentration were not more than 4.25×10^{-3} M. Beyond this limitation, the film was in a cauliflower-like structure.

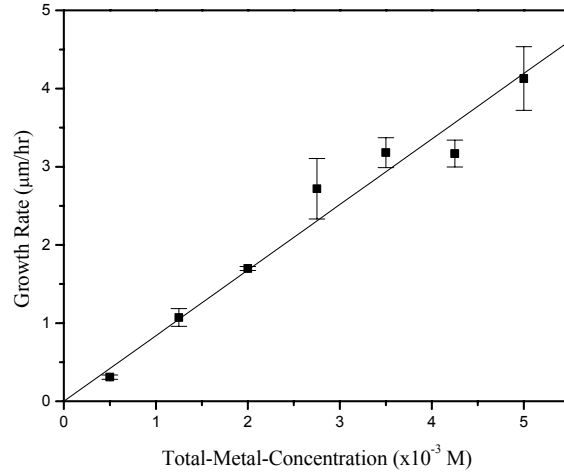


Fig. 2. Film growth rate versus total-metal-concentration in the liquid solution.

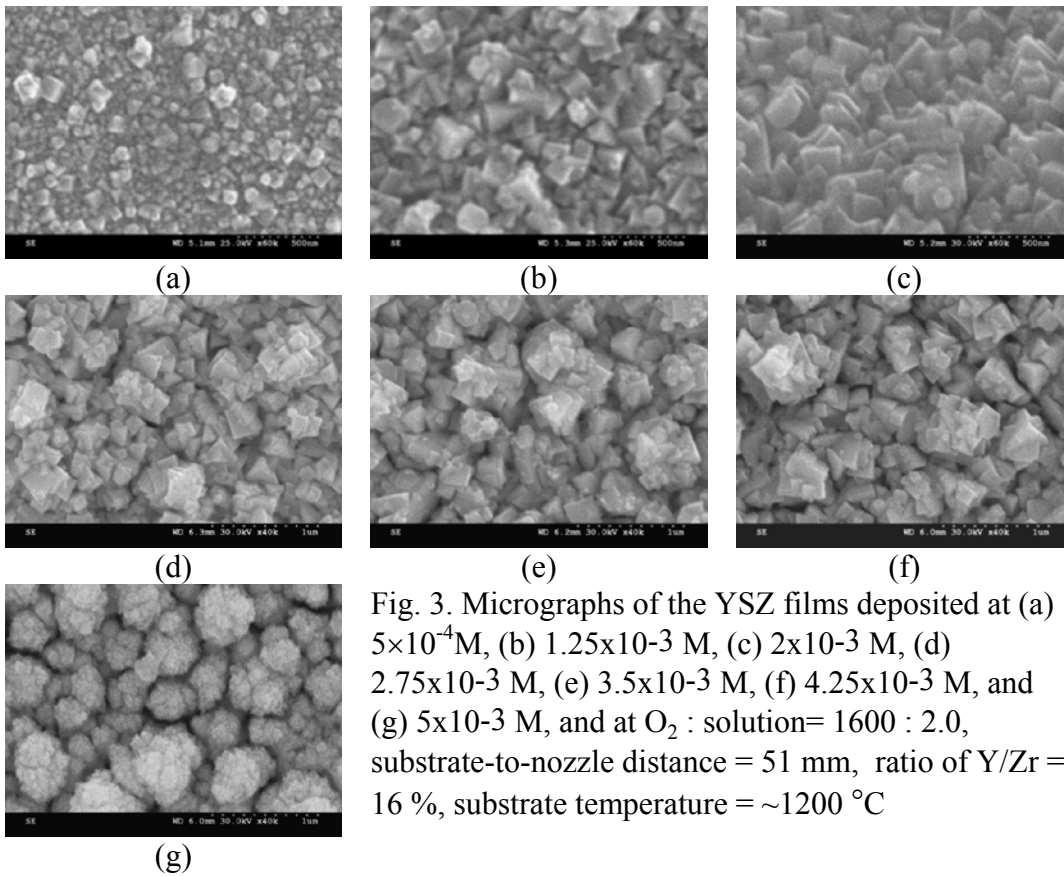


Fig. 3. Micrographs of the YSZ films deposited at (a) 5×10^{-4} M, (b) 1.25×10^{-3} M, (c) 2×10^{-3} M, (d) 2.75×10^{-3} M, (e) 3.5×10^{-3} M, (f) 4.25×10^{-3} M, and (g) 5×10^{-3} M, and at O_2 : solution = 1600 : 2.0, substrate-to-nozzle distance = 51 mm, ratio of Y/Zr = 16 %, substrate temperature = ~ 1200 °C

Status of Milestones

On Schedule

Communications/Visitors/Travel

None

Problems Encountered

None

Publications

1. Z. Xu, S. Yarmolenko, J. Sankar, "Enhancement of YSZ thin film deposition rate in CCVD," ICCE/10, Edited by David Hui, July 20-26, 2003, New Orleans, LA, pp. 861-862.
2. Z. Xu, S. Yarmolenko, J. Sankar, "Deposition of composite thin films of YSZ and Al₂O₃ using CCVD," ICCE/10, Edited by David Hui, July 20-26, 2003, New Orleans, LA, pp. 863-864.
3. C. Hilton, B. Watkins, Z. Xu, S. Yarmolenko, J. Sankar, "Thermophoresis effect of YSZ thin film deposition using combustion chemical vapor deposition," ICCE/10, Edited by David Hui, July 20-26, 2003, New Orleans, LA, pp. 865-866.
4. G. Rajaram, D.M. Pai, Z. Xu, J. Sankar, X. Jiang and S. Sarin, "Combustion chemical vapor deposition process optimization for solid oxide fuel cells," ICCE/10, Edited by David Hui, July 20-26, 2003, New Orleans, LA, pp. 851-852.

NDE Development for Ceramic Valves for Diesel Engines

J. G. Sun, J. M. Zhang, W. A. Ellingson, and M. J. Andrews *
Argonne National Laboratory
***Caterpillar, Inc.**

Objective/Scope

Emission reduction in diesel engines that are designated to burn several types of fuels has led to assessing ceramic engine valves to mitigate valve corrosion and extend service lifetimes. The objective of this work is to evaluate several nondestructive evaluation (NDE) methods to detect defect/damage in structural ceramic valves for diesel engines. The primary NDE to be utilized is the elastic optical scattering or laser scattering method. The goal is to demonstrate that investigations using this method can identify defects/damage that can be used for predicting material microstructural and mechanical properties. There are two tasks to be completed: (1) Characterize surface/subsurface defects and machining damage and correlate NDE data with mechanical properties for rectangular and cylindrical flexure test specimens of candidate silicon nitrides selected for fabricating into prototype valves. Laser-scattering studies will be conducted at various wavelengths using a He-Ne laser and a tunable-wavelength solid-state laser to optimize detection sensitivity. NDE studies will be coupled with examination of surface and subsurface microstructure and fracture surface to determine defect/damage depth and fracture origin. NDE data will also be correlated with mechanical properties. (2) Assess and evaluate accumulated damage in full-size ceramic valves due to rig or engine tests. All prototype silicon nitride valves will be examined at ANL prior to bench tests, after accumulating a specified number of test hours, and at the end of the planned test runs.

Technical Highlights

Work during this period (April-June 2003) focused on acquiring and analyzing laser-scattering NDE data for cracks and damage induced by cyclic impact tests on a NT551 and a SN235P Si₃N₄ rectangular test specimen.

1. Elastic Optical Scattering NDE for Subsurface Defect/Damage

During this period ANL obtained from Dr. Andrews of Caterpillar Inc. one NT551 and one SN235P rectangular test specimen that had been subject to cyclic impact tests. There were four loads applied at four different locations on each test specimen: 2000, 2500, 3000, and 4000 Newtons. The flat polished surface of the test specimens were loaded with a specialized polished silicon nitride sphere that had a radius of 3.18 mm. A constant load was applied for 10⁶ cycles in order to assess the initiation of cracks and subsequent contact damage. The purpose of this investigation was to evaluate/calibrate laser-scattering detection sensitivity on cyclic impact damage and to identify experimental and/or system conditions that limit detection sensitivity. Laser scattering measurements were conducted for the two specimens using the tunable laser at the wavelengths of 721 and 750 nm and with a scan resolution of 2, 5, and 10 μ m.

Figure 1 shows the typical laser-scattering images for the impact-tested NT551 and SN235P specimens. For the NT551 specimen, Fig. 1a, dendrite-like structure is evident and this structure has been identified as the secondary or glassy phase. This phase of NT551 material exhibits a

stronger subsurface scattering intensity. The cyclic impact damage is also evident at the 3000 and 4000 N locations (showing brighter in image). For the SN235P material, Fig. 1b, all impacted regions appear darker, due to a lower subsurface-scattering intensity. This feature was also observed within the wear-scar region of the 100-hour rig-tested NT551 valve (#277, see Fig. 6 in the Jan-Mar 2003 quarterly report of this project). It is believed that the increased surface roughness caused intensity reductions across the surface when incident light is transmitted into and the backscattering emerges out from the subsurface. The size of impact region increases with increasing load as evidenced from the plastic deformation. All impact regions appear as rings, indicating that the impact damage to be Hertzian in nature.

The surface microstructure of all impact spots was examined by photo microscopy. Figure 2 shows the photomicrographs of the four impact spots on the NT551 specimen. It is apparent that cracks exist at the edges of all impact regions. However, laser scattering appears to detect only the cracks at impact spots with 3000 and 4000N loads, presumably because these cracks are deeper. By comparing the photomicrographs with scattering images, as shown in Fig. 3, cracks with different scattering intensities are detected in scattering images, suggesting that these cracks have different depths and "severity". In contrast, all cracks appear similar in the photomicrographs in Fig. 3. For the 4000N-load impact spot, several areas with high scattering intensity within the impact region were further examined. They were found to have sharp boundaries and are raised above the surrounding area. It was concluded that they are thin deformed chips mostly debonded from the bulk material and ready to spall. The significantly increased subsurface scattering comes from the interface under the chips.

Figure 4 shows the photomicrographs and scattering images of the four impact spots on the SN235P specimen. Similarly, micro cracking occurred at all impact spots. Close examination of the NDE images showed that laser scattering detected all cracks, however, the contrast was generally low for this material. For the 3000N-load impact spot, the crack at top edge appears extended laterally upward in subsurface; this is, however, not apparent as seen from the surface photomicrograph.

The sensitivity and resolution of laser-scattering measurement depends on several optical and material parameters. First, the detector collects all subsurface scattering within a certain depth. Detection sensitivity is at optimum if the scattering-detection depth is comparable (or shallower) to the crack depth. When detection depth is deeper than crack depth (presumably true for current measurements), the detection sensitivity becomes lower. The detection depth is related to the optical attenuation property of the material, and it is deeper for NT551 than for SN235P, so crack detection sensitivity for SN235P is better than for NT551. Secondly, the resolving power of a scanning optical system depends on the size of the focused laser beam. The laser-spot size for the tunable laser setup is large at $\sim 35 \mu\text{m}$ while the width of cracks is typically $\sim 1 \mu\text{m}$. The detection resolution/sensitivity can be significantly improved if the laser-spot size is reduced. It is planned to examine these specimens again using the He-Ne laser setup which has an approximate $15 \mu\text{m}$ spot size and also a shallower detection depth for these materials. This laser is currently being repaired and should be available in the next quarter.

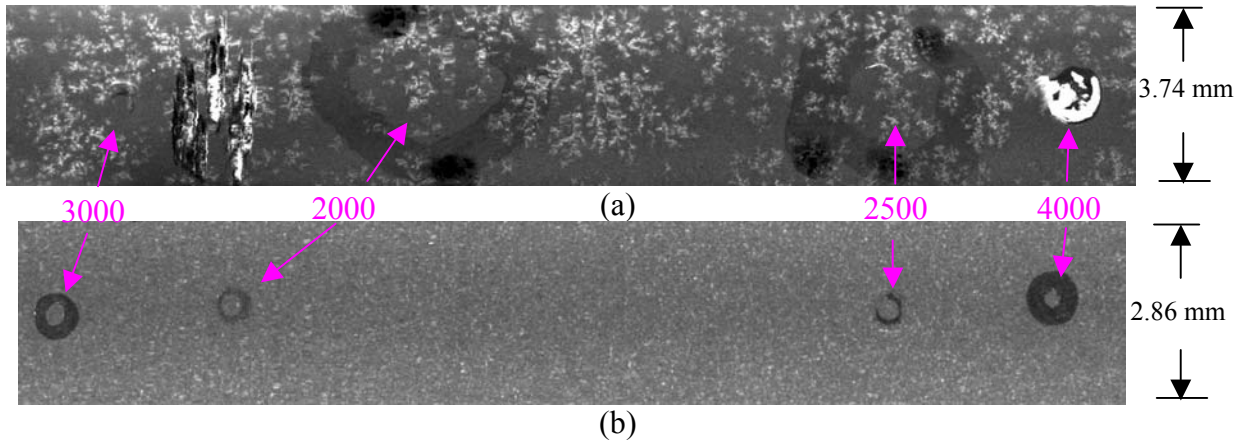


Fig. 1. Laser-scattering images of (a) NT551 and (b) SN235P ceramics each with four impact locations at impact load of 2000, 2500, 3000, and 4000 N as indicated. Images obtained at 750 nm wavelength with a scan resolution of 5 μm .

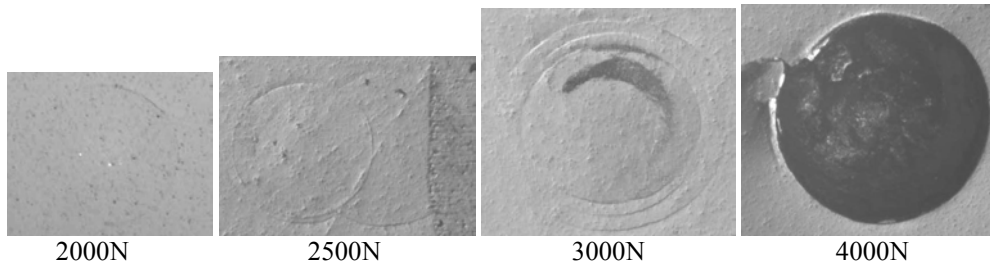


Fig. 2. Photomicrographs at 50X for four impact spots in NT551 specimen.

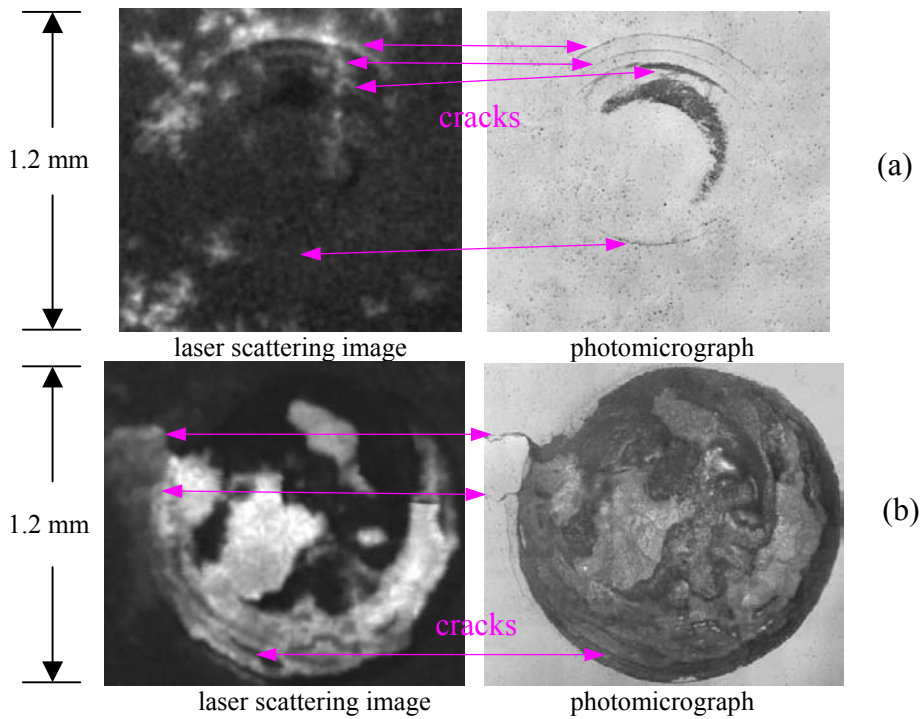


Fig. 3. Comparison of laser-scattering images and photomicrographs at 200X for impact spots with (a) 3000N and (b) 4000N load in NT551 specimen.

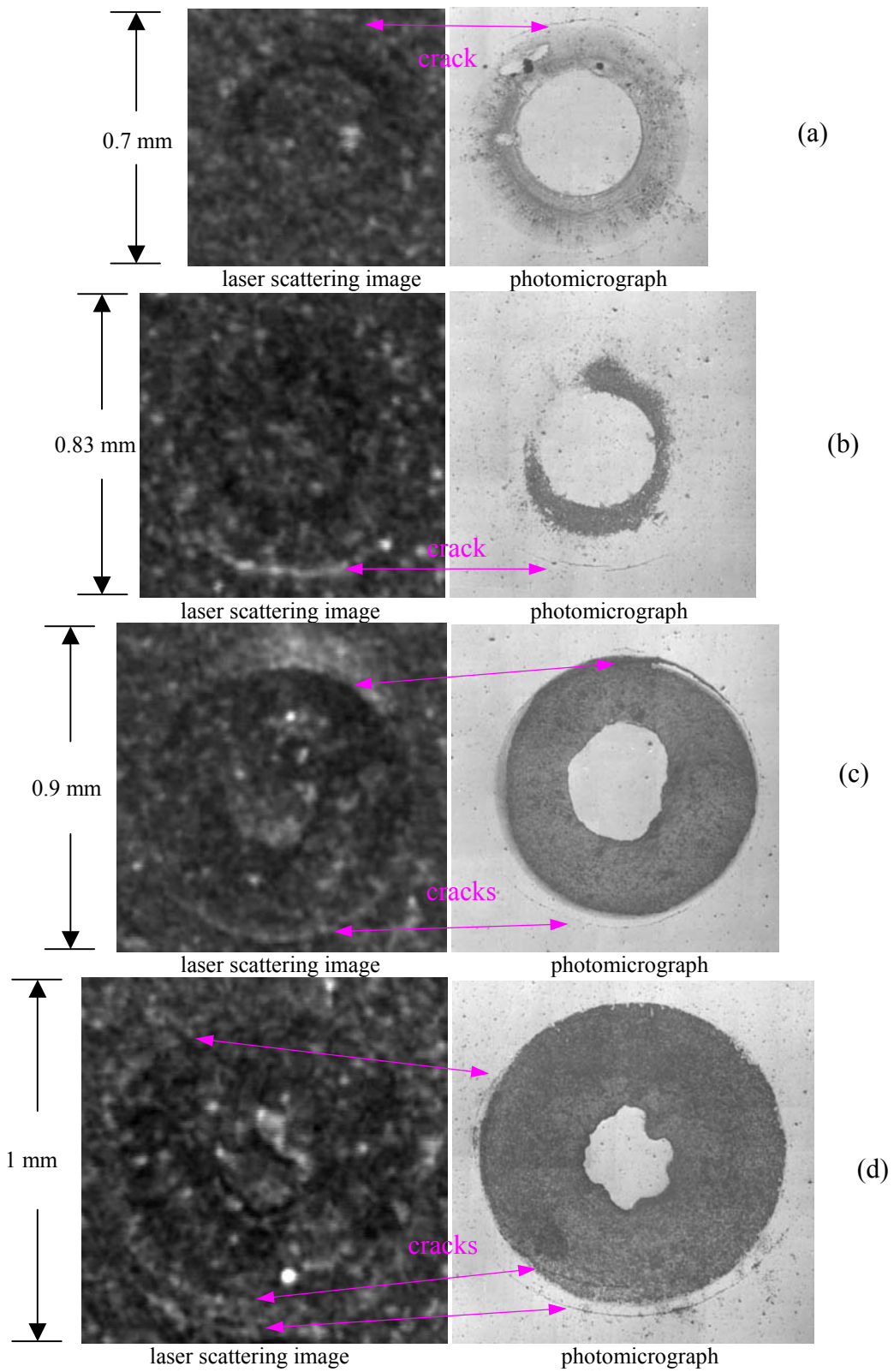


Fig. 4. Comparison of laser-scattering images and photomicrographs at 200X for impact spots with (a) 2000N, (b) 2500N, (c) 3000N, and (d) 4000N load in SN235P specimen.

2. Laser-Scattering Characterization of Si₃N₄ Valves

During this period we also obtained from Dr. Andrews two NT551 valves that were rig tested for 100 hours with eccentric valve-seat alignment. Laser scanning tests will be conducted in the next period. We have also ordered a new translation stage with a 250-mm motion range that is capable for covering the entire valve length in a single scan. The stage is expected to arrive in next period.

Status of Milestones

Current ANL milestones are on schedule.

Communications/Visits/Travel

J. G. Sun visited Dr. M. J. Andrews of Caterpillar Inc. on June 5, 2003 to discuss project issues.

Problems Encountered

Our He-Ne laser was broken at the beginning of this period, and a replacement laser was ordered. Tests requiring this laser were postponed to the next period.

Publications

None this period.

Durability of Diesel Engine Component Materials

Peter J. Blau
Oak Ridge National Laboratory

John Truhan
University of Tennessee, Knoxville, TN

Jun Qu
ORISE Post-Doctoral Fellow

Objective/Scope

The objective of this effort is to enable the development of more durable, low-friction moving parts in diesel engines for heavy vehicle propulsion systems by conducting friction, lubrication, and wear analyses of advanced materials, surface treatments, and coatings. The scope of materials and coatings is broad and includes any metallic alloy, intermetallic compound, ceramic, or composite material which is likely to be best-suited for the given application. Parts of current interest include scuffing-critical components, like fuel injector plungers and EGR waste gate components. Bench-scale simulations of the rubbing conditions in diesel engine environments are used to study the accumulation of surface damage, and to correlate this behavior with the properties and compositions of the surface species. The effects of mechanical, thermal, and chemical factors on scuffing and reciprocating sliding wear are being determined. Results will be used to refine material selection methodology and to suggest materials for durability-critical engine components.

Technical Highlights

A ‘pin-on-twin,’ reciprocating sliding test was recently developed to enable the characterization of scuffing behavior in materials for fuel-lubricated systems [1,2]. It is based on an analysis of friction force versus time traces of individual sliding cycles and verified by studies of the wear scar morphology [2]. The new method was applied to investigate the effects of fuel type, normal load, and reciprocating frequency on the scuffing characteristics of hardened 52100 steel, as well as zirconia ceramics and intermetallic alloy-containing cermets.

Effects of Fuel-Lubricity, Load, and Reciprocating Frequency on Scuffing Characteristics

Tests were conducted in the Jet A aviation fuel with three loads (20, 50, and 100 N) and two reciprocating frequencies (5 and 10 Hz). The same three loads were also applied to tests lubricated with #2 diesel fuel (at 5 Hz only). The sliding distances required for scuffing initiation at these test conditions are summarized in Fig. 1. Regardless of which fuel was used, the steel specimens generally resisted scuffing longer at the lower load and higher reciprocating frequency. At the 20 N load, scuffing did not occur at all during the 60 m sliding tests for two out of three cases (i.e., 5 Hz in diesel fuel and 10 Hz in aviation fuel). The friction coefficient traces (not shown here) also contained more evidence for aggressive scuffing propagation at the higher load and lower reciprocating frequency. At the same load and frequency, scuffing initiated later and propagated slower in diesel fuel than that in aviation fuel. These observations confirm that the fuel-injection system is more vulnerable to scuffing at higher pressure, lower sliding speed, and in poorer lubricity fuel, and are consistent with Stribeck curve behavior [3,4].

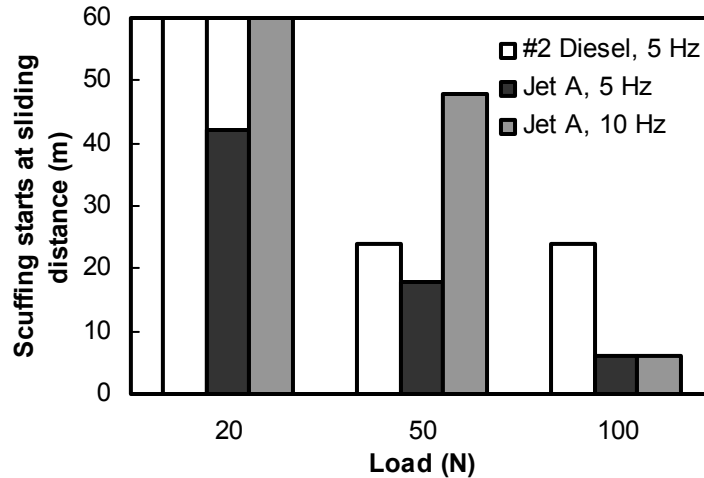


Figure 1. Effects of fuel-lubricity, load, and reciprocating frequency on the distance to produce scuffing initiation in hardened 52100 steel pin specimens.

Cermets for Fuel Injector Plunger Scuffing.

Two new, intermetallic composite materials (cermets) based on Ni₃Al and TiC were tested on the pin-on-twin rig in fuel-lubricated environment. Both were developed with support from the DOE Heavy Vehicle Propulsion Materials Program. One, designated here as ‘C-10’, was obtained from T. N. Tiegs, ORNL, and has a TiC content of 50 vol %. The second cermet, containing 40 vol % TiC in Ni₃Al, was processed by D. Wittmer and his students at Southern Illinois University (SIU). Two SIU cermets were prepared by different processing conditions. One, denoted SIU 1-20, was processed at vacuum, low-pressure hot isostatic pressed (V-LPHIP) at 1450°C, and another more porous one (SIU 3-27) was conventionally sintered (CS) at 1400°C.

The pin-on-twin method for detecting the onset of scuffing was used. In this case, twin cermet specimens were used as the bottom pins and hardened 52100 steel was used as the reciprocating upper pin. Comparative tests were also conducted on hardened 52100 steel and zirconia, a combination that has been used in commercial diesel fuel injectors. All contact surfaces were polished by 400 grit SiC abrasive paper and the arithmetic average surface roughness (R_a) was controlled in the range of 0.18 ~ 0.22 μm . Tests were conducted for 60 m sliding distance, at 50 N load, 5 Hz reciprocating frequency, 10 mm stroke, and in both Jet A aviation fuel and #2 diesel fuel. Tables 1 and 2 show the ranking of the resistance to scuffing’s onset and propagation of these metal, ceramic, and cermet materials in diesel and aviation fuels, respectively.

In summary,

- Zirconia sliding on hardened 52100 steel, performed better in #2 diesel fuel than in the lower-sulfur Jet A aviation fuel, as expected. This couple resisted scuffing initiation for longer sliding distances, and had slower surface damage propagation, in diesel fuel.
- Zirconia sliding against 52100 steel showed the highest overall scuffing resistance in the diesel fuel and did not scuff at all in the 60-meter reciprocating sliding test. However,

this pair scuffed after sliding 33 m in the ultra low-sulfur aviation fuel. This indicates the need to use new fuel injector materials to resist scuffing in the next generation of low-S diesel fuels required by the stricter emissions rules.

- Promisingly, the new cermet materials showed comparable or higher scuffing resistance in Jet A aviation fuel compared to that in #2 diesel fuel. The cermet SIU 1-20 against 52100 steel pair survived after the sliding 60 meters, and ranked at the top in the low sulfur fuel. The other material combinations began scuffing at some time during the 60-meter sliding test in Jet A aviation fuel.
- All material combinations had very similar average friction coefficients in #2 diesel fuel. Cermets showed lower friction coefficient than zirconia when sliding against 52100 steel in aviation fuel. Unexpectedly, the friction coefficient of cermet/steel pairs was slightly lower in aviation fuel, even though aviation fuel was supposed to have poorer lubricity than diesel fuel. That behavior still remains to be explained.

Table 1. Scuffing Resistance Rankings in #2 Diesel Fuel
(Upper pin: hardened 52100 steel)

Bottom pins	Average μ^*	R1, Relative resistance to scuffing initiation (sliding distance (m))	R2, Relative resistance to scuffing propagation	Overall scuffing resistance (total R1+R2)
52100 steel	0.12	3 (30)	2	3 (5)
Zirconia	0.12	1 (>60)	1	1 (2)
C-10	0.12	2 (36)	2	2 (4)
SIU 1-20	0.12	4 (18)	2	4 (6)
SIU 3-27	0.12	5 (15)	5	5 (10)

* kinetic friction coefficient

Table 2. Scuffing Resistance Rankings in Jet A Aviation Fuel
(Upper pin: hardened 52100 steel)

Bottom pins	Average μ^*	R1, Relative resistance to scuffing initiation (sliding distance (m))	R2, Relative resistance to scuffing propagation	Overall scuffing resistance (total R1+R2)
52100 steel	0.12	5 (12)	5	5 (10)
Zirconia	0.12	3 (33)	2	2 (5)
C-10	0.11	2 (36)	3	2 (5)
SIU 1-20	0.10	1 (>60)	1	1 (2)
SIU 3-27	0.09	3 (33)	4	4 (7)

* kinetic friction coefficient

Future Plans

1. Conduct scuffing experiments on cermets and on fuel injector plungers coated with TiN.
2. Investigate the causes for the unexpectedly low friction of cermets in aviation fuel environments.

Travel

None.

Status of Milestones

1) Evaluate and report on the usefulness of scanning acoustic microscopy for characterizing the extent of subsurface damage arising from high-temperature scuffing. (March 31, 2003 – completed.)

2) Report on the effects of sulfur in the fuel on the scuffing behavior of current and future candidate fuel injection system materials (September 30, 2003).

Publications

J. Qu, J. Truhan, and P.J. Blau, “Detecting the Onset of Localized Scuffing with the Pin-on-Twin Fuel-Lubricated Test for Heavy Duty Diesel Fuel Injectors,” Conference on Boundary Lubrication for Transportation, Copper Mountain, Colorado, Aug. 3-8, 2003 (accepted for presentation).

Text References

[1] J. Qu, J. Truhan, P.J. Blau, and R. Ott (2003) “A Scuffing Test for Heavy Duty Diesel Fuel Injector Materials,” Poster No. 41, 14th International Conference on Wear of Materials, Washington D.C., Mar. 30 – Apr. 3, 2003.

[2] J. Qu, J. Truhan, and P.J. Blau, “Detecting the Onset of Localized Scuffing with the Pin-on-Twin Fuel-Lubricated Test for Heavy Duty Diesel Fuel Injectors,” Boundary Lubrication for Transportation, Copper Mountain, Colorado, Aug. 3-8, 2003 (accepted for presentation).

[3] R. Stribeck (1902) “Die Wesentlichen Eigenschaften der Gleit- und Rollenlager,” *Z. Verein. Deut. Ing.*, 46 (38), pp. 1341-1348; (39) 1463-1470.

[4] P. J. Blau (1995) *Friction Science and Technology*, Marcel Dekker, Inc., New York.

Life Prediction of Diesel Engine Components

H. T. Lin, T. P. Kirkland, A. A. Wereszczak, M. K. Ferber, and M. J. Andrews*
Oak Ridge National Laboratory
***Caterpillar Inc.**

Objective/Scope

The valid prediction of mechanical reliability and service life is a prerequisite for the successful implementation of structural ceramics and advanced intermetallic alloys as internal combustion engine components. There are three primary goals of this research project which contribute toward that implementation: the generation of mechanical engineering data from ambient to high temperatures of candidate structural ceramics and intermetallic alloys; the microstructural characterization of failure phenomena in these ceramics and alloys and components fabricated from them; and the application and verification of probabilistic life prediction methods using diesel engine components as test cases. For all three stages, results are provided to both the material suppliers and component end-users.

The systematic study of candidate structural ceramics (primarily silicon nitride) for internal combustion engine components is undertaken as a function of temperature ($< 1200^{\circ}\text{C}$), environment, time, and machining conditions. Properties such as strength and fatigue will be characterized via flexure and rotary bend testing.

The second goal of the program is to characterize the evolution and role of damage mechanisms, and changes in microstructure linked to the ceramic's mechanical performance, at representative engine component service conditions. These will be examined using several analytical techniques including optical and scanning electron microscopy. Specifically, several microstructural aspects of failure will be characterized:

- (1) strength-limiting flaw-type identification;
- (2) edge, surface, and volume effects on strength and fatigue size-scaling
- (3) changes in failure mechanism as a function of temperature;
- (4) the nature of slow crack growth; and
- (5) what role residual stresses may have in these processes.

Lastly, numerical probabilistic models (i.e., life prediction codes) will be used in conjunction with the generated strength and fatigue data to predict the failure probability and reliability of complex-shaped components subjected to mechanical loading, such as a silicon nitride diesel engine valve. The predicted results will then be compared to actual component performance measured experimentally or from field service data. As a consequence of these efforts, the data generated in this program will not only provide a critically needed base for component utilization in internal combustion engines, but will also facilitate the maturation of candidate ceramic materials and a design algorithm for ceramic components subjected to mechanical loading in general.

Technical Highlights

Studies of dynamic fatigue behavior in four-point bending for Kyocera SN235P silicon nitride were completed during this reporting period. The SN235P silicon nitride billets were fabricated with the same powder batch used to process the SN235P exhaust valve blanks. The SN235P exhaust valves will be employed for bench rig as well as engine tests at Caterpillar after the completion of valve machining. This study was carried out in order to verify the mechanical performance of co-processed valve materials and to ensure consistent mechanical properties to those evaluated previously. The co-processed SN235P (here designated as SN235P-CP) silicon nitride bend bars were longitudinally machined per the revised ASTM C116 standard with 600 grit surface finish. Note that those test bend bars, machined previously prior to the recent revision of ASTM C116 standard, were with 320 grit surface finish. The dynamic fatigue tests were carried out at 20 and 850°C and at stressing rate of 30 and 0.003 MPa/s in air per ASTM C1465.

Results of dynamic fatigue tests at 20°C showed that the SN235P-CP silicon nitride exhibited inert characteristic strengths that were about 9% lower and 23% higher than those previously obtained for SN235 and SN235P silicon nitride, respectively (Table 1, and Figs. 1 and 2). The higher inert characteristic strength of the SN235P-CP could be attributed to the finer surface finish (600 grit) with respect to the 320 grit surface finish employed for the SN235P MOR bars tested previously. In addition, the SN235P-CP exhibited a lower Weibull modulus ($m = 11.9$) than the values obtained for SN235 ($m = 23.8$) and SN235P ($m = 38.1$), as shown in Table 1. The obtained lower Weibull modulus of SN235P-CP might result from the different strength limiting flaw population present in the SN235P-CP as illustrated in its lower portion of strength distribution curve (Fig. 1). A detailed analysis of fractography will be carried out to identify the critical strength limiting flaws in those lower strength samples. Similar higher strength response of SN235P-CP with respect to SN235P was also observed at 850°C under the same stressing rate. On the other hand, the failure stress versus stressing rate curves at 20 and 850°C showed that the SN235P-CP exhibited high fatigue exponents ($N \sim 111$ and 93, respectively), indicative of high resistance to slow crack growth process (Figs. 3 and 4). The high fatigue exponents obtained for SN235P-CP were consistent to the high N values obtained previously for SN235P as well as SN235. Therefore, dynamic fatigue results suggest that the SN235P-CP would meet the application criteria for exhaust valve components of diesel engines.

The machining of flexural bend bars of a commercial grade silicon nitride (i.e., SN147-31E, manufactured by Ceradyne Advanced Ceramic Operation, Inc., CA) has been completed. The SN147-31E was processed with similar sintering additives to those employed for SN147-31N evaluated previously. However, The SN147-31E contains a crystalline secondary phase achieved by a post heat treatment. The mechanical properties of SN147-31E will be evaluated under the same test matrix employed for SN147-31N, and be reported in the next quarterly. It is anticipated that SN147-31E would exhibit a higher temperature mechanical reliability than SN147-31N due to the presence of crystalline secondary phase.

Status of Milestones

Milestone: “Complete testing and analysis of prototype silicon nitride valves after bench rig testing” was on schedule.

Communications / Visitors / Travel

Update of the dynamic fatigue test results of Kyocera SN235P-CP silicon nitride with M. J. Andrews at Caterpillar.

Communication with M. J. Andrews at Caterpillar on the fractography analysis for SN235P-CP tested bend bars.

Communication with M. J. Andrews at Caterpillar on the machining status of the SN235P valves and valve test fixture.

M. J. Andrews at Caterpillar visited ORNL on May 20 to discuss the update of the silicon nitride exhaust valve program.

Problems Encountered

None.

Publications

None.

References

[1] H. T. Lin, T. P. Kirkland, M. K. Ferber, and M. J. Andrews, “Life Prediction of Diesel Engine Components,” Heavy Vehicle Propulsion System Materials Program Bimonthly Technical Progress Report to DOE Office of Transportation Technologies, Jan. – March 2001.

Table 1. Summary of uncensored Weibull and strength distributions for Kyocera SN235P silicon nitride specimens longitudinally machined per ASTM C1161. Data of

Kyocera SN235/SN235P, also machined longitudinally, generated previously are used for comparison.

Material	# of Spmns. Tested	Stressing Rate (MPa/s)	Temp. (°C)	Uncens. Weibull Modulus	± 95%	± 95%	± 95%
					Uncens. Weibull Modulus	Uncens. Chrctstic Strength (MPa)	Uncens. Chrctstic Strength (MPa)
SN235	15	30	20	23.8	15.4, 33.9	901	879, 923
SN235P	15	30	20	38.1	24.0, 55.8	666	656, 676
SN235P-CP*	30	30	20	11.94	8.58, 15.94	820	794, 847
SN235P-CP*	30	0.003	20	14.56	10.93, 18.64	741	721, 761
SN235	15	30	850	26.7	18.0, 36.7	777	760, 793
SN235P	15	30	850	19.3	12.5, 27.6	631	612, 649
SN235P-CP*	30	30	850	20.56	15.16, 26.87	684	671, 697
SN235	14	0.003	850	18.5	11.8, 26.8	744	720, 767
SN235P	15	0.003	850	18.2	11.5, 26.8	594	575, 612
SN235P-CP*	30	0.003	850	19.44	14.49, 25.01	621	608, 633

* Specimens were machined from co-processed billets of exhaust valve blanks.

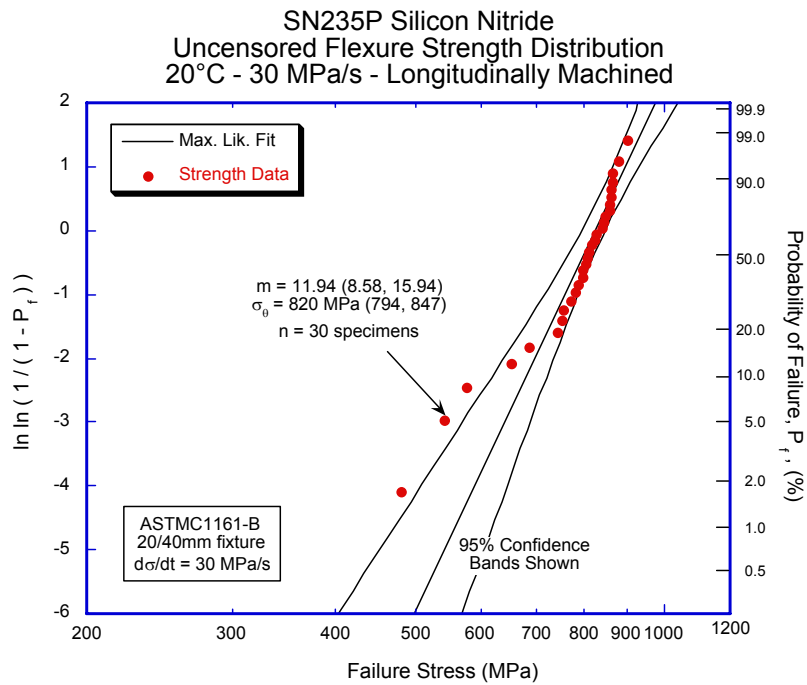


Figure 1. Strength distribution of Kyocera SN235P-CP longitudinally machined and tested at 20°C and at 30 MPa/s.

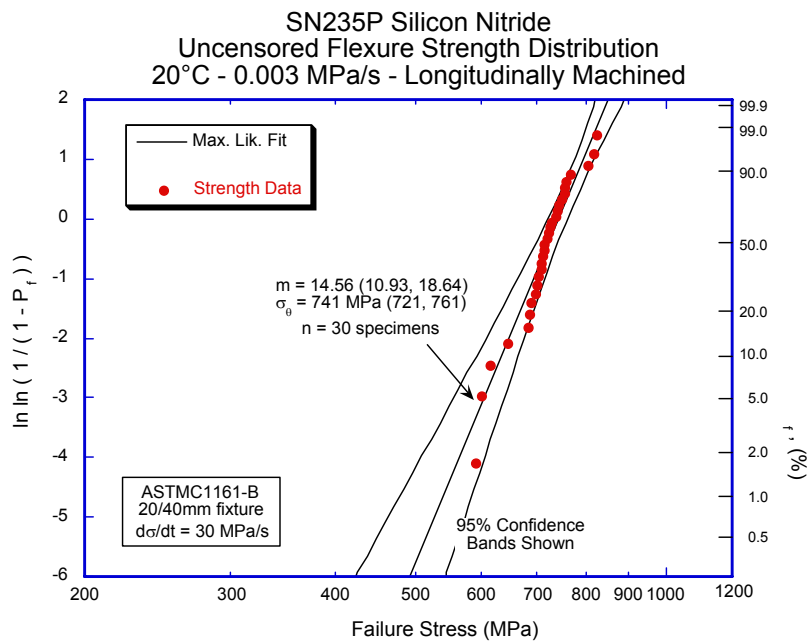


Figure 2. Strength distribution of Kyocera SN235P-CP longitudinally machined and tested at 20°C and at 0.003 MPa/s.

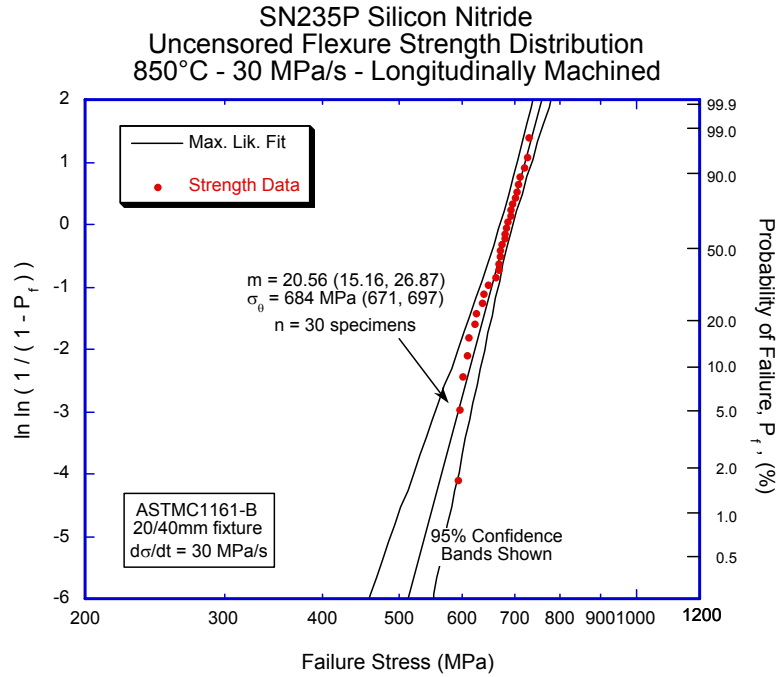


Figure 3. Strength distribution of Kyocera SN235P-CP longitudinally machined and tested at 850°C and at 30 MPa/s.

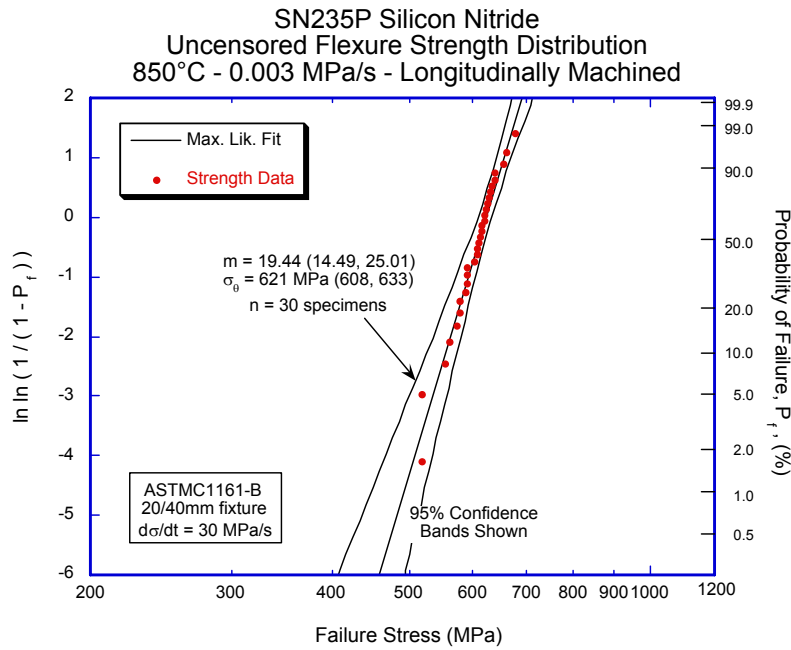


Figure 4. Strength distribution of Kyocera SN235P-CP longitudinally machined and tested at 850°C and at 0.003 MPa/s.

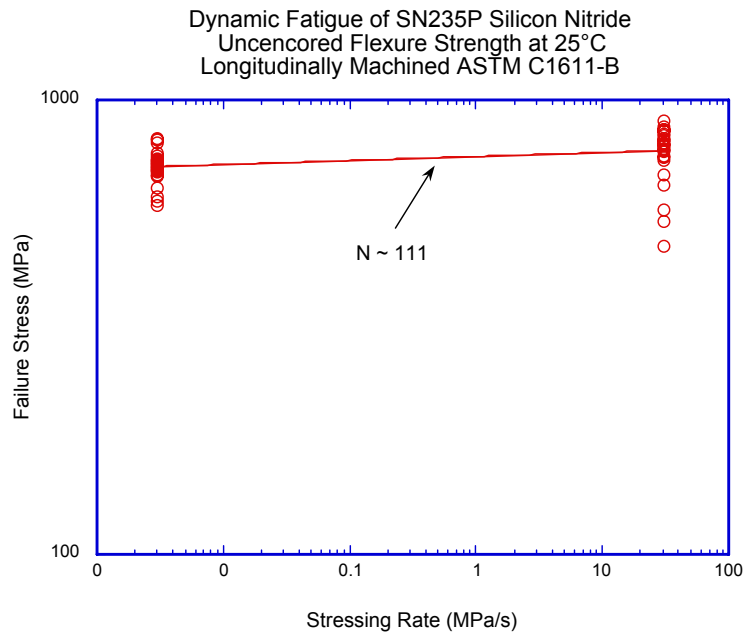


Figure 5. Failure stress versus stressing rate curve of SN235P-CP silicon nitride longitudinally machined and tested at 20°C in air.

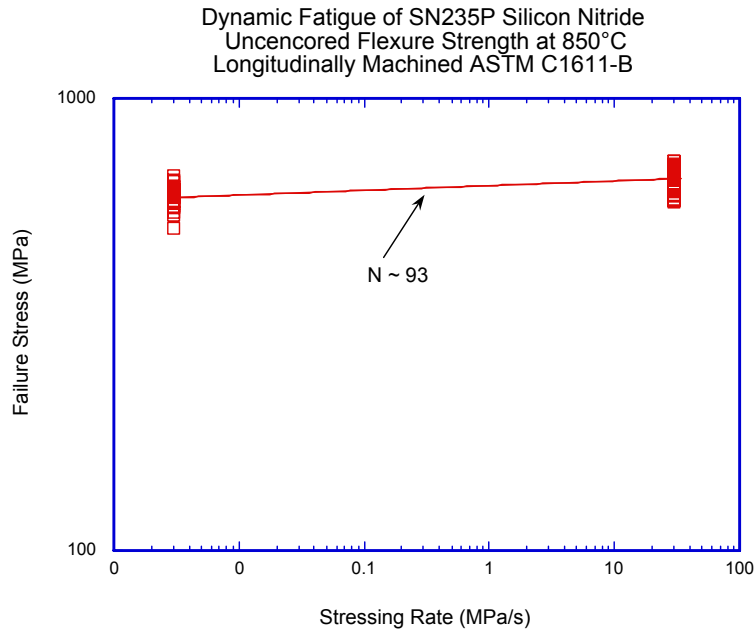


Figure 6. Failure stress versus stressing rate curve of SN235P-CP silicon nitride longitudinally machined and tested at 850°C in air.

Low-Cost Manufacturing of Precision Diesel Engine Components

S. B. McSpadden, Jr., Tyler Jenkins, Randy Parten, and Jason Braden
Oak Ridge National Laboratory

Mustafa Bakkal
(Graduate Student from North Carolina State University)

Objective/Scope

- To develop and demonstrate optimized, cost-effective fabrication processes for producing precision components for use in diesel engines.
- To develop and demonstrate optimized, cost-effective, non-destructive testing methods for detecting and preventing machining-induced damage in engine components.

Technical Highlights

Two preformed silicon nitride diesel engine valves have been received from Caterpillar for use in a machining study to be conducted on the Weldon Model AGN5 cylindrical grinder. Plans are being finalized to refurbish this grinder so that it can achieve the necessary size and form tolerances when the valves are ground. Once the final drawing requirements have been received from Caterpillar, they will be imported into our CAD/CAM software and a grinding program will be developed. The primary goal is to develop and study the machining processes required to economically produce the valves.

The recently acquired tabletop CNC milling center is being used to study the drilling characteristics of Zr-based metallic glass (BMG) material. Preliminary tests revealed that the primary drilling parameters, which include feed rate and spindle speed, must be chosen carefully due to the high hardness and low thermal conductivity of BMG material. Initial tests resulted in undesirable results such as broken drill bits and oblique holes due to the drill's tendency to "lead off" upon first penetration of the material. This is due to the high hardness of the material, and the problem was eliminated by drilling a small pilot hole to center the drill.

Drilling parameters for subsequent tests were selected as follows:

Spindle speed	10.000 rpm
Feed rate	2.5, 5, and 10 mm/min
Drilling tool geometry	1 mm diameter, 118° point angle
Tool materials	High speed steel (HSS), Solid carbide
Work piece dimensions	2 mm thick by 6.35 mm diameter BMG disks sliced from a BMG bar. (7 drilled holes per disk)

Before meaningful results can be obtained, test repeatability and reliability must be established. After these repeatability tests, drilling tests will be conducted on stainless steel work piece material to compare tool wear, tool durability, and cutting mechanics for both materials.

Typical SEM micrographs of a drilled work piece, the tip of a drill bit, and a chip produced during drilling are shown in Fig. 1.

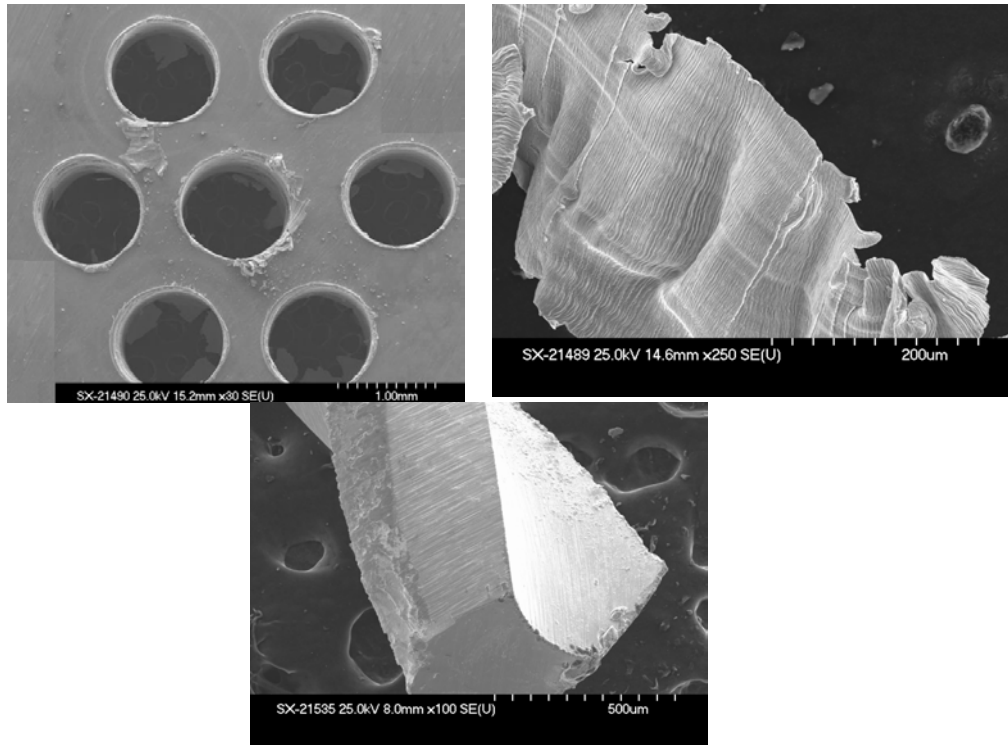


Figure 1. SEM micrographs of a) drilled work piece, b) collected chip, and c) drill bit after drilling 7 holes.

Future Plans

Cummins Engine will visit the HTML in July to conduct a grinding wheel performance study. The study will address both superabrasive cubic boron nitride (cBN) grinding wheels and conventional silicon carbide vitrified grinding wheels. Tests will be conducted under various material removal rates to optimize each type of wheel for use in grinding engine components. Components may be made from either zirconia or tool steel, depending upon the application. The challenge is to find a combination of wheels and machining conditions that can be used to grind either type of workpiece material (tool steel or zirconia) without changing wheels when switching from one material to the other. Machine setup and downtime has a significant impact on cost.

Travel

None.

FY 2003 Milestones

- (1) Two prototype valves made from silicon nitride and supplied to ORNL by a major diesel engine manufacturer will be machined on the Weldon cylindrical grinder. **(03/04)**
- (2) ORNL will work with a grinding wheel manufacturer and a major diesel engine manufacturer to test a grinding wheel that is capable of grinding both zirconia and tool steel in a single machine configuration. **(09/04)**

Publications

None this period.

Diesel Exhaust Filter Temperature Measurement and Cost-Effective Machining of Titanium Alloys

Albert Shih
University of Michigan

Objective/Scope

The objective of this research is to develop infrared-based techniques for temperature measurement in diesel exhaust after-treatment filters and to investigate cost-effective machining methods for titanium alloys.

Technical Highlights

In this quarter, researches are focusing on the low temperature measurement tests on a microwave heated diesel exhaust aftertreatment filter. As mentioned in the previous quarterly reports, the temperature measurement system, consisting of the 45° angled sapphire fiber, the PbS/PbSe two color sensor and the DAQ system, was calibrated against a blackbody heating source in low temperature range from 80°C to 400°C. Based on the calibration results, tests are performed to measure the heating history of temperature distribution in the microwave heated diesel exhaust aftertreatment filter. This quarterly report presents the temperature measurement results and discussion, as well as the parasitic heating effect during temperature measurement.

1. Filter Heating and Temperature Measurement Experiment Setup

The temperature distribution and history in microwave heating of a diesel particulate filter with SiC whisker is studied. Figure 1 illustrates the side view and front view of the ceramic filter and four locations of the fiber tip used for temperature measurement. The outer diameter of the filter is 55 mm and the length is about 76 mm. The optical fiber tip is placed inside two cavities, marked by I and II in Fig. 1(a). Cavity I is a small hole between the center and side of the filter. Cavity II is the larger hole in the center of the filter. In each cavity, two positions in the center and side of the cavity, marked as “C” and “S”, denote the fiber tip locations. The location “S” is 12 mm from the open end of the filter and the distance between “C” and “S” is 25 mm. Temperature vs. time data at four locations, designated as IC, IS, IIC, and IIS, are recorded.

To demonstrate the repeatability of microwave heating at every selected fiber tip location, four repeated temperature measurement tests under the same microwave heating conditions and the same location and orientation of the fiber tip are conducted. In total, 16 sets of temperature vs. time data at four fiber tip positions are collected and analyzed. After each heating test, the filter is cooled to room temperature within the microwave heater before starting the next heating test. Maintaining the filter’s exact location in the microwave oven ensures the same heating process and temperature distribution for each test.

Each microwave heating test lasts for 240 s under a 950 W power setting. The AC voltage outputs of both PbS and PbSe detectors are recorded at 4000 samples per second sampling rate. The RMS value of every 800 data samples is calculated to represent the sensor voltage output every 0.2 s. The RMS voltage is substituted into the calibration curves to determine the filter wall temperature.

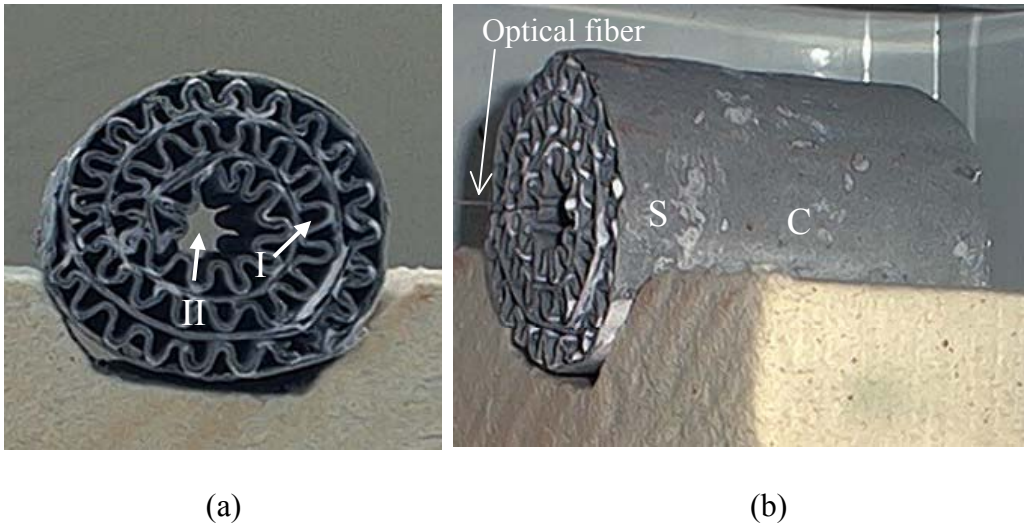


Fig. 1. Setup for filter and optical fiber inside the microwave heater; (a) front view of the filter and the designation of cavity I and II and (b) side view of filter with the center, C, and side, S, locations of fiber tip.

2. Temperature Measurement Results and Discussion

Since the sapphire fiber is transparent to microwaves, during temperature measurement, the fiber is not heated by the electromagnetic field and, the electromagnetic field distribution is also not affected by changing the fiber tip location.

Experimental results show good repeatability of the microwave heating and temperature measurement. An example is shown in Fig. 2. At fiber tip location IIS, the temperature curves of four repeated heating tests and the average of these four tests show the repeatability of the microwave heating process and temperature measurement. The maximum deviation among the four tests is less than 20°C and 10°C for the one- and two-color method, respectively. Figure 3 shows the average measured temperature vs. time results at four fiber tip locations: IC, IS, IIC, and IIS. Heating across the filter is not uniform. Among the four fiber tip locations, the highest heating rate was observed at IC, i.e., inside cavity I. The temperature steadily increases to 400°C in 60 s. In comparison to fiber tip location IIC (inside cavity II), it takes about 90 s to reach 400°C. Close to the side of the filter at fiber tip locations IS and IIS, the heating rate is about the same; both take about 120 to 140 s to reach 400°C. Due to the non-uniform electromagnetic field intensity

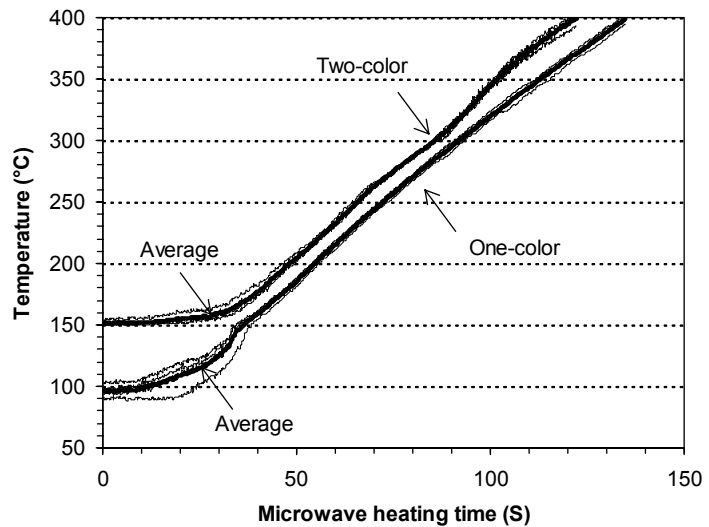


Fig. 2. Temperature repeatability at location IIS.

in microwave heating, the filter center region has a higher heating rate than on the side of the filter. The discrepancy in heating rate across the filter surface generates the non-uniform temperature distribution and chemical reaction for regeneration. The temperature gradient in the filter also creates thermal stresses and thermal cycle fatigue problem.

At the two fiber tip locations in Cavity I, as shown in Fig. 3(a), results of temperature measured using the one-color and two-color method closely match each other between 150 to 400°C. Such good agreement does not repeat at the two fiber tip locations in Cavity II. The two-color method generally predicts higher temperature than the one-color method. As shown in Fig. 3(b), the discrepancy is about 20 to 30°C. Cavity I, as shown in Fig. 1, has much smaller cross-sectional area and larger aspect ratio than Cavity II, which is the large size hole in the center of the filter. Due to the multi-reflection emissivity enhancement effect in the cavity with large aspect ratio, Cavity I has close to 1.0 effective emissivity and is almost a blackbody. This result is seen in the good match of the one- and two-color temperature measurement methods in Cavity I [Fig. 3(b)].

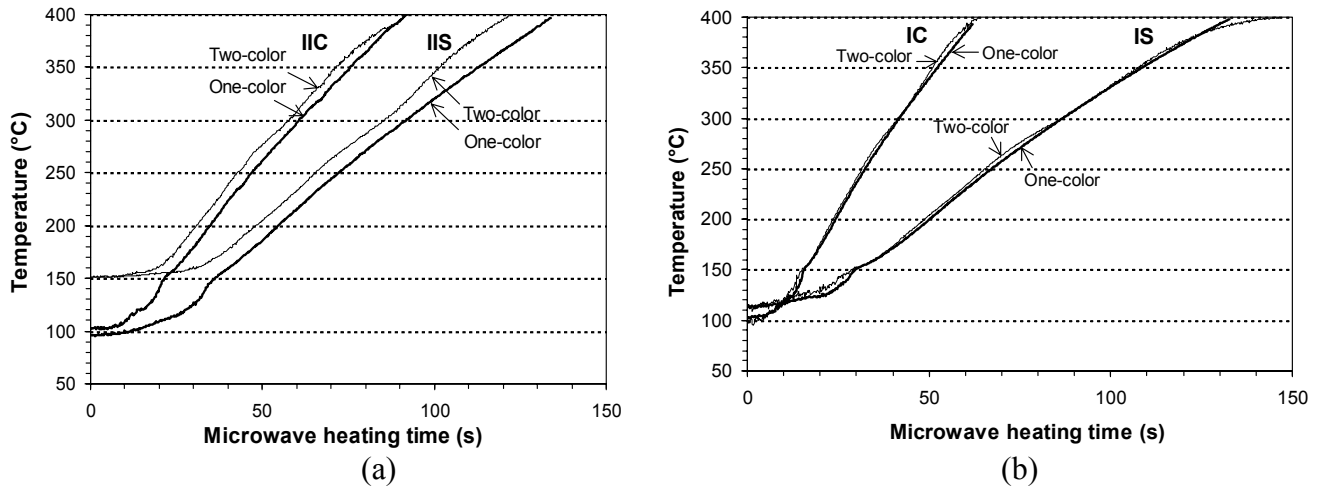


Fig. 3. Repeatability of temperature measurement at four repeated microwave heating tests.

The temperature calculated by the two-color method is generally higher than that predicted using the one-color method. This can be explained by the difference in temperature measurement strategy. The one-color method relies on the intensity of thermal radiation received by the PbS detector. The blackbody used in calibration emits theoretically the highest level of intensity. Therefore, the one-color method tends to under-estimate the temperature. The two-color method does not rely on the intensity for measurement and may over- or under-estimate the temperature due to the variation in emissivity $\epsilon(\lambda)$ and transmissivity $\tau(\lambda)$. In general, the two-color method predicts higher temperature than the one-color method, except at fiber tip location IS after 120 s.

For the low temperature measurement below 150°C, the one-color method is able to acquire temperature between 100 to 150°C. However, due to the steep slope of the calibration curves in this temperature range, the accuracy of the measured temperature below 150°C is poor. The two-color method can measure low temperatures in Cavity I with results closely matched to that obtained with the one-color method. In Cavity II, the two-color method fails to measure temperature below 150°C. This is due to the low V_{PbSe} output at low temperatures in Cavity II.

The large cavity size limits the emissivity enhancement within that cavity and the radiation intensity received by the PbSe detector for the two-color low temperature measurement.

3. Parasitic Heating Effect

During temperature measurement, the thin sapphire fiber tends to deflect and lay on the hot filter wall surface. The filter wall surface temperature in contact with the fiber may be higher than the region observed by the fiber tip. Kottmann and Stenzel [1] have studied the scattered or parasitic light effect and demonstrated that the scattered light has insignificant effect on flexible sapphire fibers for high temperature measurement. For low temperature measurement, the scattered light effect may have more noteworthy impact due to the lower intensity of spectral emission from the low temperature target. It is assumed that the thermal radiation signal from the fiber tip is not affected by other high temperature thermal radiation sources along the fiber. An experiment was designed to validate the assumption used in this study.

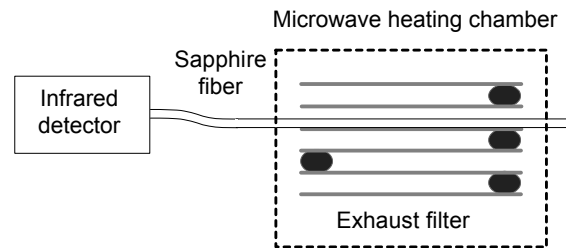


Fig. 4. Experiment setup to test the scattered light around the fiber.

The setup of the experiment is shown in Fig. 4. The fiber penetrates through Cavity I (Fig. 1) and is laying on the cavity surface. The filter is heated for 240 s using the same setup as in the temperature measurement tests described in Sec. 1. During microwave heating, the sapphire fiber is subject to an electromagnetic field. The hot, over 400°C, filter surface is in contact with the fiber. The fiber tip is exposed to the dark room background temperature, which does not generate detectable sensor output. The sensor output voltages were recorded. The PbS and PbSe detectors have less than 1.25% and 2% change in output voltage, respectively, when compared to the voltage output in the temperature measurement tests. This indicates that the scattered light from the fiber surrounding does not affect the temperature measurement. This experiment further proves that sapphire fibers can be used for low temperature measurement and the effect of scattered light is not significant.

4. Thermal Modeling for Friction Stir Welding

The finite element thermal modeling of the workpiece and tool temperature in friction stir welding has been conducted. The ANSYS finite element software was applied. Simulation results for the friction stir welding of Al 6061-T6 plate has been validated by compared with results obtained using the finite difference method [3]. The analysis is expanded to analyze the tool temperature and to predict the workpiece and tool temperature distribution in friction stir welding of titanium alloys. The high tool temperature set the selection criteria for tool material selection and the manufacturing processes to produce the tools for friction stir welding.

Status of Milestones

Milestone 1: Develop a temperature measurement system using sapphire fiber and infrared sensors for diesel exhaust filter.

Status: A fiber optic temperature measurement system consisting of angled sapphire fiber, PbS/PbSe two-color sensor, and DAQ system has been developed. With the 45°-angled tip, the sapphire fiber is able to precisely collect the radiation emitted from the internal wall surface of filters. Tests are underway to study the capability to measure temperature below 150°C.

Milestone 2: Establish calibration methods for the infrared temperature measurement system.

Status: Calibration methods have been studied and reported. The system is capable to accurately measure temperature in the range of 150 ~400°C. Study will be conducted to further enhance the low temperature sensing ability of the system down to 100°C level.

Milestone 3: Identify the sensitivity and external noise in infrared temperature measurement.

Status: Parasitic heating effect during temperature measurement has been studied and reported. Results show there is no significant impact on the temperature measurement.

Milestone 4: Investigate the cylindrical abrasive waterjet machining of titanium alloys.

Status: Nothing to report in this quarter.

Milestone 5: FEM modeling and setup cutting experiments to evaluate new cutting tools and coatings for machining of titanium alloys

Status: The direction of the titanium machining research has been shifted to the modeling of friction stir welding and machining of titanium alloys. Thermal modeling using the finite element method is completed.

Communications/Visit/Travel

- John Kong, the PhD student who is working on the infrared-based diesel exhaust aftertreatment filter temperature measurement, continues working at Cummins Technical Center in summer 2003 semester.
- Albert Shih visited Cummins on April 23rd and ORNL on April 24th.
- Albert Shih visited ORNL on June 23rd.

Publications

J. Kong, A.J. Shih, "Infrared Thermometry for Diesel Exhaust Aftertreatment Filter Temperature Measurement," *SAE Transactions*, (submitted).

References

- [1] J. Kottmann and C. Stenzel, 1999, "Characterization of Flexible Sapphire Fibers in High-Temperature Pyrometers," *Sensors and Materials*, Vol. 11, No. 4, pp. 233–246
- [2] D.P. Dewitt and G.D. Nutter, 1989, *Theory and Practice of Radiation Thermometry*, John Wiley and Sons, pp. 231–337.
- [3] M. Song and R. Kovacevic, 2003, "Thermal Modeling of Friction Stir Welding in a Moving Coordinate System and its Validation," *International Journal of Machine Tools and Manufacture*, Vol. 43, pp. 605-615.

Advanced Cast Austenitic Stainless Steels For High Temperature Components

P. J. Maziasz, R. W. Swindeman, John P. Shingledecker, N. D. Evans, and M. J. Pollard*
Oak Ridge National Laboratory
***Caterpillar, Inc.**

Objective/Scope

The objective of this new CRADA project is commercial scale up of the new modified cast austenitic stainless steels developed by Caterpillar and ORNL as cost-effective high-performance alternatives to the standard SiMo ductile cast iron used for most diesel engine exhaust manifold and turbocharger housing components. Cast austenitic stainless steels can withstand prolonged exposure at temperatures of 750°C or above, and are much stronger than SiMo cast iron above 550-600°C. The new modified stainless steels (CF8C Plus and CN12 Plus) have better aging resistance and ductility after creep than standard commercial grades of the same steels. These data would indicate better fatigue and thermal fatigue resistance than commercial cast stainless steels, and much better than SiMo cast iron. Resistance to cracking during the severe thermal cycling is necessary for exhaust components. This project provides the more comprehensive properties data needed by designers to qualify these new alloys for component applications and optimize component designs. This new advanced diesel engine CRADA (Cooperative Research and Development Agreement) project (ORNL02-0658) began on July 21, 2002, and will last at least three years. More detailed information on this project must be requested directly from Caterpillar, Inc.

Technical Highlights, 3rd Quarter, FY2003

Background

Advanced large diesel engines must have higher fuel efficiency as well as reduced exhaust emissions, without sacrificing durability and reliability. They require exhaust manifolds and turbocharger housings made from materials that can withstand temperatures ranging from 70 to 750°C or higher in a normal duty cycle. Such materials must withstand both prolonged, steady high-temperature exposure as well as more rapid and severe thermal cycling. New technology to reduce emissions and heavier duty cycles will push temperatures in these critical components even higher.

Current diesel exhaust components are made from SiMo ductile cast iron, and higher engine temperatures push such materials well beyond their current strength and corrosion limits. The previous CRADA produced systematic data comparing cast CN12 stainless steel and SiMo cast iron for such diesel exhaust component applications. That data demonstrated a clear tensile strength advantage of standard CN12 steel above 550-600°C, and even larger advantages in creep strength and fatigue life above 700°C. The previous CRADA project also developed new modified CN12 and modified CF8C steels with better creep strength, and significantly better aging resistance and thermal fatigue resistance than standard CN12. The purpose of this new CRADA project is commercial scale up of these new modified stainless steel heats, and development of the systematic and thorough database required by designers to optimize component design, and to qualify them for trial component production.

Approach

Prior work on lab-scale (15-lb induction melts with argon cover gas) heats of modified CN12 and modified CF8C and screening tests (aging, tensile, creep) at 800-850°C at ORNL provided a composition of each alloy for commercial scale up. High-temperature fatigue testing at Caterpillar Technical Center has identified a significant advantage of the modified CN12 steel. Two commercial stainless steel foundries have produced 500-lb heats of the modified CN12 and modified CF8C steels for testing and evaluation. One of those commercial foundries has been chosen to produce an addition static cast and a new centrifugally cast heat of the new modified CF8C steel. ORNL is also producing another set of laboratory heats to verify establish the effect of other minor additions on the high temperature strength of the new modified CF8C steel.

Technical Progress

Creep tests of standard CN12 and the modified CF8C (CF8C Plus) at 850°C and 35 MPa ended last quarter. The modified CF8C ruptured after 24,100 h with about 7.8% creep strain, and the test of the standard CN12 was stopped at 15,500 h without failure and less than 1% creep strain. The CF8C Plus clearly had much better creep resistance than standard, commercial CF8C at 850°C, and was comparable to CN12 (Fig. 2).

Tensile and fatigue testing were completed previously, and thermal fatigue testing was completed this quarter at Caterpillar. Tensile data on the new commercial scale-up heats of the standard and modified cast stainless steels show that the CF8C Plus is about as strong as the standard and modified CN12 steels, but still has the same high ductility as the standard CF8C steel (Fig. 1). An “engineered microstructure” alloy design approach gives the new CF8C Plus steel a very stable austenite parent matrix phase that is free of the δ -ferrite typically found in standard CF8C steel in the as-cast condition. Creep strength of CF8C-Plus at high temperatures comes from nano-scale dispersions of NbC precipitates that form and remain stable, and are much finer than found in standard CF8C steel. Because CF8C-Plus has no δ -ferrite, it is also free of σ -phase relative to standard CF8C.

CF8C-Plus was deliberately designed to have a combination of good strength and ductility at both higher and lower temperatures in order to achieve its best thermal fatigue resistance. Aging of tensile/fatigue specimens for 10,000 h at 700-850°C continued at ORNL this quarter. Aging to 1000 h was completed last quarter, and specimen tensile testing began at Caterpillar this quarter. Aging to 10,000 h continues this quarter. Microstructural analysis of previous aged or creep-tested specimens of lab-scale heats of CF8C-Plus and CN12-Plus steels was completed this quarter, and tested specimens of the new commercial heats have been identified for microcharacterization next quarter.

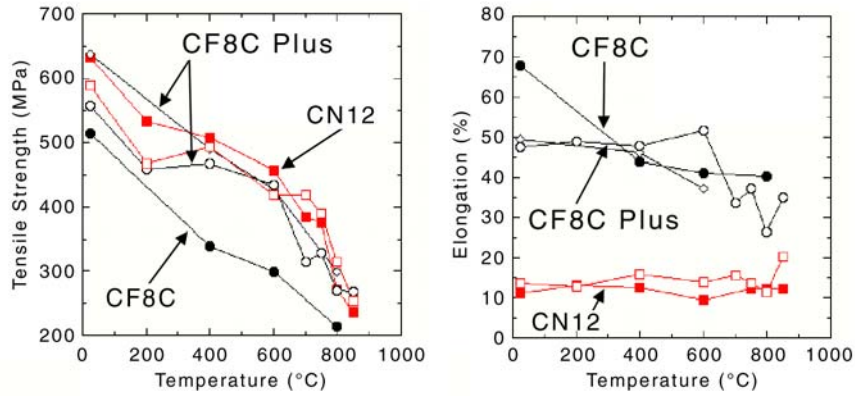


Figure 1 – Tensile properties measured by Caterpillar for the commercial scale-up heats of the new modified CN12 and CF8C stainless steels at room temperature to 850°C in air.

Isothermal fatigue testing and data analysis of the new commercial scale-up heats of CF8C Plus and CN12 Plus were completed last quarter at Caterpillar, thermal fatigue testing continued this quarter. Additional lab-heats of CF8C-Plus were cast at ORNL to define the effects of other minor alloying additions and establish their limits for commercial heats. One of the commercial foundries was chosen by Caterpillar to produce another static sand cast heat and a centrifugally cast heat of CF8C-Plus, and specimens will be made next quarter.

Communications/Visits/Travel

Detailed team communications between ORNL and Caterpillar occur regularly, at least once or twice a week. The new 3 year CRADA began on July 21, 2002, when the previous CRADA ended.

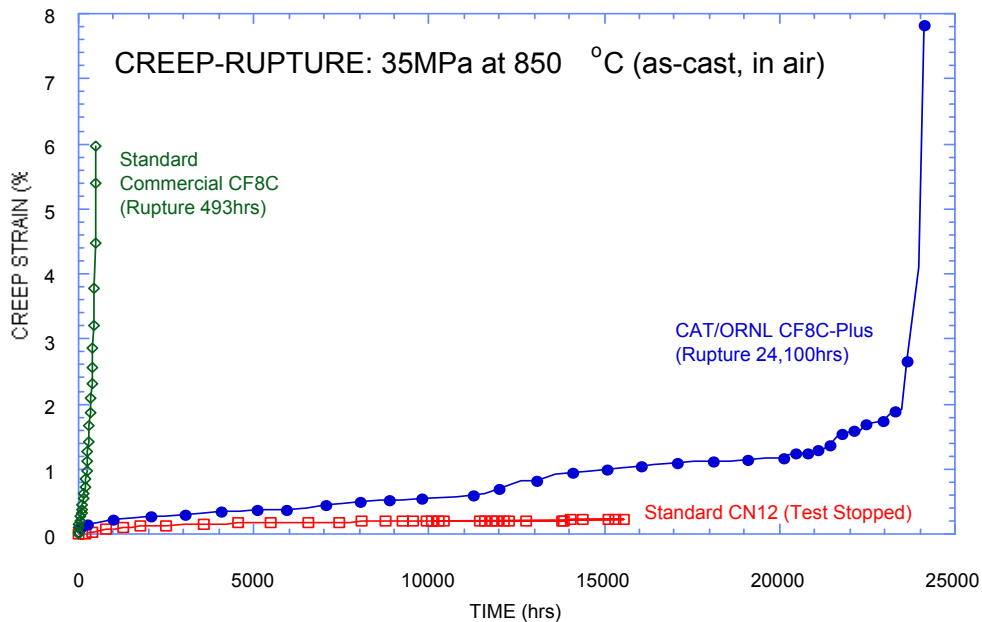


Figure 2 – Creep-rupture testing (at ORNL) of standard, commercial CF8C and and CN-12 cast stainless steels and a lab-scale heat of the new CF8C-Plus steel.

An invention disclosure and patent application on cast austenitic stainless alloys with improved performance were completed by Caterpillar and filed with the U.S. Patent Office in December 2000. It is entitled "Heat and Corrosion Resistant Cast Stainless Steels With Improved High Temperature Strength and Ductility," by P. J. Maziasz (ORNL), T. McGreevy (U. of Bradley/CAT), M. J. Pollard (CAT), C. W. Siebenaler (CAT), and R. W. Swindeman (ORNL). Several quarters earlier, two separate new patent applications were developed and submitted to the U.S. Patent Office, one on the CF8C Plus steel and the other on the CN12 Plus steel.

Status of Milestones

Formal milestones were imbedded in the previous CRADA and in the new CRADA, which is part of the DOE/OFCVT Heavy Vehicle Propulsion Materials Program, but a task in the ORNL FWP. As before, all milestones have been successfully achieved on or significantly ahead of schedule.

Publications/Presentations/Awards

An R&D 100 Award Nomination Package was submitted to R&D Magazine entitled "CF8C-Plus, Cast Stainless Steel for High-Temperature Performance," by ORNL and Caterpillar last quarter and won a 2003 R&D 100 Award this quarter. Several articles on this project have appeared in newspapers, Energy Insider, and several technical publications.

MICROSTRUCTURE AND CREEP PROPERTY OF HOT-EXTRUDED TiAl/Ti₃Al IN-SITU COMPOSITES

Luke L. Hsiung

Lawrence Livermore National Laboratory

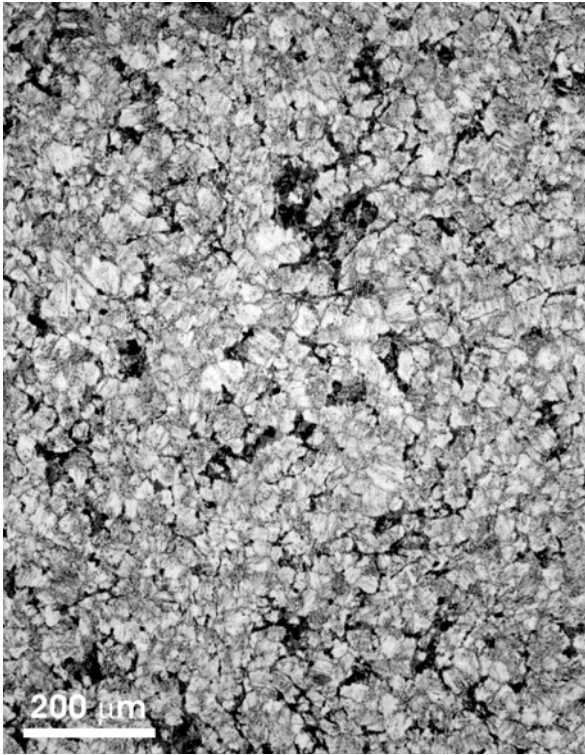
Objective/Scope

The objective of this effort is to exploit advanced thermomechanical-processing techniques to fabricate in-situ TiAl/Ti₃Al laminate composites containing ultrafine lamellar microstructure with the width of constituent lamellae down to submicron or nanometer length-scales. This project is a joint LLNL/ORNL effort to design and fabricate TiAl/Ti₃Al nanolaminate composites for advanced Diesel engine applications. The LLNL portion of this joint effort is to experimentally verify microstructural stability and mechanical properties (room-temperature ductility and strength, and elevated-temperature creep resistance) of the composites, and to investigate the fundamental interrelationships among processing, microstructures, alloying additions, and mechanical properties of the composites so as to achieve the desired properties and performance of the composites for high-temperature structural applications.

Technical Highlights

We have investigated during the third quarter report-period the microstructures and creep properties of TiAl(γ)/Ti₃Al(α_2) in-situ composites fabricated by the hot extrusion of cast Ti-46.5Al-3Nb-1W-0.1B (1W hereafter) and Ti-46.5Al-3Nb-2W-0.1B (2W hereafter) alloys at 1345°C with the extrusion ratio of 1:5. The resulted microstructures observed by optical metallography shown in Fig. 1 indicate that both the 1W and 2W composites contain very fine grain size which is in average smaller than 40 μm . Results of TEM observations shown in Figs. 2 and 3 indicate that 1W composite has a duplex microstructure, i.e. the microstructure contains both single-phase grains [Fig. 2(a)] and lamellar colonies [Fig. 2(b)], and 2W composite however has a nearly fully-lamellar microstructure [Fig. 3(a)], i.e. the microstructure contains mainly lamellar colonies with some fine single-phase grains existed at colony boundaries. An ultrafine lamellar microstructure is developed within some lamellar colonies. A typical example is shown in Fig. 3 (b). Here, the average width of γ lamella is $\leq 100\text{nm}$, which is significantly finer than that of γ lamellae (varies between 100 nm and 350 nm) within the fully lamellar Ti-47Al-2Cr-2Nb hot-extruded at 1400°C [1]. These results suggest that the alloying addition of tungsten has effects on both enhancing the formation of lamellar microstructure and refining the lamellar microstructure.

The steady-state creep rate of the nearly fully-lamellar 2W composites tested at 760°C and 815°C under stresses ranging between 50 MPa and 400 MPa is shown in Fig. 4(a). Similar to previously reported creep data of fully-lamellar Ti-47Al-2Cr-2Nb hot-extruded at 1400°C [2], there exists two creep regimes, i.e. low-stress (*LS*) and high-stress (*HS*) regimes, in which a nearly linear or nearly quadratic creep behavior [i.e. steady-state creep rate = $k\sigma^n$, where σ is applied creep stress and $2 > n > 1$] was observed in low-stress (*LS*) regime (i.e. $\sigma < 200$ MPa), and power-law break down ($n > 6$) was observed in high-stress (*HS*) regime (i.e. $\sigma > 200$ MPa). This suggests that similar to previously proposed creep mechanisms in Ti-47Al-2Cr-2Nb, the creep mechanism in *LS* regime is controlled by the sliding of lamellar interfaces, and that in *HS* regime is predominated by deformation twinning within γ lamellae. However, regardless of a higher W content in 2W composite, there is a significant reduction of creep resistance for 2 W composite. The creep rate at 760°C is approximately $7 \times 10^{-8} \text{ s}^{-1}$ under 100 MPa, which is approximately an order higher than that of fully-lamellar Ti-47Al-2Cr-2Nb, which is approximately $8 \times 10^{-9} \text{ s}^{-1}$ under 100 MPa. This reduction of creep resistance can be attributed to the existence of many single-phase grains within the nearly fully-lamellar 2W composite. The creep testing for 1W composite is currently underway. The deformed substructures of both 1W and 2W composites will be presented in the report of next period.

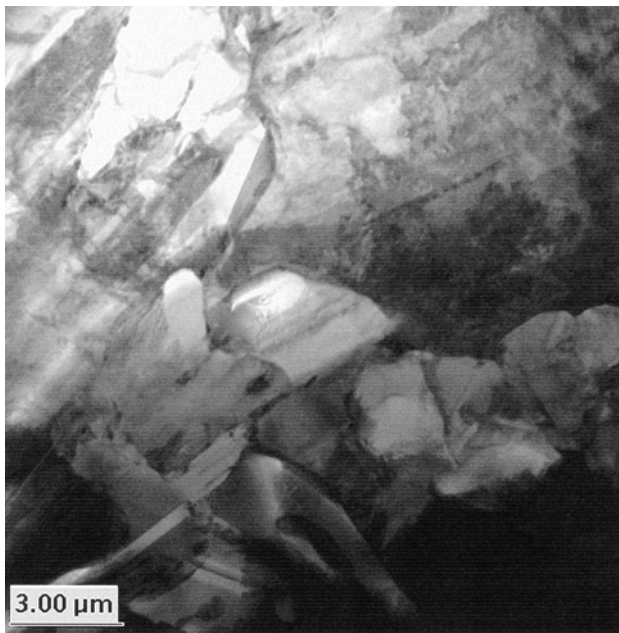


(a)

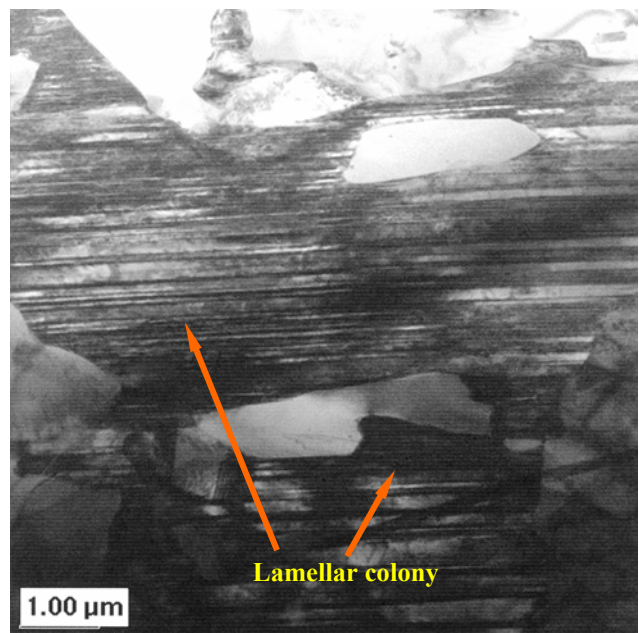


(b)

Fig. 1. Optical micrographs showing the grain morphology of TiAl/Ti₃Al composites, (a) 1W composite and (b) 2W composite, hot extruded at 1345°C.



(a) 1W composite



Lamellar colony

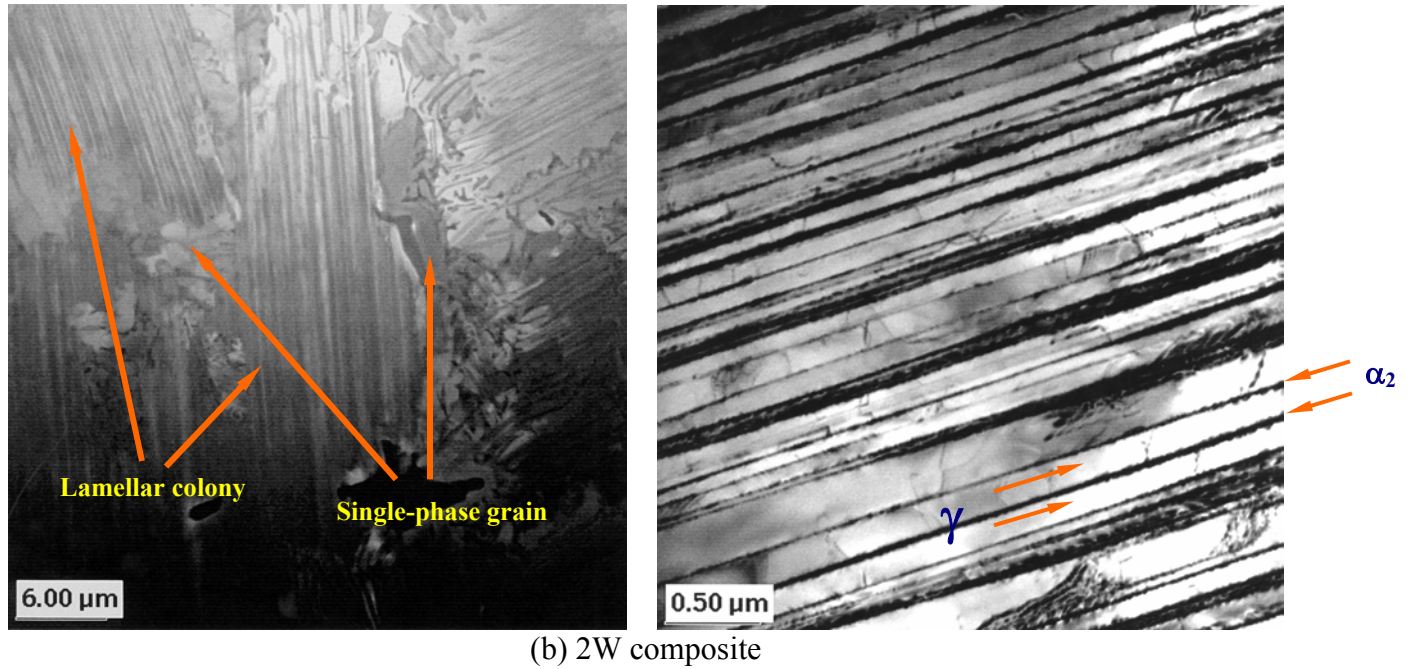


Fig. 2. Bright-field TEM micrographs showing typical microstructures observed from (a) 1W composite and (b) 2W composite.

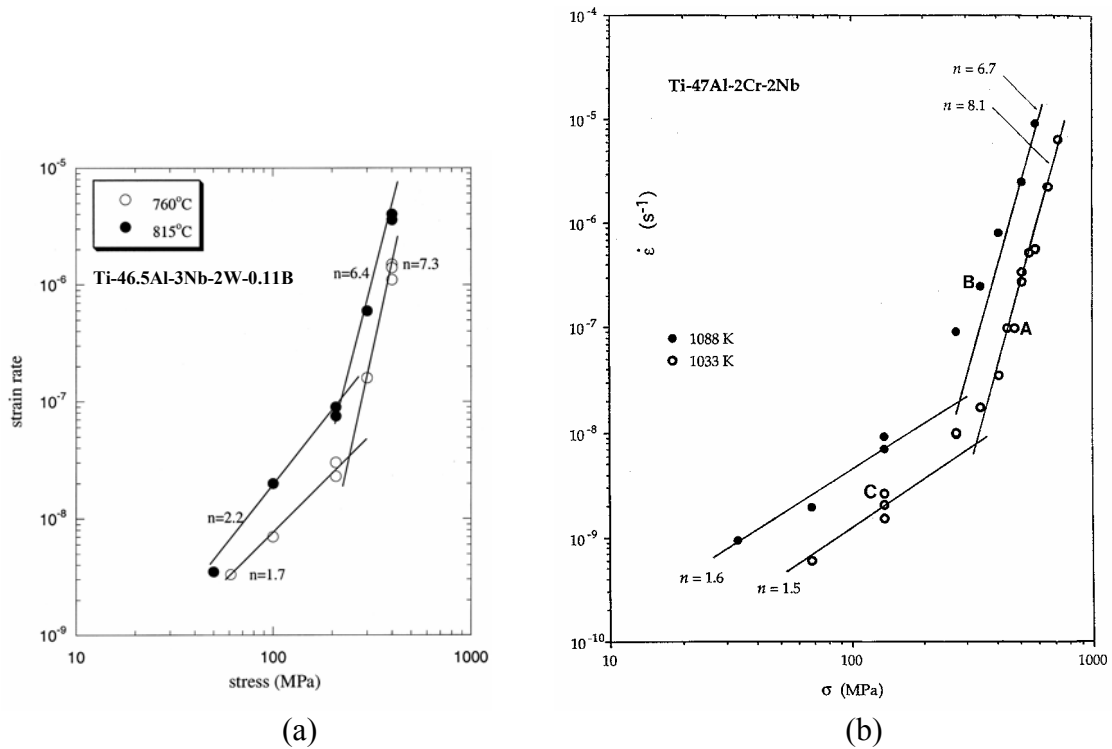


Fig. 3. Steady-state creep rate plotted as a function of applied stress at 760 and 815 $^{\circ}$ for (a) the currently investigated Ti-46.5Al-3Nb-2W-0.11B and (b) previously reported Ti-47Al-2Cr-2Nb [2].

Future Plans

1. Continue creep tests to investigate the creep resistance and microstructural stability of the laminate composites at elevated temperatures up to 850 $^{\circ}$ C.

2. Investigate the effects of prolonged annealing (at 800°C) on the thermal stability and creep resistance of the 2W composites.
3. Collaborate with ORNL to fabricate and characterize the oxidation-resistant class of in-situ TiAl/Ti₃Al laminate composites with high Nb content (>10 at.%).
4. Investigate the influence of high Nb content (up to greater than 10 at.%) to the microstructures and high-temperature creep property of the lamellar alloys.
5. Incorporate computer simulation and modeling to the study of interface sliding within the lamellar alloys (an effort collaborating with Professor Hanchen Huang of RPI).

Travel

Attended International Conference on Processing & Manufacturing of Advanced Materials (*THERMEC'2003*), July 7-11, 2003, Madrid, Spain.

Status of FY 2003 Milestones

Milestone: "Conduct in-situ TEM experiment to record a direct observation of interface sliding" was completed.

Milestone: "Collaborate with ORNL to fabricate in-situ TiAl/Ti₃Al laminate composites from cast Ti-46.5Al-3Nb-1.0W-0.1B and Ti-46.5Al-3Nb-2W-0.1B alloys using hot-extrusion processing techniques" was partially completed.

Milestone: "Conduct TEM characterization and microanalysis to measure the extent of solute segregation at lamellar interfaces" was on schedule and will be completed in September 2003.

Milestone: "Continue characterize the effect of alloying modification on creep resistance of the TiAl/Ti₃Al in-situ composites" was on schedule and will be completed in September 2003.

Publication

L.M. Hsiung, "Interface Control of Creep Deformation in Ultrafine Lamellar TiAl," Mater. Res. Soc. Symp. Proc. (Materials Research Society), Vol. 740 (2003), 287.

References

[1] L. M. Hsiung and T. G. Nieh, *Intermetallics* **7**, 821 (1999).

[2] L. M. Hsiung, T. G. Nieh, B.W. Choi, and J. Wadsworth, *Mater. Sci. Eng.*, **A329-331**, 637 (2002).

AUSPICE

This work was performed under the auspices of the U.S. Department of energy by University of California, Lawrence Livermore National Laboratory under contract No. W-7405-Eng-48.

Synthesis of Powders for Titanium Carbide /Nickel Aluminide Cermets

Christopher J. Gump and Alan W. Weimer (PI)
University of Colorado

Objective/Scope

The objective of this effort is to study methods for directly synthesizing titanium carbide and nickel aluminide, both independently and together as a cermet intermetallic composite, for use in high temperature applications. Two methods have been focused upon thus far: one batch process and one continuous process. The batch process involves the use of diluent materials in the reaction mass to absorb excess heat and thereby prevent coalescence of molten aluminum and aluminide product, and has been done on the small (1-5 g) scale, as well as the large (50-100 g) scale. The continuous process involves the use of an aerosol transport tube to rapidly heat the reactants to temperature, and then rapidly cool them to prevent particle growth.

Technical Highlights

Nickel Aluminide Synthesis

During this quarter, the continuous processing of the materials was emphasized. To begin, a series of experiments on the synthesis of nickel aluminide was performed. Previous batch results from a Differential Thermal Analyzer suggested that the reaction initiated at ~630°C. While the reaction did proceed rapidly at those conditions, higher temperatures would be required to have the reaction go to completion in the 1-3 second residence times of the continuous reactor.

Initially, the reaction to form tri-nickel aluminide was to be studied (Reaction 1)



However, upon mixing the feed it became obvious that this might be difficult. Because of the difference in the molecular weights of the two reactants, there was significantly more nickel volume in the feed than aluminum. It was therefore a concern that mass transfer resistances would prevent the majority of the feed from reacting. Coupled with the additional complexity of a reaction with four constituents, it was decided to instead focus on the formation of mono-nickel aluminide (Reaction 2)



If this proved successful, then additional nickel could be re-mixed with the product and passed through the reactor again in order to increase the nickel content to Ni₃Al. A limited run of Ni₃Al was performed simply to see if those concerns were well founded.

The matrix of experiments run is outlined in Table 1. The reactant powders were easily fed to the reactor (no jamming of the feeder, no slugging of the powder flow). In most cases, it was possible to monitor a drop in the power consumption of the furnace while the powders were being fed to the reactor. This implies that additional heat was being supplied to the reactor by the exotherm of the aluminide synthesis reaction.

Table 1. Experimental Matrix for the Aluminide Syntheses

		Temperature			
		1000°C	1200°C	1400°C	Ni ₃ Al at 1400°C
Residence Time	1.0 s	X	X	X	X
	2.0 s	X	X	X	X
	3.0 s	X	X	X	X

Analysis of the product powders is ongoing, but the initial results are encouraging. Figure 1 shows the XRD patterns for four of the experiments, all at 1400°C. In each case, the products show varying degrees of residual nickel and aluminum peaks, but each also shows a combination of nickel aluminide peaks (both NiAl and Ni₃Al). This implies that the final stoichiometry of the product is a function of the local concentrations of Ni and Al, and that good mixing of the feed is critical to achieving a homogeneous composition. However, such control should be possible with further study. The XRD patterns for the remaining samples will be measured in the near future.

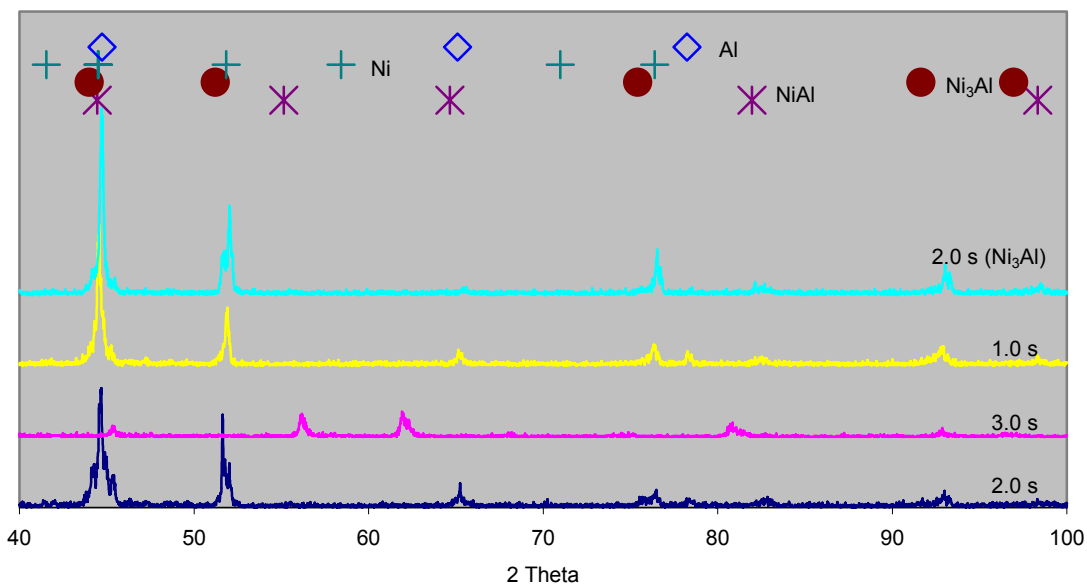


Figure 1. XRD Patterns for the Aluminide Syntheses performed at 1400°C at the residence times shown. Patterns are for NiAl (except as noted).

TiC Synthesis

Having successfully synthesized TiC as detailed in the previous report, efforts were now made to increase the conversion of the reaction to achieve greater than 80% TiC. To that end, a new feed preparation procedure was employed. Whereas previously the titania and the carbon black were simply ball-milled together to achieve the feed mixture, this time the carbon was supplied via cornstarch. Cornstarch was dissolved into a quantity of water. The titania was slowly stirred in until a thick slurry was generated. The slurry was then heated while stirring continued until the

cornstarch congealed into a gel. The gel was then dried in a tube furnace at 150°C. The resulting white flake was then calcined in nitrogen gas flow to 450°C to carbonize the starch. This feed was then fed to the reactor at 1800, 1900, and 2000°C, using a residence time of 1.5 s. The XRD patterns of the products are shown in Figure 2. In each case, the product shows strong TiC peaks, and titania peaks are only apparent in the lowest temperature run. This indicates that the starch-based feed is much more reactive than the dry-milled feed, as the dry-milled feed had still had 10% TiO₂ remaining after reaction at 2100°C.

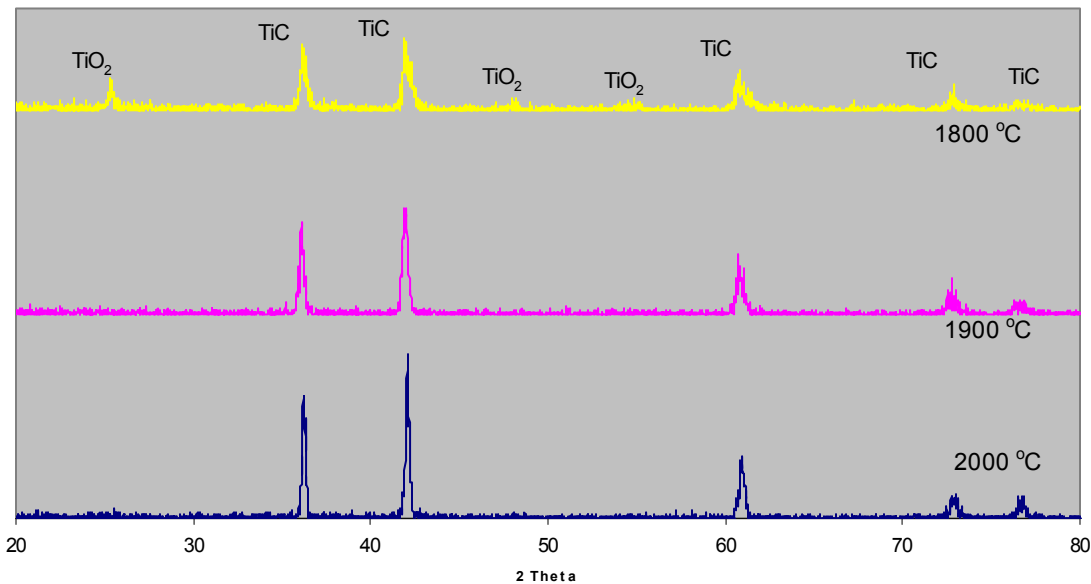


Figure 2. XRD Spectra for TiC synthesized at the given temperatures using a 1.5 s residence time.

Future Plans

Nickel Aluminide

The reacted samples must be further analyzed. The rest of the XRD patterns must be measured, as well as surface areas and particle size distributions. The greatest analytical challenge will be determining the extent of reaction for the products. Based on the preliminary analysis, additional experiments will probably need to be run at higher temperatures (1600°C). Ultimately, adjustment of the feed preparation technique and stoichiometry may be necessary

Titanium Carbide

Further analysis is also required here (surface area, particle size analysis, carbon and oxygen content). Since feed preparation is so critical, additional work must be done on optimizing the preparation technique so as to substitute a percentage of carbon black for the cornstarch.

Cermet Synthesis

Once the separate syntheses have been further optimized, it may be possible to perform a simultaneous synthesis of the cermet in one step; i.e., flow all four reactants through the reactor at the same time and generate a submicron scale cermet. Should the reactants fail to form the

products under these conditions, it may still be possible to synthesize the TiC first, and then mix it in with the nickel and aluminum to synthesize a submicron cermet.

Travel

A paper on the batch synthesis of the cermet was presented at the American Ceramics Society meeting in Nashville, TN.

FY 2003 Milestones

Continuous processing of both the nickel aluminide and the titanium carbide was successfully achieved.

Publications

Three in preparation

Laser Surface Texturing Of Lubricated Ceramic Parts

Peter J. Blau and Laura Riester
Oak Ridge National Laboratory

Objective/Scope

The objective of this effort is to evaluate the frictional benefits of laser dimple patterns on the lubrication of ceramic surfaces. This project is part of a joint Argonne National Laboratory/ORNL analysis of the benefits of a laser surface texturing (LST) process developed by Prof. Itzhak Etsion, Surface Technologies, Ltd., Israel. That process uses a computer-controlled laser to produce a pattern of shallow, rounded dimples on bearing surfaces. Based on calculations, preliminary tests, and limited field trials, the developer claims that LST enhances the ability of a lubricated surface to establish a load-bearing hydrodynamic film that decreases friction relative to a non-dimpled surface. The ORNL portion of this joint effort is focused on two aspects of LST: (1) conducting reciprocating tests of ceramic surfaces using lubricating fluids with various viscosities, and (2) determining the microstructural changes associated with the LST process.

Technical Highlights

Effects of LST on the Nanoindentation of Silicon Carbide. In the last report, nanoindentation hardness numbers were reported for taper-cross-sectioned LST surfaces of zirconia. Tests were done to see whether the localized micro-mechanical properties were altered by rapid heating and cooling. Using a three-faced Berkovich indenter, 300 nm-deep nanoindentations were made in several of the regions surrounding the dimples, avoiding as best as possible noticeable micro-cracks. In addition, the load-displacement data were used to estimate the modulus of elasticity of the materials in those regions.

Recent results for dimpled SiC (Hexalloy SA) are compared with previous data for TTZ in Table 1. Test results for regions near dimples and well away from them in the bulk, are listed separately. SiC had a nanoindentation hardness about twice that of TTZ, but as with the previously reported data, there was no significant difference in indentation properties (within the standard deviation of the data) between areas near the dimples and in the bulk material.

Table 1.
Nanoindentation Hardness and Elastic Modulus Data for
Polished Cross-Sections of LST Transformation Toughened Zirconia and Silicon Carbide

Quantity	Location	TTZ	SiC
Average nanoindentation hardness (GPa)	Bulk	16.1	37.0
Average nanoindentation hardness (GPa)	Near dimples	15.2	32.4
Average elastic modulus (GPa)	Bulk	262.	493.
Average elastic modulus (GPa)	Near dimples	257.	502.

Clear nanoindentations are difficult to make near the edges of polished specimens because even slight rounding or polishing artifacts can significantly affect results. Data interpretation was also complicated because the regions of interest lay just below the bottom of the dimples (e.g., see Fig. 1). In addition, if an indentation is made on or just above a submerged grain boundary, the

apparent NH number drops. Some of the test data were rejected because the load-displacement records were suspect, and such suspect data are not included in Table 1.

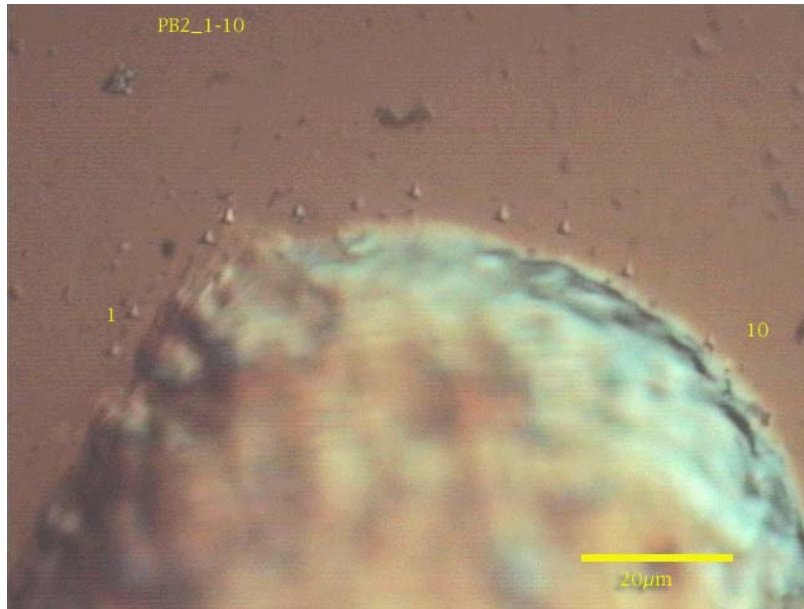


Figure 1. Array of nano-scale indentations below the bottom of a dimple.

Comparison of Dimpled with Shock-Peened Ceramics. Laser shock peening (LSP) represents a promising, new way to modify the properties of the surfaces of materials. In a program partly sponsored by DoD several organizations, including Lawrence Livermore National Laboratory, LSP Inc., and Metal Improvement Co. helped to develop this process. Since LSP can presumably affect friction and wear, it was of interest to compare the surface properties of LST ceramics with LSP ceramics. M. Ferber and A. Werescszak, ORNL, are planning to visit key developers of the LSP process in August, and we will explore the possibility of comparing LSP effects to dimpling effects on the current TTZ material.

Future Plans

- (1) Continue microstructural analysis of the LST TTZ and SiC.
- (2) Compare the tribological behavior of LST ceramics with laser shock-peened ceramics, if the latter process proves to be feasible with ceramics.

Travel

None this period.

FY 2003 Milestones

- 1) Complete studies on the effects of LST on the frictional behavior and microstructural changes produced on ceramic bearing surfaces. Submit final report. (09/03)

Publications

None this period.

High Density Infrared Surface Treatment of Materials For Heavy-Duty Vehicles

**T. N. Tiegs, H. S. Craft, D. C. Harper, F. C. Montgomery, and C. A. Blue
Oak Ridge National Laboratory**

Objective/Scope

High Density Infrared (HDI) technology is relatively new to the materials processing area and is gradually being exploited in materials processing. For many applications in heavy-duty vehicles, superior properties, such as corrosion and wear resistance, are only required at the material surface. The project using HDI technology will be exploratory and will examine (1) application of wear-resistant coatings, and (2) modification of plasma-sprayed coatings.

Technical Highlights

The project has been initiated and base materials have been procured. Three different iron-based alloys were chosen (gray cast iron, 4140 alloy steel, and D2 tool steel). Slurry coatings of WC-Ni, WC-Co, WC-Ni₃Al and TiC-Ni₃Al were fabricated and applied to the surface of the different metals. The surfaces were then exposed to the IR lamp under an argon cover gas. The appearance of the coated metals before and after HDI exposure is shown in Figs. 1 and 2, respectively.

Cross-sections of the coatings and base alloys revealed that the coatings are well bonded to the substrates with some chemical interaction evident. Some examples are shown in Figs. 3 and 4. Some large porosity within the coatings and at the interface with the underlying alloy is also observed. The coatings appear to be highly dense although no quantitative determinations have been made to date. Initial testing showed a significant improvement of the hardness in the as-fabricated coatings. Further characterization and testing is in progress.

Status of Milestones

On schedule.

Communications/Visits/Travel

None.

Problems Encountered

None.

Publications

None.

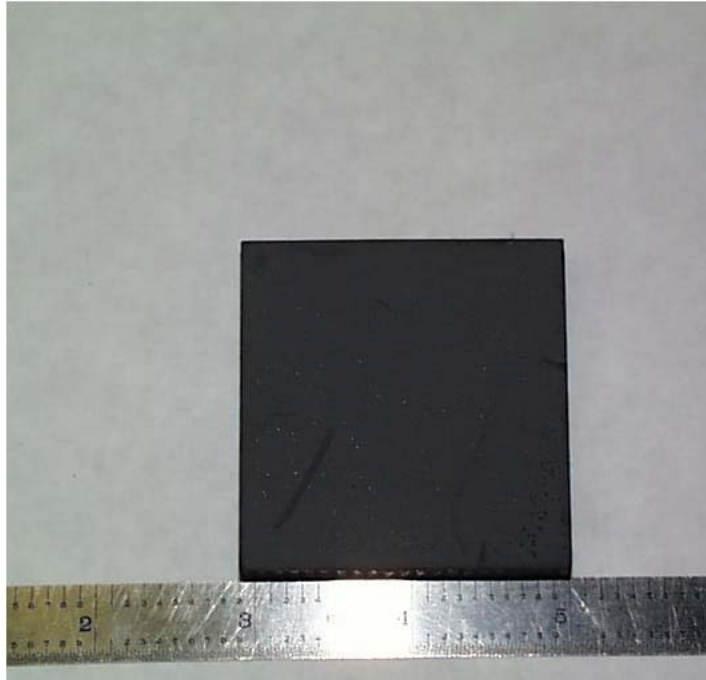


Fig. 1. Visual appearance of cast iron sample with unprocessed WC-Ni coating on surface.



Fig.2. Visual appearance of D2 tool steel sample with HDI processed WC-Ni coating on surface.



Fig. 3. Cross-section of WC-Ni coating on 4140 alloy steel after HDI processing.

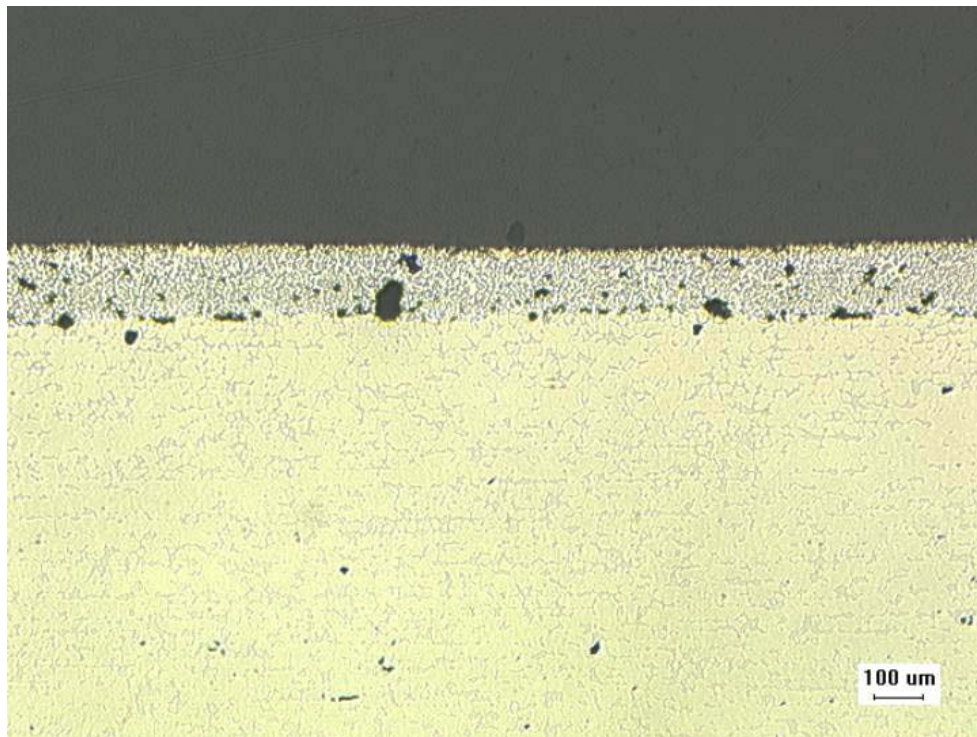


Fig. 4. Cross-section of WC-Ni₃Al coating on D2 tool steel after HDI processing.

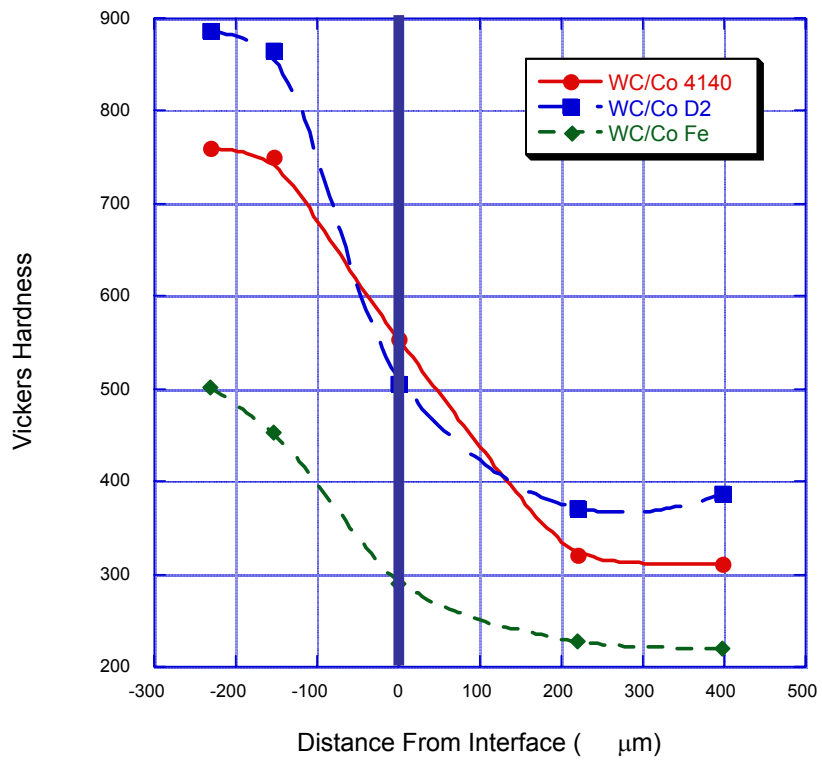


Fig. 5. Hardness improvements with HDI-treated WC-Co surface coatings on 4140 alloy steel, D2 tool steel and cast iron.

Surface Modification of Engineering Materials for Heavy Vehicle Applications

(Formerly: Standards for Reliability Testing of Heavy Vehicle Propulsion Materials)

**Stephen Hsu, Lew Ives, X. Wang, Y. Chae
National Institute of Standards and Technology**

Preface

A meeting was held on March 11, 2003, at NIST to review the existing program on contact damage and to explore new technical thrusts. Program managers from DOE HQ, ORNL, ANL, and PNNL attended, as well as researchers from these labs. A new program on integrating surface textures, thin film coatings, and surface lubricating films was proposed by NIST. Researchers from Argonne and Oak Ridge presented their earlier work on surface texturing by dimples and carbon hard coatings. PNNL presented a surface modification technique using friction stirring to harden the surface. The conclusion was that an integrated surface modification program at this time is very attractive in terms of durability and potential fuel economy benefits.

In May 2003, DOE made the decision to initiate a new activity at NIST focusing on the proposed surface modification concept. The existing contact damage assessment project was transferred to ORNL under the guidance of Dr. Andy Wereszczak. A new work statement for NIST was implemented.

Objective/Scope

The objective of this project is to develop tools and methodology to improve durability and energy conservation through an integrated approach to modify the surface properties of materials typically used in transmissions, gears, and engines. The goal is to reduce friction by 5% and increase power density of energy transmission devices by 30%.

The approach to reach these goals will be to develop theoretical basis and predictability of the effects of surface textures. This includes size and shape of the surface features, patterns on the surface, and materials of the surface features. Once we understand what surface features will do, the additional synergistic effects of thin overcoats and lubricating chemistries to protect/reinforce the surface textures will be examined. At the end, a “tool chest” of surface modifications, surface texturing, coatings, and surface modification technologies will be provided for various applications under different environments. Initial effort will focus on transportation industries where energy usage is most intense. NIST will also coordinate various research efforts in various DOE laboratories to achieve coordination and synergy. Additionally, NIST will involve members of the international community in the surface modification study and, in concert with the DOE Office of Fuel Cell and Vehicle Technology (OFCVT) and the Oak Ridge National Laboratory (ORNL), will propose to the IEA-Executive Committee the formation of a new annex to study surface modification.

In support of this goal we will pursue five research thrusts: 1) fundamental understanding between size and shape of surface features with friction reduction, 2) fabrication technique development for specific surface features, 3) development of relationship modeling between

surface patterns and surface features with friction and wear reduction 4) development of evaluation protocols of surfaces incorporating surface textures, coatings, and lubricant chemistries; 5) organization of an international cooperative research activity for pre-standardization round robin testing to establish testing methodologies for patterned surfaces.

Technical Highlights

Since the beginning of this project, a special technical symposium on Integrated Engineered Surfaces has been organized at the ASME/STLE Joint Conference in Oct. 2003 at Sawgrass Marriott Resort and Beach Club, Ponte Vedra Beach, Florida. The technical program is shown below:

INTEGRATED ENGINEERED SURFACES

SESSION 1

Session Chair and Organizer: Dr. Stephen Hsu, NIST, Gaithersburg, MD

Engineered surfaces involve surface texturing, thin film modifications, and lubrication chemistry. We intend to explore this emerging field with many invited speakers around the world to assess the current knowledge, identify future potentials, and establish a community network. This symposium will seek to bridge academic research with industrial applications.

8:30 AM – "An integrated approach S. M. Hsu, NIST, USA

9:00 AM - "Tribology opportunities from surfaces engineered at the nanoscale," Jorn Larson Basse, NSF, USA

9:30 AM - "State of the art in laser surface Texturing," Izhak Etsion, Technion, Israel

10:30 AM - "The effect of surface texture on stiction, friction, and wear," Koji Kato, Tohoku University, Japan

11:00 AM - "Tribological mechanisms of textures in dry and boundary lubricated sliding" Prof. Staffan Jacobson, Uppsala University, Sweden

11:30 AM - "Challenges for the application of engineered surfaces to tribosystems subjected to multiple contact modes" Peter Blau, Oak Ridge National Laboratory, USA

2:00 PM - "Effect of Laser texturing on lubrication regime transitions" L. Ajayi, Argonne National Laboratory

2:30 PM - "Slippery questions of boundary conditions for oil and gasoline flow," Steve Granick, University of Illinois, USA

3:00 PM - "Shakedown of integrated engineering surfaces," A. Kapoor, University of Sheffield, UK

4:00 PM – "Surface distress modeling fro engineered surfaces in low lambda regime," Diann Hua, Caterpillar, USA

4:30 PM - "Wear of oxide ceramics and diamond coatings," K. Miyoshi, A. Sayir, S.C. Farmer, NASA Glenn Research Center, USA

5:00 PM - "Nanoscale engineering of surface coatings for improved boundary lubrication," Ali Erdemir, Argonne National labs, USA

5:30 PM - "Curvature and roughness on magnetic slider air bearing surface," Y. S. Hor, M. Zhang, B. Liu, DATA Storage Institute, Singapore

5:45 PM - "Surface texturing to produce specific size and shape of UHMWPE particles for biomaterial application," H. W. Fang, S. M. Hsu, NIST, USA

As can be seen from the program, representatives from Sweden, U.K., Israel, Japan, U.S. national labs, universities, and U.S. industry will speak in this symposium.

We have begun internal laboratory research on surface texturing. Two postdoctoral fellows have been added to the program and preliminary surface textures have been fabricated. A pin on disk machine is being modified to enable flat on flat evaluation of textured surfaces.

Travel

- 1) Attended STLE annual meeting in New York City on April 27-29, 2003, and discussed with a number of companies on interest in this activity.
- 2) Attended ICMCTF coating conference in San Diego on April 30-May 1, 2003, and discussed with a number of companies on their interests and participation in this activity
- 3) Visited Caterpillar on May 7, 2003, to discuss Caterpillar's interest and participation in this activity.

Status of FY 2003 Milestones

- 1.) Organize a symposium on contact reliability to compare testing procedures used in different countries (Oct. 2002).

—done— Completed a symposium among the participating countries on IEA activities on Oct. 29, 2002, during the ASME Tribology Conference in Cancun, Mexico.

- 2.) Propose to the IEA Executive Committee the formation of a new Subtask related to performance testing of nanostructured coatings for friction reduction (Jan. 2003).

Proposed a new subtask to the DOE program managers on an integrated surface technology. A workshop was held at NIST on March 11, 2003, in which ORNL, ANL, BNW and DOE headquarters were represented. A general agreement was reached to embark on this technology.

- 3.) Prepare draft progress report on international collaboration on rolling contact fatigue testing (March 2003)

The proposed IEA international round robin was modified at the March 11 meeting because of the closing of NTN Technical Center in the US. The new round robin is being initiated and solicitation of participants are requested from various country representatives.

4.) Complete preliminary round robin rolling contact fatigue testing (June 2003).

--deleted—due to change of plans

5.) Report progress of IEA Annex III activities to the Executive Committee (July 2003)

-- IEA Annex III meeting at Istanbul in June 2003 was cancelled due to the unstable situation in the Middle East.

6.) Develop a preliminary analytical model for prediction of rolling contact fatigue lifetime (September 2003)

-- project transferred to ORNL

New milestones:

1.) Preparation of a draft annex for an IEA study of surface modification for improved performance of materials in surface-property-limited applications in heavy vehicles (June 2003)

-- IEA Executive Committee meeting scheduled in Istanbul, Turkey in June 2003 was cancelled; the next meeting is scheduled in Oct. 2003.

2.) Organize an IEA international study after obtaining approval from the IEA Executive Committee (Sept. 2003)

-- Since the IEA Executive Committee will meet in Oct. 2003, the target date will be moved. Preliminary organization has already taken place.

3.) Organize a special symposium at an international conference to assess the current state of the art in this area from the world community (Fall 2003)

4.) Evaluate the effects of surface texture size and shape on friction and wear at the bench test level (Dec. 2003)

Publications

None

Implementing Agreement For A Programme Of Research And Development On Advanced Materials For Transportation Applications

**M. K. Ferber
Oak Ridge National Laboratory**

Objective/Scope

The International Energy Agency (IEA) was formed via an international treaty of oil consuming countries in response to the energy crisis of the 1970s. A major objective of the IEA is to promote secure energy supplies on reasonable and equitable terms. The governing board of the IEA, which is composed of energy officials from each member country, regularly reviews the world energy situation. To facilitate this activity, each member country provides energy experts who serve temporary staff assignments at IEA headquarters. These staff or secretariat support the governing board by collecting and analyzing energy data, making projections in energy usage, and undertaking studies on specialized energy topics. The governing board is also assisted by several standing groups; one being the committee on energy research and technology (CERT), which encourages international cooperation on energy technology. Implementing agreements (IAs) are the legal instruments used to define the general scope of the collaborative projects. There are currently 40 active implementing agreements covering research topics such as advanced fuel cells, coal combustion science, district heating and cooling, enhanced oil recovery, fluidised bed conversion, fusion materials, solar heating and cooling, pulp and paper, hydropower, heat pumping technologies, hybrid and electric vehicles, high temperature super conductivity, wind turbines, and high temperature materials. A complete listing can be found at the IEA website, www.iea.org.

This progress report summarizes recent activities in the implementing agreement entitled, “Implementing Agreement For A Programme Of Research And Development On Advanced Materials For Transportation Applications.” This implementing agreement currently consists of one active annex entitled, “Annex II: Co-Operative Program on Ceramics for Advanced Engines and Other Conservation Applications”. The motivation for this IA is the development of new and improved ceramic materials, brittle material design methods, and life prediction methodology. The objective of Annex II is coordinated R&D on advanced ceramics leading to standardized methods for testing and characterization.

The Executive Committee for the IA on Advanced Materials is also exploring the possibility of adding new efforts (Annex III and Annex IV). Annex III focuses on the characterization of contact damage (fatigue) while Annex IV deals with materials for hydrogen storage.

Technical Highlights

The final draft of the United States report for Subtask 11 was completed. The primary objective of this effort was to develop and verify techniques for the measurement of thermal and mechanical fatigue of structural ceramics. National efforts in Japan and the United States focused on the development of procedures for evaluating the mechanical fatigue behavior of silicon nitride ceramics using either uniaxial flexure or biaxial test specimens. Specific activities within the United States included the measurement of static, dynamic, and cyclic fatigue properties of a commercial silicon nitride. The national effort in Germany consisted of the development of thermal fatigue procedures using the laser thermal shock equipment evaluated in Subtask 9 [1].

Subtask 11 also included an international effort in which the thermal and mechanical fatigue behavior of a single silicon nitride was compared with the mechanical fatigue data generated at a temperature which is the same as that at the fracture point in thermal fatigue test. Germany was responsible for the thermal fatigue testing while both Japan and the United States conducted mechanical fatigue testing.

A major finding from this work concerned the excellent correlation between static and dynamic fatigue. The static fatigue data measured at 850°C using the GS44 silicon nitride flexure specimens are shown in Figure 1 (circles). As discussed in [2], the susceptibility of GS44 to time-dependent loss in strength was much greater at this temperature than that observed at temperatures <700°C. The associated strength degradation mechanism was attributed to softening of the intergranular phases, which ultimately led to viscous flow and separation of grain facets. Given sufficient time, this viscous flow was ultimately responsible for the formation of cavities within the intergranular phase. For example, Figure 10 compares the fracture surfaces of two dynamic fatigue specimens; one tested at 30 MPa/s and other at 0.003 MPa/s. At 0.003 MPa/s there was sufficient time for the cavitation to occur as evidenced by the skeletal pattern of the intergranular phase outlining the interfaces between adjacent grains. It should be noted that similar behavior was observed for a hot-isostatically pressed silicon nitride when tested under tensile loading at temperatures above 1200°C [3]. In that study, however, the temperatures were sufficiently high to activated addition deformation mechanisms including cavitation of the silicon nitride by a solution-precipitation process.

The experimental static fatigue data were subsequently fit to the generalized slow crack growth expression

$$[1 - (S_f / S_i)^{N-2}] = (N - 2)/2 V(K_{IC}) (Y S_i / K_{IC})^2 (\sigma / S_i)^N t. \quad (1)$$

where Y is a constant. K_{IC} is the fracture toughness, $V(K_{IC})$ and N are the slow crack growth constants, V is the crack velocity, t is time, σ is the applied stress, S_i is the inert strength, and S_f is the strength after time, t. Failure occurs when $S_f = \sigma$.

The curve fitting process involved choosing values of S_i , N, and $V(K_{IC})$ which minimized the sum of the square of errors between predicted and measured lifetimes. The fracture toughness at 850°C was assumed to be comparable to the room-temperature value reported by the vendor (8 MPa m^{1/2}). The resulting values of the crack growth parameters estimated using this iterative procedure are provided in Table 1. The solid line in Figure 1 illustrates the model prediction. Note that the value of $V(K_{IC})$ is relatively low. One might expect that it should be comparable to the speed of sound given that it associated catastrophic fracture. However, this parameter actually represents the velocity occurring at the intersection of the Region I slow crack growth curve with Region III curve as shown schematically in Figure 2. Because the Region III crack growth makes very little contribution to the time-dependent failure, it is treated as a vertical line in the development of the equations describing static, dynamic, and cyclic fatigue.¹

¹ The contribution of Region II slow crack growth to time-dependent failure is also ignored.

Table 1: Crack growth parameters.

Parameter	Value	Comments
Y	1.5	Based on surface cracks
K_{IC} (MPa m ^{1/2})	8	Based on vendors information
V (K_{IC}) (m/s)	5×10^{-6}	
S_i (MPa)	800	
N	25	

The triangles in Figure 1 illustrates the results of the dynamic fatigue testing conducted at 850°C. For these data the time was calculated by dividing the stress by the stressing rate. Note that the experimental dynamic fatigue data points are shifted to longer times due to fact that in a dynamic fatigue test the stress is not constant but increases linearly from zero to final fracture strength. The same relationship is reflected by the predicted static and dynamic fatigue curves. In the latter case the curve was predicted from the static fatigue results by applying the slow crack growth parameters in Table 1 to the expression:

$$[1 - (S_f / S_i)^{N-2}] = [(N-2)/(2(N+1))] V(K_{IC}) (Y S_i / K_{IC})^2 (\bar{\sigma} S_i)^N t. \quad (2)$$

where the stress, σ , now increases linearly with time. Again at the point of failure, $S_f = \sigma$.

Status of Milestones

All milestones are on track.

Communications/Visits/Travel

None.

Publications

None.

References

- [1] M. K. Ferber, Kirchoff, G., Hollstein, T., Westerheide, R. Bast, U., Rettit, U., and Mizuno, M., "Thermal Shock Testing of Advanced Ceramics – Subtask 9 (Final Report)," Oak Ridge National Laboratory, Oak Ridge, Tennessee, Report No. MOO-107208, March 2000.
- [2] A. A. Wereszczak, H.-T. Lin, T. P. Kirkland, "Strength and dynamic fatigue of silicon nitride at intermediate temperatures," *J. Mater. Sci.* **37** 2669 – 2684, (2002).
- [3] M. K. Ferber and M. G. Jenkins, "Evaluation of the Strength and Creep-Fatigue Behavior of a HIPed Silicon Nitride," *J. Amer. Ceram. Soc.*, **75**, [9], 2453-62, 1992.

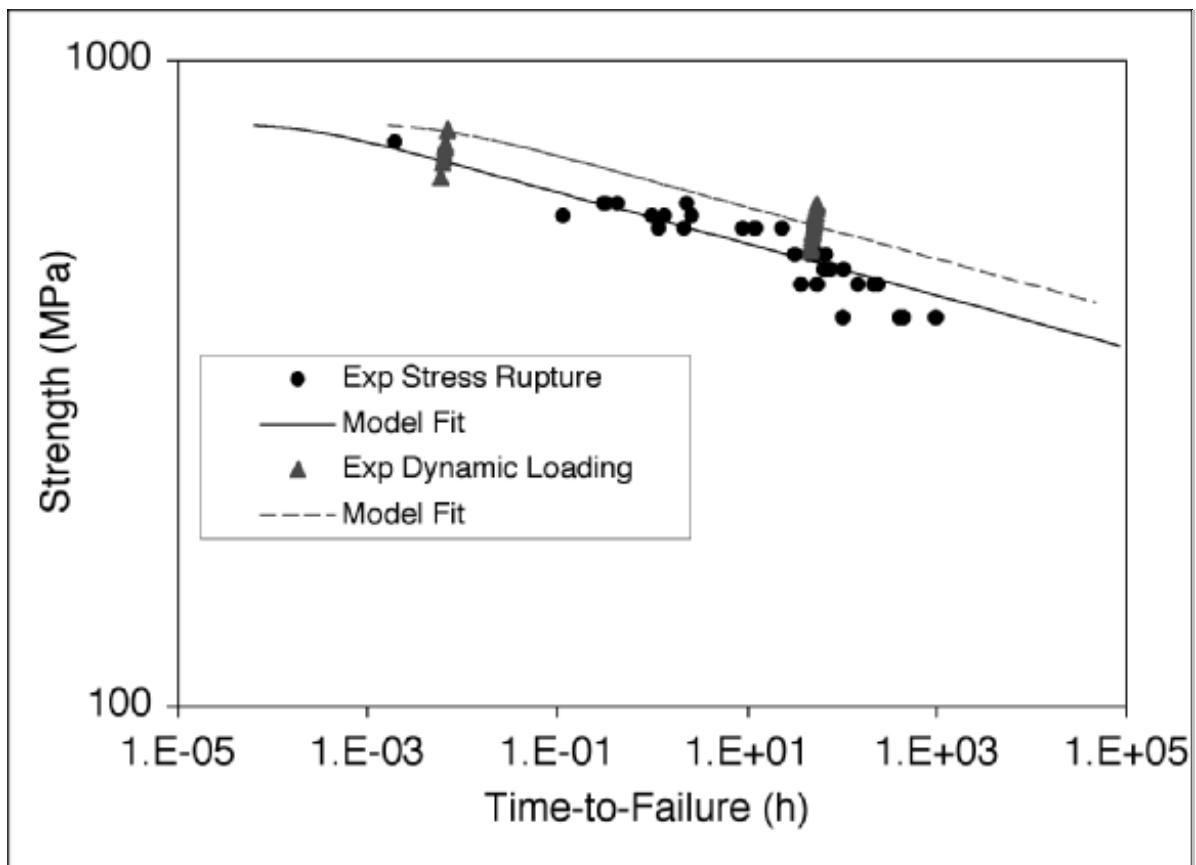


Figure 1: Comparison of static and dynamic fatigue data.

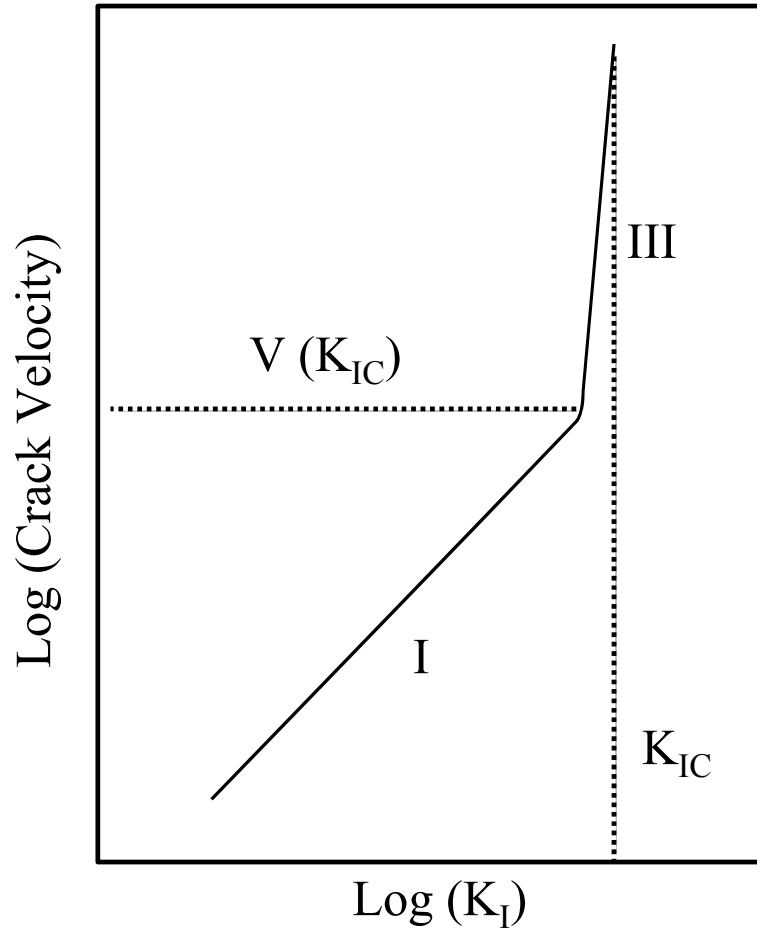


Figure 2: schematic representation of V - K_I behavior showing two regions of crack growth. Because the slope of Region III is very high, its contribution to time-dependent failure can be neglected. In this case, $V (K_{IC})$ represented the intersection of the Regions I and III curves.

Mechanical Property Test Development

George Quinn
NIST

Objective/Scope

This task is to develop mechanical test method standards in support of the Propulsion Systems Materials Program. Test method development should meet the needs of the DOE engine community but should also consider the general USA structural ceramics community as well as foreign laboratories and companies. Draft recommendations for practices or procedures shall be developed based upon the needs identified above and circulated within the DOE engine community for review and modification. Round robins will be conducted as necessary. Procedures will be standardized by ASTM and/or ISO.

Technical Highlights

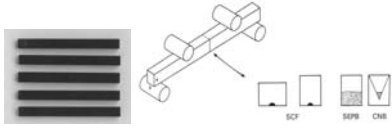
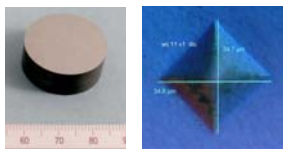
1. General

In this quarter, the new Vickers hardness standard reference material 2831 finally went on sale. Planning continued for a new Applications Subcommittee in ASTM Committee C 28, Advanced Ceramics. The large NIST Special Publication 996 on machining damage cracks in silicon nitride was printed and is being distributed. Nearly all the administrative work in updating the older ASTM standards and advancing the comparable new ISO standards is now complete. Several publications went to press during this quarter as well. We look forward to resuming work on new test method standards.

2. Fracture Toughness

No activity this quarter. Most work is finished on this topic. The ISO final draft international standard FDIS 18756, Fracture Toughness by the SCF method is done and is ready for final ISO balloting. A review of ISO DIS 15732 Fracture Toughness by the SEP method was completed last quarter. There was no additional work on the R-curve characterization of the Ceradyne sintered reaction bonded silicon nitride. A manuscript has been submitted to a Journal. In May we revised the manuscript on the fracture toughness Standard Reference Material 2100 for the 8th International Fracture Mechanics of Ceramics Conference in Houston in February 2003.

Table 1 Standard Reference Materials that are now available from NIST to support ASTM and ISO test method standards and materials specifications. All are available off the shelf. The fee per unit covers only a portion of the actual cost to prepare each SRM.

SRM	Specifics	Availability	Images
# 2100 Fracture Toughness of Ceramics K_{Ic}	(5) silicon nitride bend specimens with certified fracture toughness values: $4.57 \text{ MPa}\sqrt{\text{m}}$. Any method may be used.	Immediate \$365	
# 2830 Knoop Hardness of Ceramics HK2	(1) hot-isopressed (NBD-200) silicon nitride disks with 5 NIST 19.6 N (2 kgf) indentations HK ~ 14.0 GPa; 1,400 kgf/mm ²	Immediate \$575	
# 2831 Vickers Hardness of Ceramics and Hardmetals HV1	(1) hot-isopressed tungsten carbide disk (12% cobalt) with (5) NIST 9.8 N (1 kgf) indentations. HV ~ 15.0 GPa; 1500 kgf/mm ²	Immediate \$625	

For more information about these SRMs, or any of the NIST powder size standards, see:

<http://ts.nist.gov/ts/htdocs/230/232/232.htm>

3. Flexural Strength of Advanced Ceramics – Rectangular Specimens

Nearly all work on updating the ASTM standards and advancing the ISO standards is now complete. We expect C 1161-02c will be definitive version and no further changes will be necessary in the foreseeable future. In mid April, the revised ASTM Elevated Temperature Flexural Strength standard C 1211 came back from ASTM for a proof review. Unfortunately the proof copy was in very poor shape. Some changes were done badly or not at all. This standard was overhauled in late 2002. Twenty separate revisions were balloted in late 2002 and good comments or negatives were received from Jon Salem, Mike Jenkins, Sung Choi, and Vic Tennery. The proof was finally prepared properly by ASTM in June 2003. C 1211-02 is now finished. The ISO 14704 room temperature flexural strength is complete and the elevated temperature flexural strength standard ISO 15765 is in its final “FDIS” voting stage.

4. Fractography

A proof copy of revised ASTM Standard C 1322, Fractographic Analysis of Advanced Ceramics was finally received from ASTM in June 2003. The proof incorporated changes that were approved in late 2002. The proof was satisfactory except that some of the layout is still poor (e.g., figures separated from accompanying text) and some of the images deteriorated in quality in the process of printing and converting to PDF format. This is exasperating since we sent good quality TIFF files and even original photo figures in some cases and we continually complained to ASTM about this matter.

NIST management feels that there is a need for a separate user-friendly “Guide to Best Practice” for fractographic analysis. Work will commence on this topic in July 2003. Many fracture origin and fractography related photos were scanned in preparation for this task.

5. Flexural Strength Testing of Cylindrical Ceramic Specimens

A major 104 page NIST Special Publication on the findings of the fractography of machining damage cracks in Ceradyne SRBSN was finally printed and is now being distributed. It is a tour de force of fractographic analysis of machining cracks. Some of the key highlights are:

- The **depth of grinding cracks** is controlled primarily by the grinding wheel grit size. Many silicon nitrides fit the same general trend.
- **Deeper machining cracks** form in materials with enhanced fracture toughness. This paradox is discussed and accounted for by machine work piece interactions.
- Numerous **illustrations and schematics** of grinding cracks are included. A new nomenclature is proposed to distinguish between the various grinding cracks. Illustrations depict how they form and the telltale characteristics that may be detected by simple fractographic methods.
- Stray, **“renegade” abrasive grits** in a grinding wheel may control strength and reliability.
- The **size of the severest machining cracks varied** by as much as a factor of 2 in batches of identically prepared rods or bars. This variability was matched by a corresponding (40%) strength variability.
- New **damage maps** for grinding silicon nitride are included.
- **R-curve effects appear to have been minimal** in the Ceradyne material, despite the interlocking microstructure that enhanced the plateau fracture toughness.

A brief four-page article on this work was written for the Bulletin of the American Ceramic Society on short notice. It was published in the July 2003 issue of the Bulletin, but unfortunately only the title and abstract actually appeared in the printed copy off the bulletin. The full rendition for this (and five

other articles) was published on line in the Ceramic Society web site. It remains to be seen how much impact this approach will have.

Contact was reestablished with Professor Phillip Koshy of McMaster University in Canada. He is helping with the analysis of experimental errors in cylindrical rod strength testing. Experimental work on verifying errors in rod testing is expected to resume at NIST in July 2003.

6. Hardness

Most of our hardness activities are now complete after years of work. We finished preparing SRM 2831, Vickers Hardness of Ceramics and Hardmetals in October 2002. Ninety-six disks were accepted for distribution by the NIST Reference Materials Office. It finally cleared the administrative chores and went on sale in June 2003. It is now available off the shelf for immediate delivery. A set of minor revisions to the two ASTM standards for hardness (C 1326 for Knoop and C 1327 for Vickers) were prepared and sent to Committee C-28 for balloting in the summer of 2003. Only 4 changes are being made to the Vickers standard and 3 to the Knoop standard. One involves relaxing the numerical aperture of the objective lens of the microscope used to measure the indentations slightly to make the ASTM version compatible with the ISO 14705 standard that was adopted two years ago. A specification for the allowable asymmetry of a Vickers indentation, also taken from the ISO standard, will be added to C 1327. Statements encouraging collection of hardness at more than one indentation load will be added to both standards.

7. New Applications Subcommittee for ASTM Committee C-28 Advanced Ceramics

ASTM Committee C 28 decided to reorganize itself at the November 2002 meeting in Miami. The sense was that the committee had done a good job in preparing generic standard test methods since the committee's inception in 1986, but that interest was petering out on the generic property work, in part since many of the key properties have indeed been standardized. Through the years, we had been aware that industry was desirous of having test methods and standards for specific components and applications. These are not generic property standards such as strength of a laboratory test piece such as a button-head tension specimen or a bend bar, but instead the strength of a honeycomb structure for a diesel filter or a catalytic converter substrate. A new applications subcommittee could even construct materials specifications standards. Such specifications standards, based in part on Committee C-28's generic standards, have already been prepared in ASTM by committees F-34 on Bearings and F-04 on Surgical and Medical Devices. The executive committee of C-28 decided that the time had come to organize a C-28 subcommittee devoted to just such new applications and specifications standards.

There have been delays getting this subcommittee up and running, so in June 2003, George Quinn and Steve Gonczy agreed that a new initiative proposed by Corning will be brought into subcommittee C 28.01, Properties and Performance.

8. Other

An inquiry was received from the National Physical Laboratory in England about our ASTM elastic moduli standards C 1198 and C 1259. Both ASTM methods use the resonance of beams in bending to measure elastic moduli. NPL was surprised that the effects of altering a beam cross-section shape on the resonant frequency could be analytically accounted for through adjustments to the beam moment of inertia. This approach was the subject of a paper by Mr. Quinn and Jeff Swab in 2000. In response to the new NPL inquiry, we reviewed the equation derivations and confirmation of the approach to NPL. They are now satisfied. They have been resonating hollow tubes, and the change in the resonant frequency compared to that for a solid rod is easily accounted for by adjusting the moment of inertia.

Status of Milestones

412149 Prepare ballot-ready first ASTM draft of cylindrical rod flexure strength test	April 2002 Delayed
412150 Prepare paper on effect of machining on strength of SRBSN rods. Cocoa Beach paper, Major NIST special publication	May 2002 Completed Nov. 2002 ✓ Completed June 2003 ✓
412151 Prepare review paper on flexural testing of cylindrical rods.	October 2002 Delayed by completion of SRM 2831, HV

Communications/Visits/Travel

Small glass spheres were sent to Edgar Lara-Curcio at ORNL for crush test strength evaluation.

This is an outgrowth of our plans for diametral compression strength testing.

Mr. Quinn had discussions with Steve Gonczy about applications standards in ASTM Committee C28.

Mr. Quinn discussed applications standards with Corning engineers in June.

Publications and Presentations

1. G D. Quinn, K. Xu, J. A. Salem, and J. J. Swab, "SRM 2100: the World's First Fracture Toughness Reference Material," subm. to 8th International Conference on the Fracture Mechanics of Glasses and Ceramics, Houston, Feb 2003.
2. J. A. Salem, G. D. Quinn, and M. G. Jenkins, "Measuring the Real Fracture Toughness of Ceramics –ASTM C 1421," *ibid*.

3. G. D. Quinn, "Weibull Strength Scaling for Standardized Rectangular Flexure Specimens," *J. Am. Ceram. Soc.*, 86 [3] (2003) pp. 508-510
4. G. D. Quinn, "Weibull Effective Volumes and Surfaces for Cylindrical Rods Loaded in Flexure," *J. Am. Ceram. Soc.*, *idem*, pp. 475-478.
5. G. D. Quinn, L. K. Ives, and S. Jahanmir, "On the Fractographic Analysis of Machining Cracks in Ground Ceramics: A Case Study on Silicon Nitride," NIST SP 966, May, 2003.
6. G. D. Quinn, L. K. Ives, and S. Jahanmir, "Machining Damage Cracks: How to Find and Characterize Them by Fractography," to be publ. *Ceram. Eng. Sci Proc.*, Vol. 24, Issue 3 or 4, 2003.
7. G. D. Quinn, L. K. Ives, and S. Jahanmir, "On the Nature of Machining Cracks in Ground Ceramics: Part I: SRBSN Strengths and Fractographic Analysis," *subm. to Machining Science and Technology*, Dec. 2002.
8. G. D. Quinn, L. K. Ives, and S. Jahanmir, "On the Nature of Machining Cracks in Ground Ceramics: Part II: Comparison to Other Silicon Nitrides and Damage Maps," *idem*.
9. G. D. Quinn, L. K. Ives, and S. Jahanmir, "Fractography Reveals Machining Cracks," *Bul. Amer. Ceram. Soc.*, 82 [7] (2003) p. 11.
10. G. D. Quinn, J. J. Swab, and M. J. Motyka, "Fracture Toughness of a Toughened Silicon Nitride by ASTM C 1421," *J. Am. Ceram. Soc.*, 86 [6] (2003) pp1043-1045.